X-661-74-71
PREPRINT

NASA TM X- 70622

CHARGE COMPOSITION OF HIGH ENERGY HEAVY PRIMARY COSMIC RAY NUCLEI

ROBERT D. PRICE

MARCH 1974

GODDARD SPACE FLIGHT CENTER
GREENBELT, MARYLAND

I

For information concerning availability
of this document contact:

Technical Information Division, Code 250
Goddard Space Flight Center
Greenbelt, Maryland 20771

(Telephone 301-982-4488)

THE CATHOLIC UNIVERSITY OF AMERICA

CHARGE COMPOSITION OF HIGH ENERGY HEAVY PRIMARY COSMIC RAY NUCLEI

A DISSERTATION
Submitted to the Faculty of The
Engineering and Architecture School
Of The Catholic University of America
In Partial Fulfillment of the Requirements
For the Degree
Doctor of Philosophy

by
Robert D. Price

Washington, D.C.
1974

ACKNOWLEDGEMENTS

I wish to express my sincere thanks to the many people who contributed to the success of this research, which was conducted in its entirety with the High Energy Cosmic Ray Experiment Group of the Laboratory for High Energy Astrophysics at NASA/Goddard Space Flight Center. In particular, I wish to thank Dr. F. B. McDonald, Chief, LHEA, for giving me the opportunity to conduct this research while an employee of his laboratory, for encouraging me to obtain the Ph.D. degree, for allowing me the time necessary to complete the degree, for continued patience with me throughout the duration of the research, and for providing all the facilities necessary for the conduct and completion of this work. Indeed, I am indebted to him for the privilege of working in the LHEA.

It is with deepest gratitude that I acknowledge my advisor, Dr. J. F. Ormes, for suggesting the topic of investigation, directing the research, and providing continuous guidance and valuable advice throughout. Without his assistance, this dissertation would not have been possible. It is a pleasure to thank Dr. V. K. Balasubrahmanyan, who acted as a second advisor to me, for his suggestions and constructive criticisms.

One of the advantages gained from working in the LHEA was to be able to draw information and advice directly from many experts in the field of cosmic ray physics via "private communication". I have benefited greatly from numerous invaluable and helpful discussions with the following people regarding many phases of this work: Dr. L. A. Fisk on solar modulation, Dr. R. Ramaty on interstellar propagation, Dr. D. Reames on nuclear interactions, and Dr. T. T. von Rosenvinge on high energy charge composition of cosmic rays.

From the start this has been a group project. Therefore the entire staff of the HECRE Group is to be thanked for their close support and skillful assistance: Mr. J. Laws, electronics engineer, who was responsible for the electronics design and provided leadership and support for all electronics development and testing; and the technicians, Messrs. G. Cooper, R. Greer, M. Powers, T. Puig, J. Purvis, and L. Stonebraker who provided invaluable technical support in the form of experience, initiative, responsibility for fabrication and assembly of the experiment components, and long hours which contributed directly to the success of the experiment.

Messrs. A. Thompson, H. Trexel, and F. Shaffer were responsible for the initial mechanical design of the experiment. They are to be thanked for their continued swift and excellent quality drafting support, both for the mechanical design and layout of the experiment and for the drawings used in this dissertation. Appreciation is also expressed to Ms. B. Dallas for the patient, diligent, and careful preparation of this manuscript. Additional secretarial support was provided by Ms. B. Shavatt, Ms. M. A. Spruill, and Ms. G. Evans.

Lastly, but certainly most important to me, I wish to recognize the contributions of my parents, Mr. and Mrs. W. H. Price, that have helped to make this goal possible. They have always stressed to me the value of obtaining as full and complete an education as possible. They gave me the opportunity to pursue a higher education by providing me with financial assistance at great sacrifice to themselves during my undergraduate education. They have been a constant source of encouragement and moral support throughout the trying years of my graduate education. I am deeply

indebted to them and wish to express my sincerest gratitude for their aid. To them I dedicate this dissertation.

ABSTRACT

A detailed study of the charge composition of primary cosmic radiation for about 5000 charged nuclei from neon to iron with energies greater than 1.16 GeV/nucleon is presented. Integral flux values of $10 \leq Z \leq 14 = 9.58 \times 10^{-1}$, $15 \leq Z \leq 19 = 1.80 \times 10^{-1}$, $20 \leq Z \leq 23 = 1.15 \times 10^{-1}$, and $24 \leq Z \leq 28 = 2.37 \times 10^{-1}$ particles/m^2-sec-ster for rigidity greater than 4.9 GV and $10 \leq Z \leq 14 = 1.54 \times 10^{0}$, $15 \leq Z \leq 19 = 2.90 \times 10^{-1}$, $20 \leq Z \leq 23 = 2.10 \times 10^{-1}$ and $24 \leq Z \leq 28 = 3.60 \times 10^{-1}$ particles/m^2-sec-ster for rigidity greater than 3.25 GV are reported and compared to other recent measurements at similar geomagnetic latitude. These values are obtained after corrections have been made for detector dependences, atmospheric attenuation and solar modulation. New values of 38.5, 32.4, 23.7, and 16.8 g/cm^2 for the attenuation mean free paths in air for these same charge groups are presented.

An ionization spectrometer was used to measure the charge spectrum. This detector system consisted of 3 parts: (1) a charge identification module with 2784 cm^2-ster geometry factor, consisting of two plastic scintillators, one inorganic scintillator (CsI), and one Lucite plastic Cerenkov radiator, (2) a four-grid (2 X-Y pairs) spark chamber to determine each particle's trajectory through the spectrometer, and (3) an energy deposition module consisting of layers of tungsten, and iron interspersed with scintillator for measuring ionization energy loss. This detector measured the charge of a nucleus to an accuracy estimated to be $\leq \pm 0.7$ of a unit charge. The spectrometer was flown from Holloman Air Force Base, New Mexico (5.0 GV rigidity cutoff) and floated at an altitude of 7.4 g/cm^2 for 16 hours.

The observed charge composition has been corrected for detector dependences and atmospheric attenuation. This charge distribution, extrapolated back to the source using an exponential path length distribution of pure hydrogen, is consistent with a mean amount of matter of 5 g/cm^2. The results of this propagation back to the source imply the source is predominantly iron, neon (Ne/Fe = 1.44), magnesium (Mg/Fe = 1.68), silicon (Si/Fe = 1.38), with admixtures of sulfur (S/Fe = 0.29), and calcium (Ca/Fe = 0.18), all other elements of charge between $10 \leq Z \leq 26$ being absent at the source and being produced by cosmic ray fragmentation in interstellar hydrogen. This source charge composition is quite similar to the solar system abundances with the exception of neon, sulfur, and argon. It is consistent with the predictions of explosive nucleosynthesis in highly evolved massive stars, i.e. a supernova origin for energetic heavy cosmic rays.

TABLE OF CONTENTS

LIST OF TABLES

LIST OF FIGURES

I. INTRODUCTION

Primary galactic cosmic radiation consists largely of ionized nuclei of the elements hydrogen through iron (Z = 1 to 26) with non-zero fluxes of elements throughout the periodic table up to uranium (Z = 92) and beyond, possibly as high as $Z \simeq 114$ (Fowler et al., 1967, 1970; Fleischer et al., 1967 a, b) with energies ranging from 10^8 to 10^{20} eV/nucleon. The chemical composition and energy spectra of these multiply charged nuclei have been the subject of intensive study since their discovery in 1947 (Freier et al., 1948a, b; Bradt and Peters, 1948). But the problems of the origin of these particles and their propagation through the interstellar medium, although the topic of much theoretical discussion since their discovery, remain essentially unsolved.

The study of primary cosmic radiation, i.e. particle astronomy, is an important source of astrophysical information regarding the physical characteristics of our space-time environment and complements the knowledge obtained by radio, optical, x-ray, and γ-ray astronomy techniques. These energetic nuclei represent a sample of matter that has survived a complex series of physical processes which are comparatively common in the universe but that are not very well understood nor well defined at present. A general picture of the history of a cosmic ray particle which has struck the Earth begins with its production in some unknown way. There are reasons for believing that cosmic rays are produced and accelerated in the expanding envelopes of exploding supernovae, or in the fields of pulsars. Considerable changes of the production composition may occur during acceleration in the source. For example, injection energies may depend on the relative ionization potential of the various nuclides;

nucleon reactions may occur during acceleration; escape of particles from an acceleration region, if that region is bounded, may depend on the mass and charge of the individual nucleus. It is thus possible that the composition of the accelerated sample is different from that present in the source region. These esoteric possibilities will be neglected in this thesis since there is no real understanding of them and they are speculation at best. It will be assumed then that the abundances of the various types of particles reveal something of the nature of processes and the characteristics of the region where they are occurring.

The next phase experienced by the nuclei is a combination of physical processes which can be included under the heading of propagation through the interstellar medium. The propagation of a cosmic ray nucleus through the Galaxy subjects the charged particle to the effects of the magnetic fields traversed. The magnetic fields randomize the arrival direction of cosmic rays, which explains why cosmic rays are observed to arrive at the Earth isotropically. The particles also suffer chance encounters with matter in space (mostly hydrogen atoms) which produce the effects of energy loss due to ionization and collision. Some of the heavy nuclei will undergo catastrophic collisions or nuclear interactions with interstellar matter causing them to break up into nuclei of smaller charge, thus changing their identity, and hence altering the source composition. The magnitude of all these effects depends on the nature and amount of matter traversed, which in turn depends on the configuration and strength of the magnetic fields experienced by the nuclei during their traversal of the medium.

Finally, as the cosmic ray particle comes within some 10 to 100 A.U. of the sun it encounters the solar wind, a plasma streaming out of the sun with its frozen-in magnetic field which tends to sweep out lower energy

particles. The interaction of the nuclei with the solar environment leads to a solar modulation of the intensity of the nuclei, decreasing the intensity detected near Earth compared to that outside the solar system and possibly reducing their energy. The magnitude of solar modulation is dependent on the charge-to-mass ratio, the energy of the nuclei, and the level of solar activity. Even at times of low solar activity, there is considerable uncertainty regarding the amount and form of the residual modulation. After running upstream against this solar wind, the particle enters the nearly dipole magnetic field of the earth which acts to deflect the charged particle. If it has enough energy to penetrate the magnetic field, it enters the earth's atmosphere and eventually interacts with one or several air molecules, ending its journey. But if the primary cosmic ray nucleus should survive this rigorous journey and be detected, since it is the only direct sample of matter originating outside the solar system that can be observed, it will bring with it many "clues" about the galaxy which, when combined with a knowledge of the galaxy's physical structure, such as the spiral arms and halo, and physical processes, such as pulsars and supernovae, and then properly interpreted, will reveal its own history as well as increase knowledge of the galaxy itself.

The experimental observables, i.e. the "clues" available for measurement, in cosmic radiation are the charge composition, the energy spectra of the nuclear components, anisotropy in arrival direction, and temporal variations. Because of the complexity of the processes undergone by cosmic rays between their origin and their observation, it is attractive and probably essential to observe all of these interrelated quantities under comparable conditions at one time. At present all experimental

observables have not been measured in one experiment, hence data collected thus far has just established its own consistency.

The balloon-borne experiment to be described in this paper has been designed to observe the energy spectra and charge composition of elements of approximately the lower one quarter of the periodic table. (The event collection time needed to delineate the features of anisotropy and temporal variations await the application of similar experiments to long duration satellite flights). The piecemeal studies of primary cosmic radiation that have been conducted to date have advanced knowledge of the galaxy, and its radiation, however, by increasing knowledge of the origin and propagation of cosmic rays. The predictions of any theory of primary cosmic radiation must match the "corrected" values of the experimental observables, i.e. the values obtained after the observed values have been adjusted for detector dependences, solar modulation, and propagational effects. Since the predictions are based on a model of the galaxy, matching the predictions pins down the model applicable to the Galaxy. Features of low energy spectral and charge composition studies have been determined by various experiments mentioned in the next paragraph. However, as indicated in later paragraphs, features determined from high energy spectral and charge composition studies have given more fruitful results when applied to galactic models.

Knowledge of the low and medium energy range ($\sim 10^7$ to 10^9 eV/nucleon) is quite extensive, and detailed observations and theoretical studies of the charge composition and the energy spectra have been made in this energy interval. (Fan et al., 1968; Price et al., 1967, 1968, 1970). It has been considered that these cosmic ray nuclei of the lowest observable energies provide the best clues concerning their sources and their propa-

gation to Earth. But the experimental results of studies of low energy particles has demonstrated that theoretical conclusions about their relative energy spectra are not borne out. (Comstock et al., 1966, 1969; Freier and Waddington, 1968a, 1968b; Fichtel and Reames, 1968). There are a number of reasons for this failure of agreement, but only two of the more important ones will be briefly presented here. Firstly, a solar demodulation correction, based on the solar activity at the time of measurement, must be applied to the data to obtain fluxes outside the solar system. This correction is large in the low energy region. Secondly, present models of particle propagation through the galaxy may break down at low energies if the diffusion coefficients are β-dependent, which would result in β-dependent path lengths. The best worked out theories about the relative charge abundances apply to the energy range 10^9 to 10^{12} eV/nuc. This is so for three reasons: (1) solar modulation is small and can be reasonably well accounted for, (Webber, 1967a) (2) fragmentation parameters are generally constant in this range and thus more likely to be known, (Cleghorn, 1967), (3) at these energies fragmentation and ionization loss have small effect on the shape of the energy spectrum, (Beck and Yiou, 1968).

The high energy regions, i.e. $\geq 10^9$ eV/nuc., should offer more promise for the solution of the major problems confronting cosmic ray physicists. Above 1.0 GeV/nuc., however, data on chemical composition and energy spectra are very sparse. Known features of the primary cosmic radiation in this energy range include the following: (1) the spectrum of each cosmic ray element is described by a power law in total energy/nucleon, the index of the integral spectrum varying from -1.1 to -2.0, depending on the element. (2) the presence of lithium-beryllium-boron in large rela-

tive abundances, (3) the high abundance of heavy nuclei ($Z \geq 10$) relative to hydrogen and helium, and (4) the intensity variation between even- and odd- numbered nuclei.

The two most abundant components of the cosmic radiation, proton and helium nuclei, have been studied extensively, and their energy spectra are well known over a wide range of energies. (See Anand et al., 1968; Fan et al., 1968; and Ormes, 1967). The most reliable and statistically significant measurements in the charge range $2 \leq Z \leq 10$ have been made by von Rosenvinge et al. (1969 a, b), Freier and Waddington (1968a), Webber and Ormes (1967), Ormes et al. (1970), and Ryan et al. (1972)

The observed numbers of cosmic ray nuclei in the light heavy ($10 \leq Z \leq 14$), medium heavy ($15 \leq Z \leq 19$), and very heavy ($Z \geq 20$) region have been insufficient to permit an element-by-element study of their energy spectra. This situation was partly remedied by studies of the VH spectrum (see Webber and Ormes, 1967; von Rosenvinge, 1969; Freier and Waddington, 1968a; Mewaldt et al., 1971), where considerable attention was directed toward determining the detailed energy spectra of heavy nuclei in primary cosmic radiation. But there is still a paucity of measurements of the intensity of individual heavy nuclei above 1.0 GeV/nuc.

Recent measurements (Juliusson et al., 1972; Ormes and Balasubrahmanyan 1973; Smith et al., 1973; and Webber et al., 1973) of cosmic ray energy spectra of small groups of elements $Z \geq 6$ with energies up to 100 GeV/nuc. have revealed startling new features which have not been included in prior theories of the origin of cosmic rays and their propagation in interstellar space. These results have indicated that: (1) the relative nuclear composition of cosmic rays changes with energy in such a manner that the ratio of galactic secondary nuclei to galactic primary nuclei decreases as

energy increases. (Juliusson et al., 1972; Ormes and Balasubrahmanyan, 1973; Smith et al., 1973; and Webber et al., 1973a, and (2) the differential energy spectra of individual nuclei are well represented by smooth power laws in total energy/nuc. with spectral indices ranging from -2.5 to -3.0, i.e. no significant structure, breaks, or steepening of the spectra have been observed at energies beyond the region of influence of solar modulation (Ryan et al., 1972 and Juliusson, 1973).

Several recent charge composition studies, which in general are integral energy measurements of individual heavy elements ($Z \geq 10$), have succeeded in achieving nearly unique charge resolution out to iron. (Mewaldt et al., 1971; Juliusson et al., 1972; Smith et al., 1973; and Webber et al., 1973a). The results of these experiments indicate a charge composition for primary cosmic radiation that is different from that observed in the solar system.

Considerable interest is attached to the energy spectra and charge composition of nuclei ($Z \geq 6$) because these studies of energetic heavy galactic cosmic radiation provide unique information on the source regions of cosmic radiation, on propagation and possibly acceleration of cosmic radiation, on interactions of cosmic ray particles in the tenuous interstellar gas, on the amount of material traversed before escaping the Galaxy, and on the age of cosmic rays. The interpretations of the experimental results of these studies are illustrated in the next few sentences. The results cited previously of energy spectra studies are interrelated, and are relevant to the origin and propagation of cosmic rays in that they can be utilized to decide whether cosmic radiation has a local origin or, to go to the other extreme, is extragalactic in origin, and whether confinement in the galaxy is energy dependent. For example, attempts to

explain the decreasing ratio with energy of secondary nuclei to primary nuclei lead to the conclusion that high energy cosmic rays must have traversed less matter than low energy cosmic rays. Since theoretical as well as experimental results indicate that spallation cross sections for daughter nuclei do not depend strongly on energy above 1 GeV/nuc., the observed decrease in the ratio must mean less matter is traversed at high energy as opposed to low energy rather than being due to the propagational effects of collision. Further implications could be (1) very energetic nuclei are produced predominantly by sources which are close to the solar system; or (2) primary cosmic ray nuclei are extragalactic in origin but secondaries are produced in the galaxy and have energy dependent confinement; or (3) cosmic radiation is of galactic origin and confinement in the galaxy is energy dependent. The results of charge composition studies have provided more constraints on the origin and propagation of cosmic radiation in that they can be utilized to decide amongst various possible sources of cosmic rays as well as place restrictions on cosmic ray propagation models. For example, the nuclei in the charge range $10 \leq Z \leq 30$, which includes the very significant iron region, are those in the primary cosmic radiation, with the exception of the very rare $Z \geq 30$, that have the shortest interaction mean free paths and greatest rates of energy loss through ionization in traversing matter. As a consequence of the large interaction cross sections, i.e. short interaction mean free paths, the relative abundances of these heavy cosmic ray nuclei are very sensitive to the amount of interstellar matter that they have traversed between their origins and the point of detection. The amount of matter traversed then is related to cosmic ray age. Furthermore the nature of the charge composition that is deduced to exist in the source region must

be directly related to the nature of the source itself and the elemental building processes that occur therein. This deduced cosmic ray source composition is different from the solar system composition. Attempts to explain these results lead to the conclusior that galactic cosmic ray elements must have had a different origin than solar system elements. Cosmic rays may have been produced and accelerated in supernova explosions (Colgate and Johnson, 1960), or are produced in the region around pulsars and accelerated to high energies by their large magnetic fields (Gold, 1969; Kulsrud et al., 1972), or are produced and accelerated during the collapse of a small mass star to a white dwarf (Cowsik, 1971).

The most plausible suggestion for the origin of cosmic rays is that supernovae represent the dominant source of cosmic rays since: (1) an enormous amount of energy is released (2) the shock wave imparts large velocities to the mass in the envelope, and (3) there is a high concentration of heavier elements ($Z \geq 6$) compared to hydrogen and helium which, during the explosion, are processed to even heavier elements. If this suggestion is correct one would expect the cosmic ray composition to reflect advanced stages of nucleosynthesis rather than abundances obtained under static conditions as would be obtained in the sun since the explosion will alter pre-supernova abundances. By comparing the cosmic ray composition measured by experiment with that predicted by models of nucleosynthesis and stellar evolution, after propagational effects on the composition have been removed, one hopes to confirm or deny the significance of specific nucleosynthesis models at the cosmic ray source, and hence identify the astrophysical site of cosmic ray origin.

Charge composition studies have always suffered to some degree from 1) lack of charge resolution and 2) counting statistics. As a result of these

very basic limitations, the finer details of chemical composition, so important for theories regarding the origin and propagation of cosmic radiation, are poorly known, particularly the abundances in the $10 \leq Z \leq 28$ charge range. However, with improved charge resolution and increased counting statistics due to large geometry factor detectors, one should be able to distinguish charges out to $Z \simeq 30$ uniquely.

This thesis will report on one aspect of a study undertaken to obtain the charge composition of primary cosmic radiation from Z = 10 to Z = 28 for energies above 1.16 GeV/nucleon. The charge resolution of the detector and the total exposure factor represent a useful advance to overcoming limitations (1) and (2) mentioned previously. In what follows will be described a charge identification module (CIM) with a large geometry factor consisting of two plastic scintillators, one inorganic scintillator (CsI), and one Lucite plastic Cerenkov radiator. The charge identification module was launched on a balloon flight on 14 November 1970 from Holloman Air Force Base, Alamogordo, New Mexico (32° 51.7' N, 106° 7.3' W), as the top module of the High Energy Cosmic Ray Experiment (HECRE) (See Figure 1) sponsored by the Laboratory for High Energy Astrophysics, Goddard Space Flight Center, Greenbelt, Maryland. The vertical geomagnetic cutoff at Holloman AFB is 5.0 GV. (This corresponds to $\beta \geq 0.93$ for all particles, or 1.5 GeV/nuc). The flight, using a 27×10^6 ft^3 balloon, carried the experiment to an altitude of 7.4 g/cm^2 residual atmosphere (110,000 ft.) where it floated for 16 hours. All systems worked as planned. The balloon also drifted across the United States to the East Coast, a change from 4.9 GV cutoff to about 3.25 cutoff at altitude.

This thesis concerns itself with a description of that instrument, the data received during that flight, its analysis and interpretation, and the

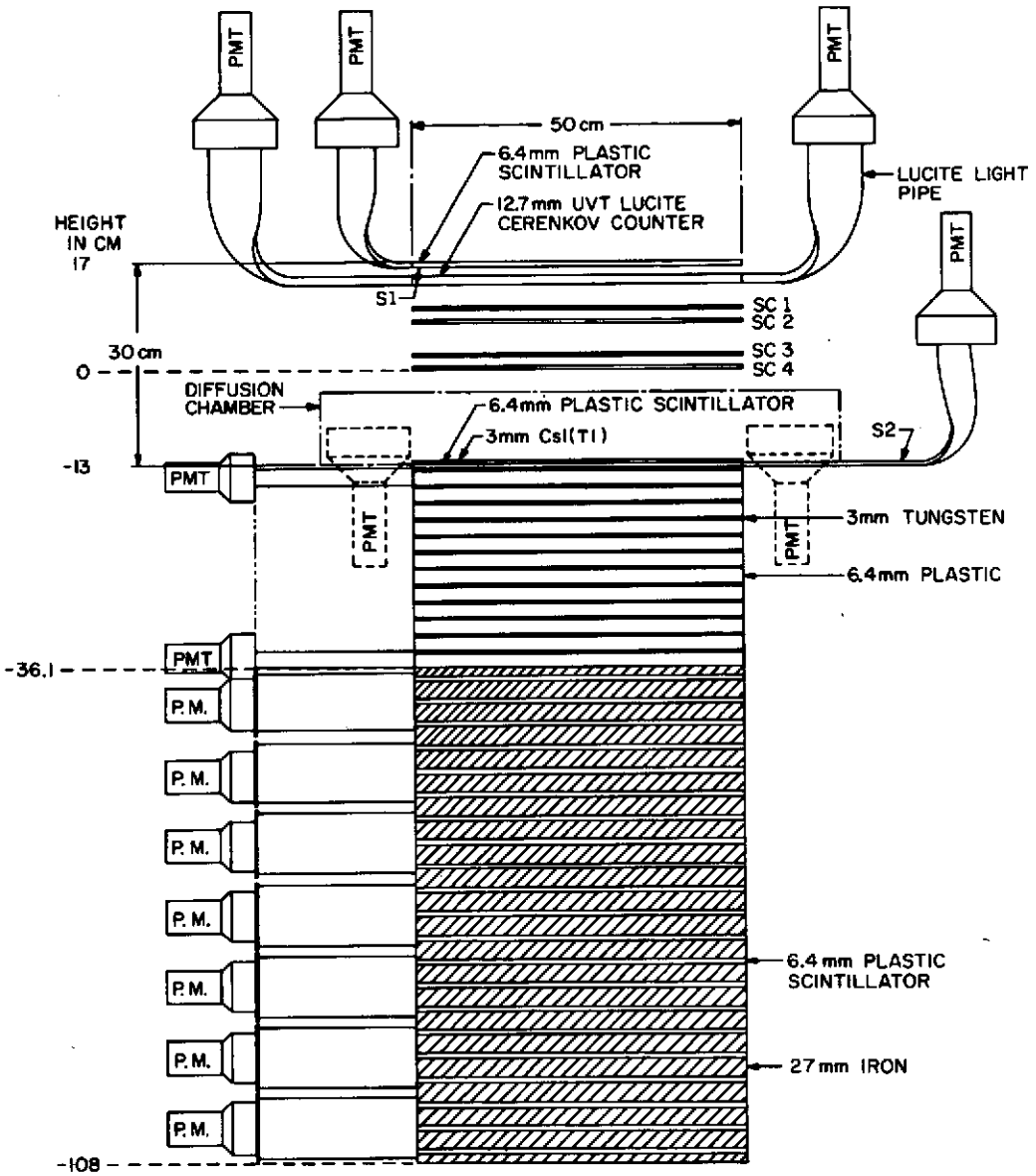

IONIZATION SPECTROMETER

Fig. 1. Schematic diagram of the High Energy Cosmic Ray Experiment, an ionization spectrometer.

implications to be drawn therefrom.

II. DESCRIPTION OF EXPERIMENT

II.A. Charge identification module

II.A. 1. Discussion

The entire High Energy Cosmic Ray Experiment (HECRE) consists of a charge identification module, a trajectory-defining system (a spark chamber with 4 sets of grids), and a varying number of tungsten and iron modules used for energy determination. Thus the basic experimental observables of primary cosmic radiation may be measured at one time in one large detector. This dissertation concerns itself with the interpretation of the data of the charge identification module (CIM); therefore, the next few sections will be devoted to describing in detail this module. Since the data analysis depends quite heavily on information gathered by the spark chamber module, it will be described briefly in a separate section. A schematic of the charge identification module, consisting of two plastic scintillators, a CsI (Tℓ) scintillator and a Lucite Cerenkov radiator, inclusive with the spark chamber grids is shown in Figure 2.

The CIM was designed to meet the following requirements:

(1) Determine the charge of the incident nucleus to $\pm$ 0.5 charge units up to Z = 30

(2) Have a large geometry factor to increase statistics for heavier nuclei

(3) Determine the trajectory to improve resolution and give path lengths through the overlying atmosphere.

The two plastic scintillators define the acceptance geometry of 2784 cm^2-ster of the system while the cesium iodide and Cerenkov counters are

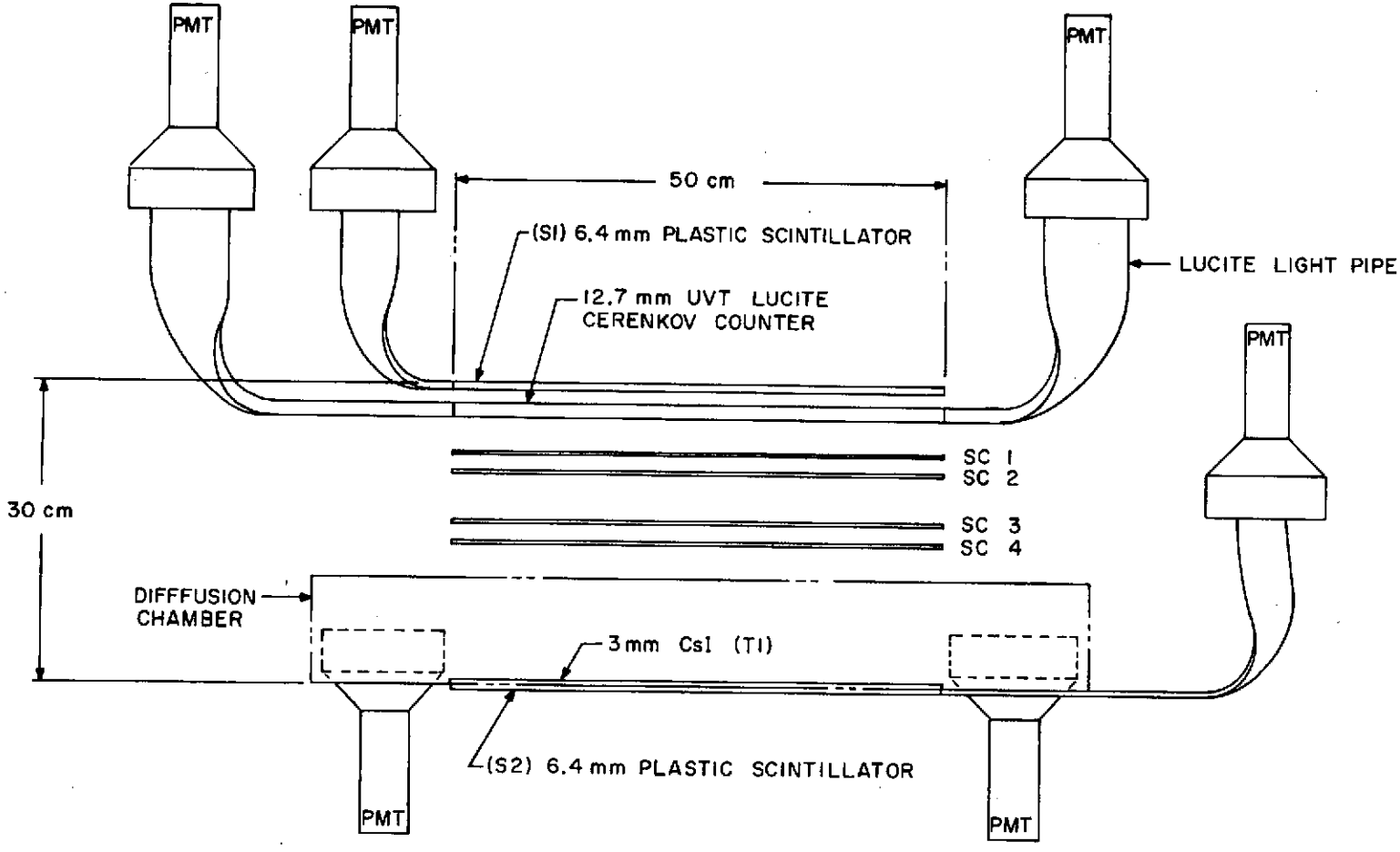

Fig. 2. Schematic diagram of Charge Identification Module (CIM), the top module of the High Energy Cosmic Ray ionization spectrometer experiment.

the principle charge-determining elements. This geometry factor, at the time it was first flown, was two orders of magnitude larger than counter telescopes commonly flown on balloons and about one order of magnitude larger than that flown by von Rosenvinge (1969). Comparably-sized geometry factors have since been attained by Juliusson et al. (1972) and Smith et al. (1973).

The pulse height data from the plastic scintillators is also used to provide a consistency check on the charge determination. These counters all have dynamic ranges of 10^4 to cover the charge range from protons to superheavy nuclei, a factor of 100 in charge or 10^4 in ionization loss. The amount of matter in the detector geometry is approximately 5 g/cm^2; hence the interaction probability is not excessive and the effects of nuclear interactions can be corrected with adequate precision. (See Section III.G). The CIM weighed about 75 kg and was enclosed in a gondola pressurized to 1 atmosphere with air. For a more detailed description of the detector and its operation, consult the references by Ormes et al. (1968, 1970).

II.A. 2. Coincidence Scintillators

Two plastic scintillators about 30cm apart in coincidence with one another define the acceptance geometry of 2784 cm^2-ster of the HECRE. Each scintillator detector consists of a square piece, 50 cm x 50 cm x 0.6 cm, of Pilot B scintillator viewed edge on through each of two opposite sides by an RCA 4524-3" photomultiplier tube which was bonded to the end of an adiabatic light guide. Note that the maximum opening angle of the telescope is given by

$$\theta_{max} = \tan^{-1} (\sqrt{2} \times \frac{50}{30}) = 67° \qquad (1)$$

where 50 cm is the lateral dimension of the scintillators and 30 cm is their separation. This means that pulses from a given charged particle can vary by a factor of 2 ($1/\cos \theta_{max} \simeq 2$) which must be taken into account in setting thresholds for given particle types and in data analysis. (See Appendix A. 2. and Section III.B.). Extensive laboratory tests were conducted on similar pieces before the scintillator final configuration was decided upon. These tests, using sea level muons as a standard measure of detection, showed that the maximum amplitude response and sharpest resolution resulted when the edges of the detector were painted with NE 560 (TiO_2) highly diffusively-reflective white paint and the entire scintillator wrapped in aluminum foil. Several other configurations were tried which did not achieve the optimum response and resolution: (1) wrapping the scintillator completely in diffusively reflective white paper, which gave both poor response and poor resolution; (2) wrapping the scintillator completely in aluminum foil, which gave the sharpest resolution but poor response; and (3) painting the scintillator completely with

diffusively - reflective white paint, which gave the maximum amplitude response but poor resolution.

Uniformity of response to within ± 13% for various positions of traversal through the large detector area were found to be the case in general. (See Figure 6 and Section III.C). However, each detector is unique in production so that individual corrections for corners, weak scintillation spots, etc. were necessary. A description of how this was accomplished is given in Section III.C.

A pulse from a coincidence event in the plastic scintillators was used to trigger the spark chamber. The efficiency of the spark chamber for registering a particle trajectory decreases as the delay between passage of the particle and the application of high voltage on the spark chamber electrodes exceeds 500 nsec. Plastic scintillators provide the necessary fast triggering pulse.

Energy loss through ionization is known to be proportional to Z^2.

$$-\frac{dE}{dx} = \frac{2 C m_e c^2 Z^2}{\beta^2} \left[\ln \frac{2 m_e c^2 \beta^2 E_m'}{(1-\beta^2) I^2(Z)} - 2\beta^2 - \delta \right] \qquad (2)$$

where $C = 0.150 \frac{Z_D}{A_D}$ gm^{-1} cm^2 and $I(Z) = 13.5 Z_D$ (B. Rossi, 1952). However, the light produced by plastic scintillators does not demonstrate this proportionality for all Z, as explained in the next paragraph.

The necessity of obtaining a fast triggering pulse for the spark chamber dictated the choice of plastic scintillators, which are ideal for this application. But plastic scintillators exhibit a non-linearity of response of light output with respect to energy loss such that relativistic nuclei tend to give outputs proportional to Z^α ($\alpha<2$) instead of the theoretically

expected Z^2. The non-linearity curves for the scintillators used in the HECRE are shown in Figure 7. The value of the exponent of Z has been found to be $\alpha = 1.64$, making resolution of charges in the range 10-30 more difficult. For iron nuclei this results in a reduction of the signal by a factor of 3 below the expected value. By way of comparison, Webber et al. (1973b) find a value for α of 1.72 for Pilot Y scintillator. (It is generally known that the light attenuating properties of Pilot Y are better than Pilot B. These results would indicate that the nonlinearity of Pilot Y is better than Pilot B).

Final resolution of the top scintillator, S1, was determined to be about 17% at charge 10. Although it was not possible to accurately determine the resolution at charge 26 due to limited statistics, indications were that the resolution was improving as charge increased. For example, the resolution determined at charge 14, the highest charge with reasonable statistics, was about 3% improved. An analysis done in section III. F. indicates that the resolution improved to 8% at charge 26 in this detector. The implications of this analysis are also given in section III. F. Similarly, the final resolution of the bottom scintillator, S2, was determined to be about 19% at charge 10 with the analysis indicating it decreased to 10% at charge 26.

The plastic scintillators were each pulse height analyzed to supplement the more linear information from the CsI scintillator. The pulse height data from the plastic scintillators provided consistency checks for the other detectors as explained in detail in Section III. F.

II.A. 3. Cerenkov Radiator

This detector consists of a square piece, 50 cm x 50 cm x 1 cm of ultraviolet transmitting (UVT) Lucite viewed by four RCA 4525-5" photomultiplier tubes, one on each side, which had been bonded to the end of a UVT adiabatic light guide. Using sea level muons for the standard measure of pulse height, the Lucite also showed that the maximum amplitude response and sharpest resolution resulted when the edges of the detector were painted white and the entire detector wrapped in aluminum foil. Thus the Cerenkov light is transported by the highly efficient process of total internal reflection. Four tubes were used on this detector due to the expected low light level of Cerenkov radiation. Only about 200 useful photons are produced by a singly charged particle.** Again uniformity of response over the entire area was found to be within $\pm 13\%$. Corrections for Cerenkov detector large area variations were also accomplished as outlined in Section III. C.

The light output of Cerenkov radiator, in contrast to that of commonly used scintillators, does not saturate for large values of Z, and instead is strictly proportional to Z^2 over the entire range of elements. The following formula is used to compute the energy loss of a charged particle due to Cerenkov radiation given off by that particle upon traversing a material in which the velocity of light in the material is less than the velocity of the particle:

$$-\frac{dE}{dx} = kZ^2\left[1 - \frac{1}{\beta^2 n^2}\right] \qquad (3)$$

**These tubes were also specially selected by RCA to have a very low dark current, ≤20 nanoamp at 2000 V with a gain of 10^6, to better separate signal from noise.

where $\frac{dE}{dx}$ = energy loss per g/cm^2 of material, $\beta = \frac{v}{c}$ = velocity of the particle, and n = index of refraction = 1.5 for the Lucite used in this experiment. The validity of this expression over the entire charge range is of decisive importance in the design because a particle of charge Z is equivalent to Z^2 independent singly charged particles which have the same velocity and follow the same trajectory.

Several practical advantages arise from the validity of this equivalence. The relative standard deviation of the pulse height distribution is proportional to 1/Z; therefore constant resolution can be maintained between neighboring elements, independent of Z. The combination of a Cerenkov radiator with scintillation counters thus provides unique charge identification up to $Z \approx 18$, and should provide a resolution of $\pm$ 1 charge up to approximately $Z \approx 30$.

The Cerenkov radiation formula indicates that this energy loss is proportional to Z^2 and to energy of the incoming particle, through the β^2 dependence. Until the response due to energy of the incoming particle reaches a plateau, the output can not be used by itself for charge composition studies since the output is proportional to both charge and energy. When the response due to energy becomes constant, as it does on the plateau, then the output response is proportional to the charge-squared. At the low end of the energy range under study here, this energy dependence property of Cerenkov radiation limits the resolution of individual charges since the pulse height distribution is spread out. Minimization of this property was accomplished by selecting events whose pulse height value was within 0.92 of the relativistic value, since the maximum energy loss per unit path length, i.e. the plateau, is reached when $\frac{1}{\beta^2 n^2}$ approaches its minimum value

which corresponds to $\beta \rightarrow 1$ for a given n, or relativistic particles.

Another property indicated by the formula is that below some energy threshold value, no Cerenkov radiation is emitted by the particle. The threshold energy is reached at $[1 - \frac{1}{\beta^2 n^2}] \rightarrow 0$ which corresponds to $\frac{1}{\beta n} \rightarrow 1$, or $\beta = 0.667$ for $n = 1.5$. This energy threshold property is an advantage to the experiment since the Cerenkov velocity threshold is used to reject low energy background particles. These may take the form of slow, heavily ionizing particles such as large angle alphas which might simulate a high Z event, or low energy secondary particles which travel upward through the charge module after being produced in interactions in the spectrometer. More importantly, the Cerenkov pulse height was used to reject non-relativistic high Z particles, as explained in more detail in section III. F.

A plastic Lucite Cerenkov radiator such as used in the CIM has an energy threshold for singly charged particles of 300 MeV and reaches a plateau in energy after several hundred MeV. Finally, it must be mentioned that the light output from Cerenkov radiators is very directional. Total internal reflection techniques are used with plastic radiators to collect this light, but some light will be lost when the angle of the Cerenkov light cone exceeds the critical angle for total internal reflection in the plastic. This also affects the resolution due to the variation in pulse height of any given charged particle.

Final resolution of the Cerenkov radiation detector was determined to be about 34%, uniformly to within a few percent, for all charges.

II.A. 4. Cesium Iodide Scintillator

The cesium iodide, thallium-activated scintillator was assembled as a mosaic of 9 small square crystals each 17 cm on a side in a large square array 50 cm x 50 cm x 0.3 mm, because these inorganic crystals cannot be "grown" to that size with any uniformity in production. Since this mosaic had no mechanical strength, the light pipe arrangement, as applied to the other scintillators, could not be used. Instead a diffusion chamber technique was employed to view the scintillation light. The crystal array was placed inside a light-tight box, the inside of which was completely painted with diffusively-reflecting white paint. Viewing of this diffusively-reflected scintillation light was accomplished by four RCA 4525-5" PM tubes, one in each corner of the box. Summing the four outputs then produced a nearly spatially uniform response.

CsI (Tℓ) scintillator response is proportional to Z^2 over a range of energy losses, since again ionization losses are proportional to Z^2. In fact, the response should be proportional to Z^2 out to at least Z = 30, and probably to Z = 40. This makes cesium iodide very desirable for Z = 10 to 30 studies. However, the rise time of the pulse from this material is approximately 1 μsec which necessitated taking special care in the pulse height analysis to insure no information was lost.

The cesium iodide detector had a final resolution of about 21% over the entire charge range.

II,B.. Spark Chamber Module

For precise charge determination, it is necessary to know the particle trajectory through the charge identification module. By utilizing the direction and position measurements to compensate the pulse heights for differences in response due to the large opening angle of the telescope and to variations in light collection efficiencies as a function of position, resolution comparable to that of much smaller detectors can be achieved. The 50 cm x 50 cm digitized wire grid spark chamber, used for the purpose of trajectory definition, consisted of four independent sets of X-Y grids of 200 wires spaced about 2.5 mm apart with about 4 mm between the X-grid and the Y-grid, (thus an X and Y measurement in each set providing 4 position measurements.) One grid of parallel wires is connected to a high voltage buss through ferrite cores, the orthogonal set being connected to a ground buss. The thin-walled pressure container for this module added only 0.315 gm cm^{-2} of matter in the particle path. Upon receiving a coincidence signal from the scintillators, high voltage is applied to the sets of grids. The ionization along the track of a charged particle causes a current to flow in a wire thereby setting its ferrite core. Later these ferrite cores are interrogated and the coordinate information passed on to the digital data handling system. A computer program was written to translate this information into trajectories which were used in the data analysis. This is described in sections III. B. and III. C.

Because the detector must be sensitive from electrons and protons up to iron nuclei, the spark chambers are required to operate over a very large dynamic range in dE/dx (almost 10^3). In addition they must operate in the presence of all the knock-on electrons produced by high Z, high energy, particles. The spark chambers are operated at the knee in the

efficiency voltage curve, about 2750 volts. This yields a track detection efficiency of approximately 98% for singly charged minimum-ionizing particles (sea level muons) with a spatial resolution of $\pm$ 0.2 cm and an angular resolution of $\pm$ 2° for a voltage of 2750V and a gas mixture of 89%-Ne, 9%-He, 1%-Ethanol. At this voltage between 1.5 and 2 wires were set per spark. During the flight this spark spreading was found to increase with Z up to about 3 at Z = 3. Unfortunately, at these large values of spreading an electronic inefficiency develops in the ability to read out the set cores and so it is not possible to measure the spreading at higher Z values. This inefficiency results in unset cores within bunches of set cores and confuses the exact location of the track. In addition, the knock-on electrons which produce satellite tracks, increase like the square of the charge. At 1.5 GeV/nuc. approximately 7% of the energy lost by a particle in crossing the spark chamber goes into electrons with sufficient range to cross all four grids.

The net result of these effects is that as Z increases, an inefficiency develops in the ability of the algorithms developed for computer analysis to determine the trajectory. This inefficiency, while greatly complicating the data analysis, can be determined in principle and so fluxes can be corrected. (Consult Appendix B).

Because of these difficulties with the spark chamber one must convince oneself that the detector is giving trajectories correct to within a few degrees. If satisfactory, then the trajectories can be used to make corrections of up to 200% to the pulse height values with confidence. In Figure 3 is plotted a histogram of carbon nuclei at various zenith angles. This can be seen to agree quite closely with the differential geometry as

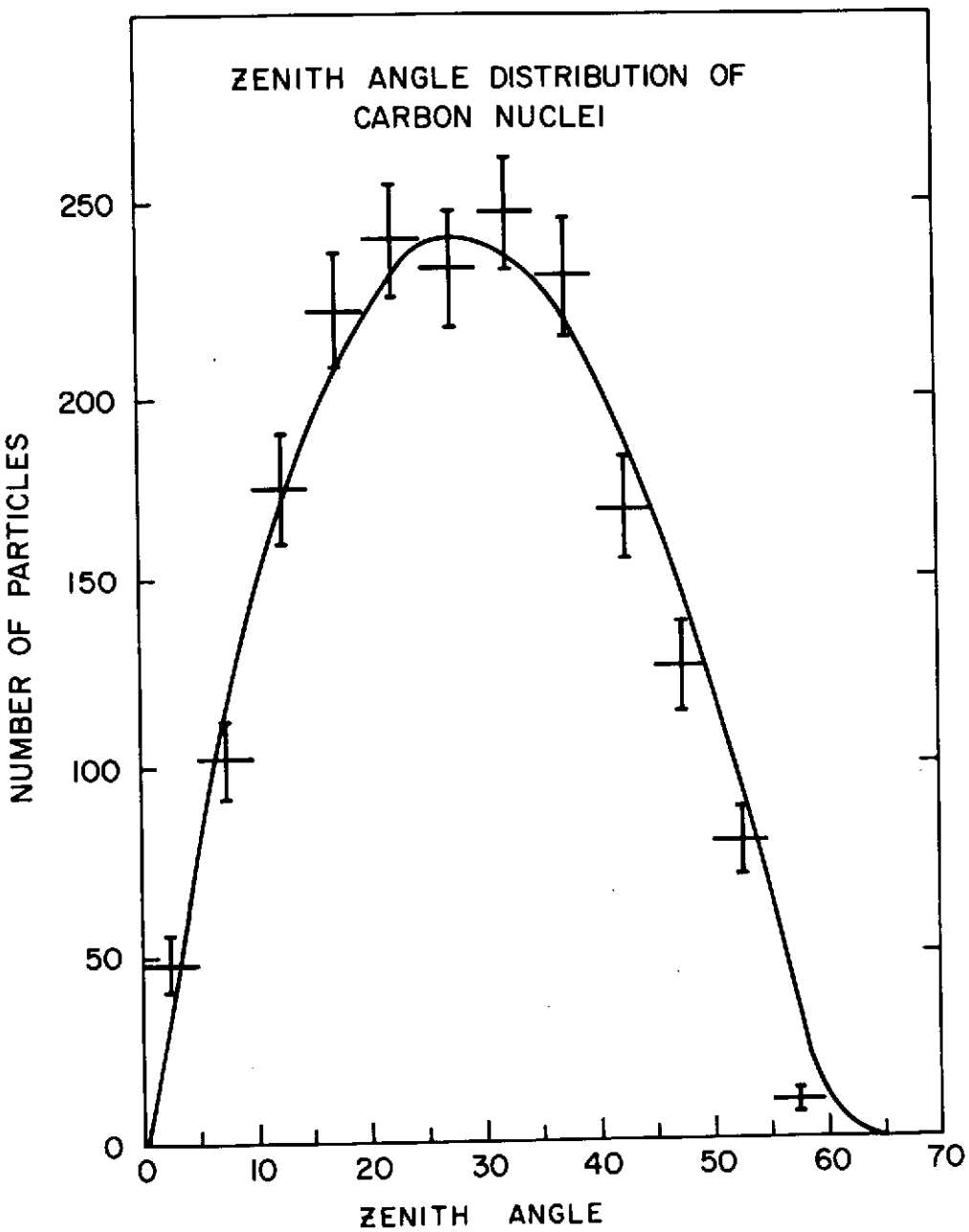

Fig. 3. Zenith angle distribution of detected carbon nuclei (histogram points) compared to the differential geometry of the Charge Identification Module (solid line) as a function of zenith angle.

a function of zenith angle, except possibly for a slight absence of particles at large zenith angles. This slight deficit can be understood in terms of the increased atmospheric absorption of carbon at larger angles. This good agreement indicates that the trajectories must be accurate to within a few degrees.

II.C. Ionization Spectrometer (IS)

For purposes of this experiment, the most straightforward technique for measuring the energy of primary cosmic rays at high energies is the ionization spectrometer ("ionization calorimeter") originally proposed by Grigorov et al. (1958), whereby the incident particle loses its energy through nuclear interactions in many nuclear mean free paths of condensed matter. The design of the ionization spectrometer that is described in the following paragraphs is based on the theory presented by those authors.

The IS consists of two sections: an electron cascade section consisting of twelve tungsten modules and a nucleonic cascade section consisting of seven iron modules. Each electron cascade module contains a sandwich structure of one sheet of tungsten 0.32 cm thick followed by a piece of 0.64 cm Pilot Y plastic scintillator which is viewed through air coupling by a pair of 3" photomultiplier tubes on opposite sides. Therefore each tungsten sheet is 6 g/cm^2 which is approximately 0.89 radiation lengths (r.l.) or 0.42 interaction mean free paths. Hence there are about 11 r.l. in the electron cascade section. Each nucleonic cascade module contains 3 layers of iron 1.25 cm thick interspersed with 3 layers of 0.64 cm thick plastic scintillator sheets, which are also viewed through air coupling by a pair of 3" photomultiplier tubes. Therefore each iron module is 66.4 g/cm^2 thick which is 0.5 nuclear interaction length or 4.8 r.l. Within each module the three scintillators are placed to provide a sampling of the cascade every 1/6 mfp. However, their total light output is viewed by only 2 PMTs, the outputs of which are added and pulse height analyzed. The active elements are thus located approximately every 1.6 r.l. of absorber material so as to thoroughly sample electromagnetic cascades, and every 1/6 nuclear interaction mfp. There are a total of 3.5 nuclear mfp

in the nucleonic cascade section.

Briefly the IS measures the energy of the incoming particle as follows. The nuclear interacting particles are incident on the appreciably large mass of condensed matter in the IS. Through a series of nuclear interactions the primary particle loses its energy to secondary particles which are mostly charged and neutral pions. The charged pions interact further contributing to the development of the nuclear cascade. The neutral pions decay rapidly into gammas whose energy is dissipated in electromagnetic cascades. About 60% of the initial kinetic energy is converted to ionization in this manner. By sampling this ionization at frequent intervals, it is possible to determine the total primary energy. The energy of an incoming primary electron is measured through the development of the cascade shower in the tungsten modules, where, due to the large number of radiation lengths for electrons, the cascade develops very rapidly. In this manner the double-sectioned IS is used to distinguish electrons from singly charged, nuclear-active particles (mainly protons). Figure 4 illustrates the example of the ionization energy loss sampling for an iron nucleus as identified by the CIM during the flight discussed here. For a discussion of how the instrument was calibrated for electrons, and protons and heavier charged particles, consult papers by Whiteside et al. (1973) on the proton calibration at the Brookhaven National Laboratory and Crannell et al. (1973), on the electron calibration at the Stanford Linear Accelerator Center. For purposes of this dissertation, where only integral fluxes above the magnetic rigidity cutoff are presented, the IS was used only to establish the energy threshold of about 0.5 GeV/nucleon. Differential and integral spectra over a wide energy range are presented in a series of papers (Ryan et al., 1972; Balasubrahmanyan and Ormes, 1973; Ormes et al., 1971

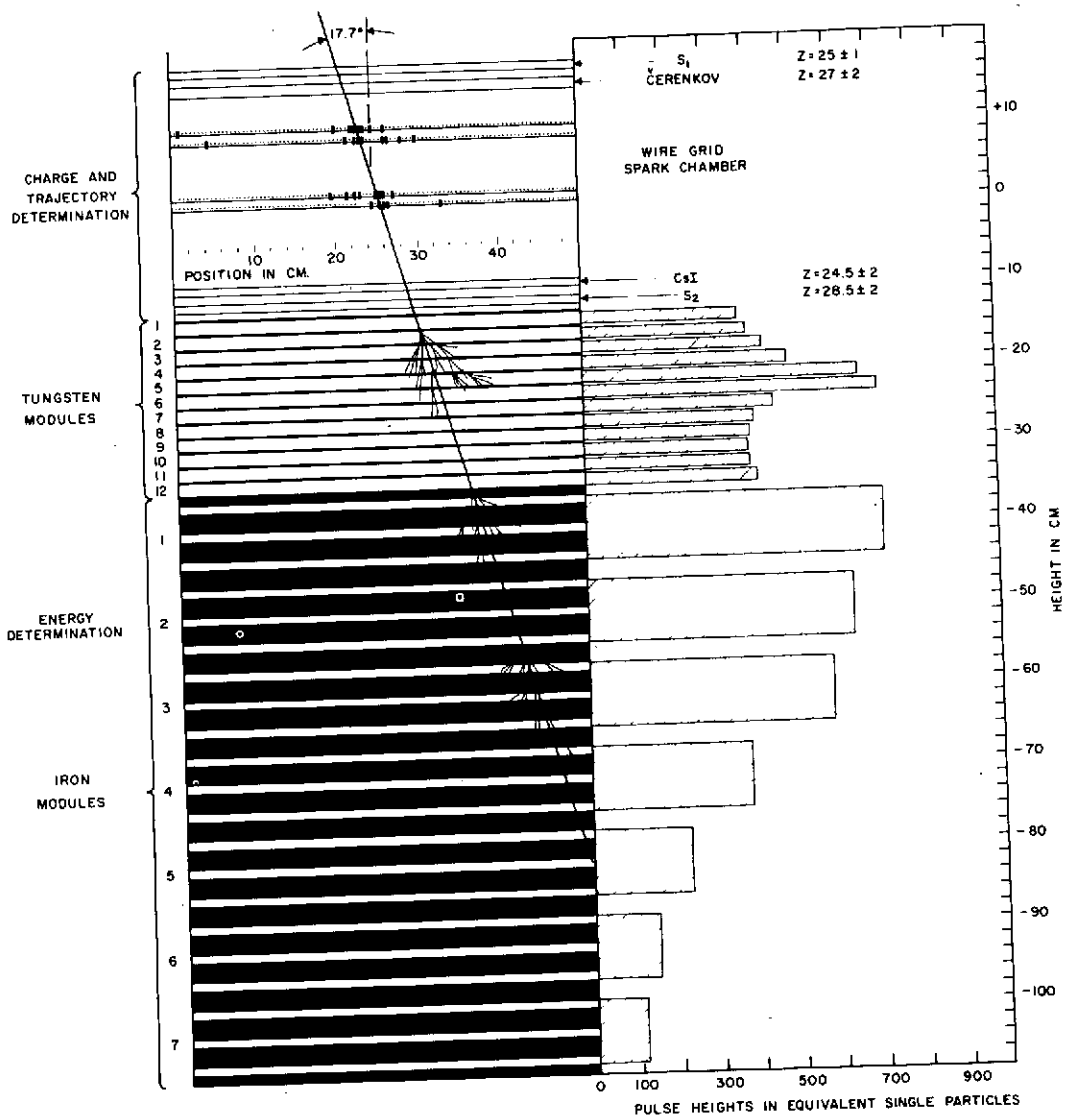

Fig. 4. Schematic diagram of a cascade shower of an iron nucleus through the ionization spectrometer.

and Silverberg et al., 1973).

III. DATA ANALYSIS

III.A. Discussion

The problems of obtaining a high degree of charge resolution while at the same time collecting a sufficient number of events for good statistics are connected. The latter requires large area times solid angle, which means large sensitive areas of counters and unavoidably introduces variations across the area of scintillation and light collection efficiency. Large solid angle means variations of emitting path length of the particle as a function of the angle of incidence, and hence also variations in light output for different directions. Both effects tend to reduce charge resolution. The two properties of charge resolution and a large geometrical factor seem by existing instrumentation to be in opposition. However by introduction of a device such as a spark chamber for determination of the particle path through the instrument this can be overcome.

A number of corrections must be made to the raw data from the balloon flight before it can be placed in usable form and conclusions drawn from it about propagation and source models, cosmic ray age, and amount of matter in interstellar space. The ultimate success of the data analysis depends on the ability of the corrections to separate adjacent charges (i.e., to improve the resolution) and to distinguish background events. The pulse height from an individual event may fluctuate from its true value due to intrinsic statistical fluctuations and detector design fluctuations. Landau fluctuations and photoelectron statistics fall in the category of intrinsic statistical fluctuations in pulse height. All geometrical effects which produce fluctuations in pulse height such as path length or zenith angle corrections, positional variations due to large size of the detector,

and nonlinearities of the electronics fall in the category of detector design fluctuations. The true pulse height for a particular event will be the convolution of all these factors.

Finally, corrections must be made to the entire set of data for solar modulation, misidentification of events, and interactions in the detector which constitute a background.

The next few sections will be devoted to discussing the intrinsic limitations on resolution, and the size of and corrections for various geometrical effects. The aim of the analysis is to determine the charge to within $\pm$ 1/2 a charge unit up to and including iron so that a resolution of $\pm$4% is required. It is possible that there is an inherent limit to the resolution. The difficulty of this task is illustrated by the corrections outlined in the following sections.

III.B. Angle Corrections

III.B. 1. Zenith Angle Compensation

Particle trajectories through the instrument are determined by using the 4 X-Y position measurements provided by the digitized wire grid spark chamber. Since all the detectors respond proportionally to path length through the detector (determined by the zenith angle), this effect represents the largest correction that must be made. As an example of the size of this correction, consider a carbon nucleus entering the CIM at such an angle that sec $\theta \geq 1.20$. This charged particle will have the pulse height of a nitrogen, and could possibly even resemble an oxygen if the angle is great enough. In the range of Z = 20 to 30, a charge 20 can look like a charge 28. By utilizing direction measurements to compensate the pulse heights for differences in response due to the large opening angle of the CIM telescope (about 60°), final resolution comparable to that of much smaller detectors can be achieved.

A simple sec θ correction has been applied to the data since this is to be expected theoretically. Carbon nuclei have been used to check this correction since they are the most plentiful and fall in the center of a range of electronic amplification where no non-linear effects are present. Pulse heights from the four detectors are selected to include only carbon nuclei. A two-dimensional histogram is then plotted with the uncorrected response of the detectors as one variable and zenith angle as the other coordinate. The variation of pulse height as a function of angle is shown in Figure 5 for the scintillators and Cerenkov detector. As can be seen from the figure, sec θ is a good representation, within 2%, for the two plastic scintillators, S1 and S2.

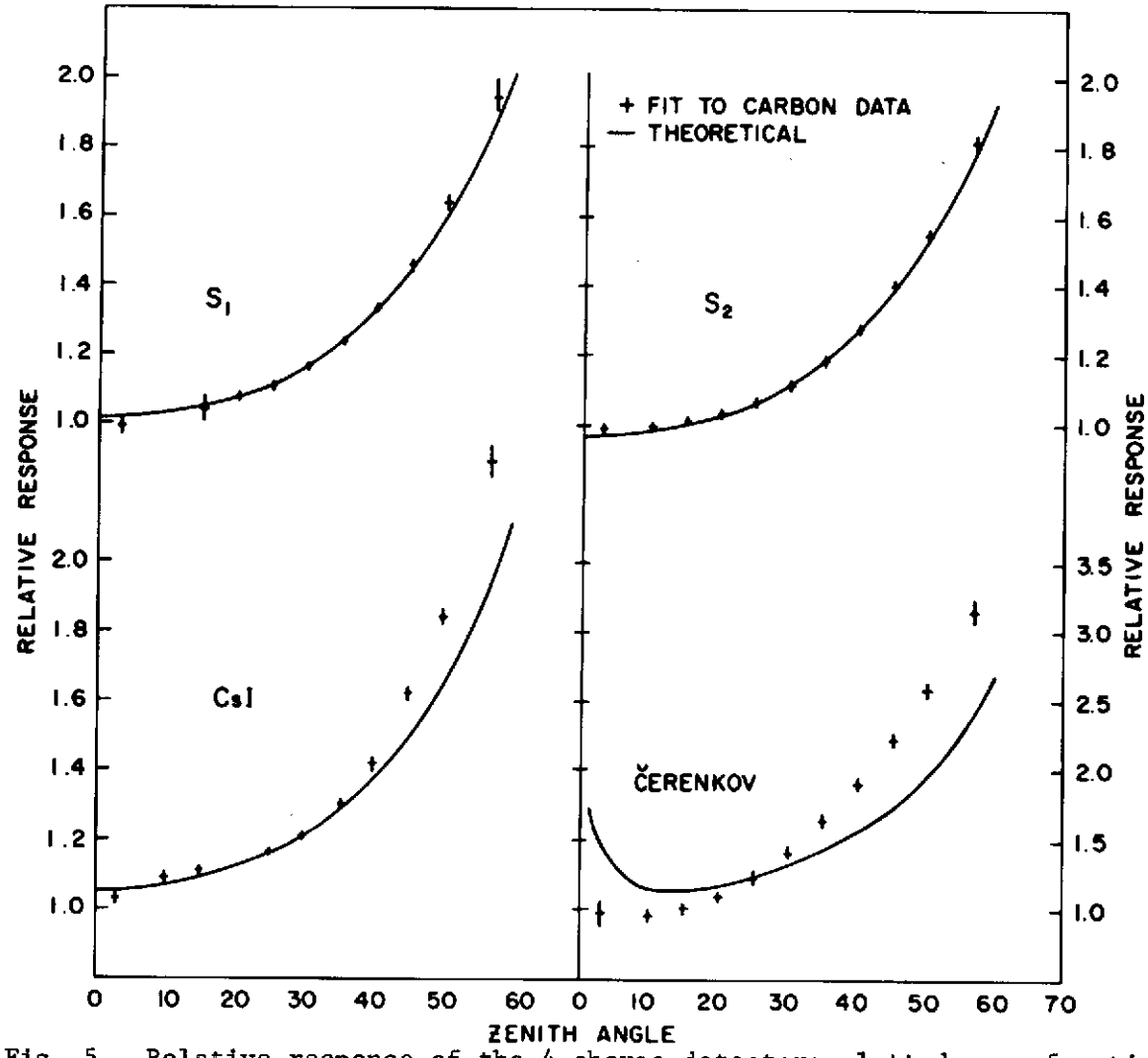

Fig. 5. Relative response of the 4 charge detectors plotted as a function of zenith angle. Solid line represents theoretical correction (sec θ), crosses represent experimental data (carbon nuclei). Note that the scale for the Cerenkov response curve on the right hand side is different from the other 3 detectors.

In the case of CsI the agreement is not good beyond 40°. This discrepancy can be understood in the following manner. The CsI scintillator was placed in a box painted white with photomultiplier tubes at the four corners. The tubes face the white surface opposite the CsI and cannot view the scintillation light directly. Light which comes from a spot near the tubes is collected more efficiently than light from the center. In fact when the detector response is examined as a function of area, the center square area is found to produce about 10% less signal than the average from the other areas. This affects the response as a function of zenith angle because extreme trajectories cannot pass through the center. The enhancement at large zenith angles is due to trajectories which come nearer to photomultiplier tubes and thus produce larger light pulses. The less extreme trajectories are distributed much more equally across the area of the detector. In any case, the variation is measured and can be compensated out.

Angular variations greater than expected have been found in the Cerenkov detector and are not completely understood. However some ideas can be put forth. Below about 15° large light losses at small angles are caused by attempting to collect the Cerenkov emission by total internal reflection methods. The Cerenkov cone lies between 45° and 48° to the particle direction. The angle for total internal reflection is 42° so all light from vertically incident particles is collected. Between 3° and 6° zenith angles, particles begin to lose some light. Losses increase rapidly with zenith angle up to about 10° to 15°. But at large angles the response is further enhanced by increased path length through the radiator. Again the compensations can be measured directly and applied to the data to obtain useful charge composition information.

III,B. 2. Azimuthal Angle Compensation

The Cerenkov radiator and CsI scintillator were both found to have azimuthal angle variations large enough to require a correction. This can probably be attributed to imbalance in gain of the photomultiplier tubes. Since four tubes were used on each of these detectors, a larger gain in any one tube will show up as a significantly larger pulse height in that tube for charged particles that pass through the detector near that tube.

The experimental variations were too large for any simple theoretical fit so an empirical curve was fitted to the data in the following manner. The scattered data from carbon nuclei were chosen again for the same reason given in section III.B. 1. A fitting routine on the computer using a 3rd order polynomial as the empirical relation, corrected the pulse heights to their average value. Variations were then reduced to about $\pm$ 2%.

III.C. Area Correction

Variations in light collection efficiencies as a function of position due to the large physical size of the detector can also be compensated for by using the spark chamber data. The light collection efficiency F (x,y) is in general a function of two variables:

$$F(x,y) = g(x)\ h(y)\ f(x,y), \tag{4}$$

a product of a separable part g(x), and h(y) and an inseparable part f(x,y).

The relative responses as functions of position are plotted in Figure 6 as percentage deviations from the mean for one of the plastic scintillators. The function h(y) varies systematically from -3% near the edges to +3% in the middle. The variation in x position is quite symmetrical reflecting good balance in the gain of the photomultiplier tubes. Thus, the function g(x) is constant within errors. Since the variations in F(x,y) are somewhat larger than those of g(x) and k(y), f(x,y) must be comparable to or greater than g and h in certain localized spots. The most extreme case is the lower right hand corner which seems to be 6 or 7% below average.

The area corrections have been made by again fitting a 3rd order polynomial to g(x) and h(y) and applying it to the data. These again are strictly empirical curves generated to correct the data. Variations in pulse height due to area position were then reduced to about 3-4%.

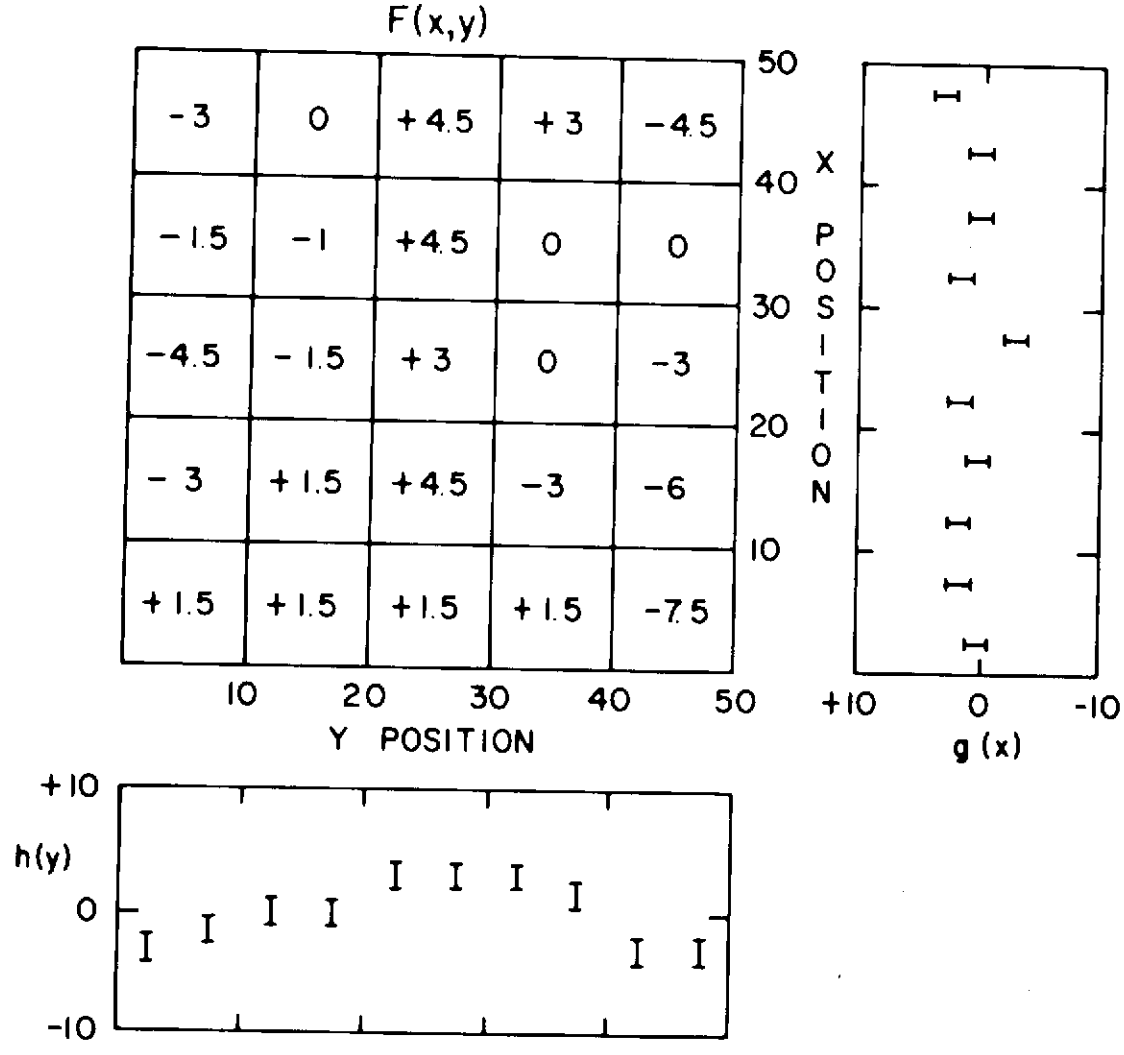

Fig. 6. Variations in pulse height as percentage deviations from the mean response as a function of position and linear dimension across the area of the scintillator, S1.

III,D. Nonlinearities of Plastics and PHAS

III.D. 1. Plastics

The nonlinearity of output response of plastic scintillators to highly charged particles is well documented in the literature (see Ormes, 1965; Badhwar et al., 1967; where nonlinearities with respect to carbon output of 20 - 30% have been reported). The response curves of the telescope elements used in this experiment have been obtained directly from the experimental data and are shown in Figure 7. The plastic scintillator S1 is seen to be fairly linear up to $Z \simeq 6$ after which it clearly falls below the linear response line. Plastic scintillator, S2, exhibits a similar response. Measurements of the slopes of S1 and S2 response curves indicate the output to be proportional to $(dE/dx)^{0.82}$. This power law correction was applied to the pulse heights to compensate for this nonlinearity.

Cesium iodide is essentially linear throughout the charge region, thus confirming it represents an independent linear charge measurement that can be used in conjunction with S1 and S2.

The poor resolution of the Cerenkov detector, about 35%, made it difficult to obtain a response curve. The resolution and response data were obtained using an iterative procedure as follows. Events were identified from the S1, S2, and CsI data using a 3-dimensional hyperellipsoid. (See section III.F.). From these results, the individual particle distributions in the Cerenkov detector were unfolded, and the resolution and response data obtained. This detector is also linear.

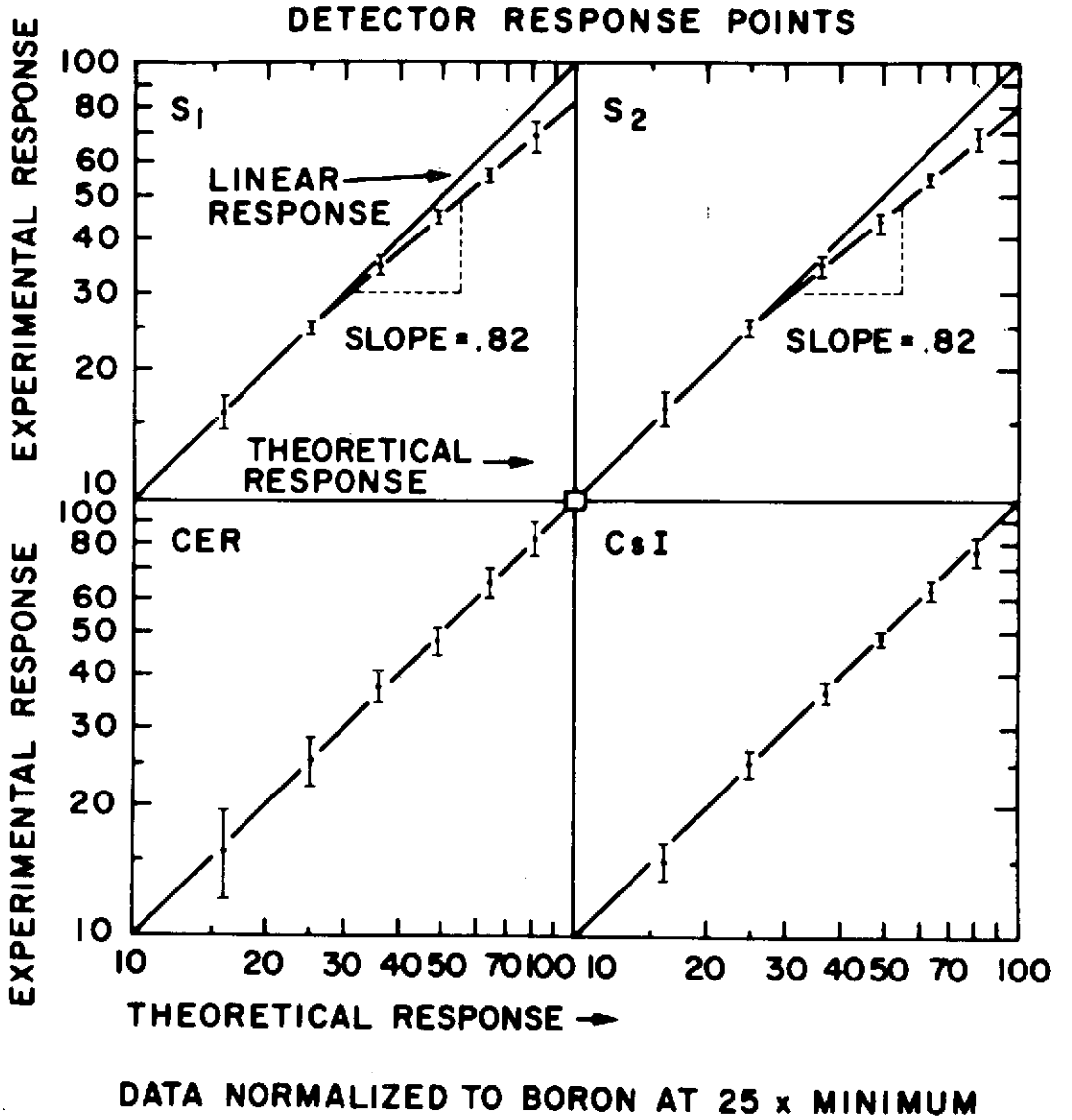

Fig. 7. Comparison of nonlinear output (points) of the 4 charge detector elements to theoretical linear response (solid line) expected for charges 4-9.

III.D. 2. PHAS

Laboratory testing of the electronics circuitry revealed some non-linearity of output response of the pulse height analyzers with respect to input for large values of input. This nonlinearity was measured simply by feeding the electronics a pulse generator output of the proper shape and amplitude to simulate a photomultiplier tube output in place of the actual tube output. A polynomial is fitted to the output response as a function of input, and this polynomial used in a subroutine of the data analysis computer program to compensate for the deviation from linearity.

III.E. Landau Fluctuations

Pulse height distributions for a given kind of particle of a given energy in a given detector element are not delta functions. This results not only from geometrical variations in light output and non-linearities of the detector system, but also results from the fact that energy loss in a scintillator is a statistical process. The theory surrounding these fluctuations in energy loss, called Landau fluctuations, is discussed in the several paragraphs that follow as well as the method used in overcoming the detrimental effect on charge resolution of these fluctuations.

The ionization energy lost in a thin detector element by cosmic ray nuclei of given charge, mass, and energy is not unique; instead a distribution of energy losses results because the energy loss is a statistical process consisting of many independent interactions between the cosmic ray nuclei and the bound electrons of the material in the detector element. The theoretical expression which describes the most probable energy loss, as taken from the work of Rossi (1952) following the work of Symon (1948), is presented here:

$$E_0 - E_p = \frac{2\pi m_e c^2 x Z^2}{\beta^2}\left[\ln\frac{4\pi m_e^2 c^4 x Z^2}{(1-\beta^2) I^2(Z)} - \beta^2 + j - \delta\right] \qquad (5)$$

This may be compared to the average energy loss formula given in chapter II (Eqn. (1)):

$$-\frac{dE}{dx} = \frac{2\pi m_e c^2 Z^2}{\beta^2}\left[\ln\frac{2 m_e c^2 \beta^2 E_m'}{(1-\beta^2) I^2(Z)} - 2\beta^2 - \delta\right] \qquad (6)$$

The difference between these 2 expressions occurs primarily in the log term, which causes the most probable energy loss to become less than the average loss as $\beta \rightarrow 1$. The distribution approaches its most asymmetrical form with a large skewness occuring toward high energy losses. This is due to the increased probability of interactions of the cosmic ray nuclei with the bound electrons producing large energy transfers to the bound electrons (the so-called knock-on electrons.) For a given charge, the effect worsens at higher energies ($\beta \rightarrow 1$) because the maximum energy transferred to knock-on's, $E'_m = 2 m_e c^2 (\beta^2/1-\beta^2)$, increases (hence the average energy loss increases), while the most probable energy loss in the scintillator remains approximately constant. When the most probable energy loss is quite a bit less than the average energy loss, the distribution is highly skewed.

An example of a distribution of energy losses by a singly charged particle in a scintillator element, called a Landau distribution, is shown in Figure 8. The distribution in pulse height, which is not symmetric with respect to its maximum, decreases the charge resolution. For example, a large statistical fluctuation in energy loss in one detector can cause a carbon nucleus to appear to be an oxygen nucleus in that detector. The ability to resolve different charges depends on minimizing the effects on charge identification of the skewness and the width of the Landau distribution.

The Landau distribution depends on the parameters λ, which determines the shape of the distribution, Δ, which determines the width of the distribution, and the most probable energy loss $E_o - E_p$, which determines the location of the peak of the distribution. The quantities λ and Δ and a term j

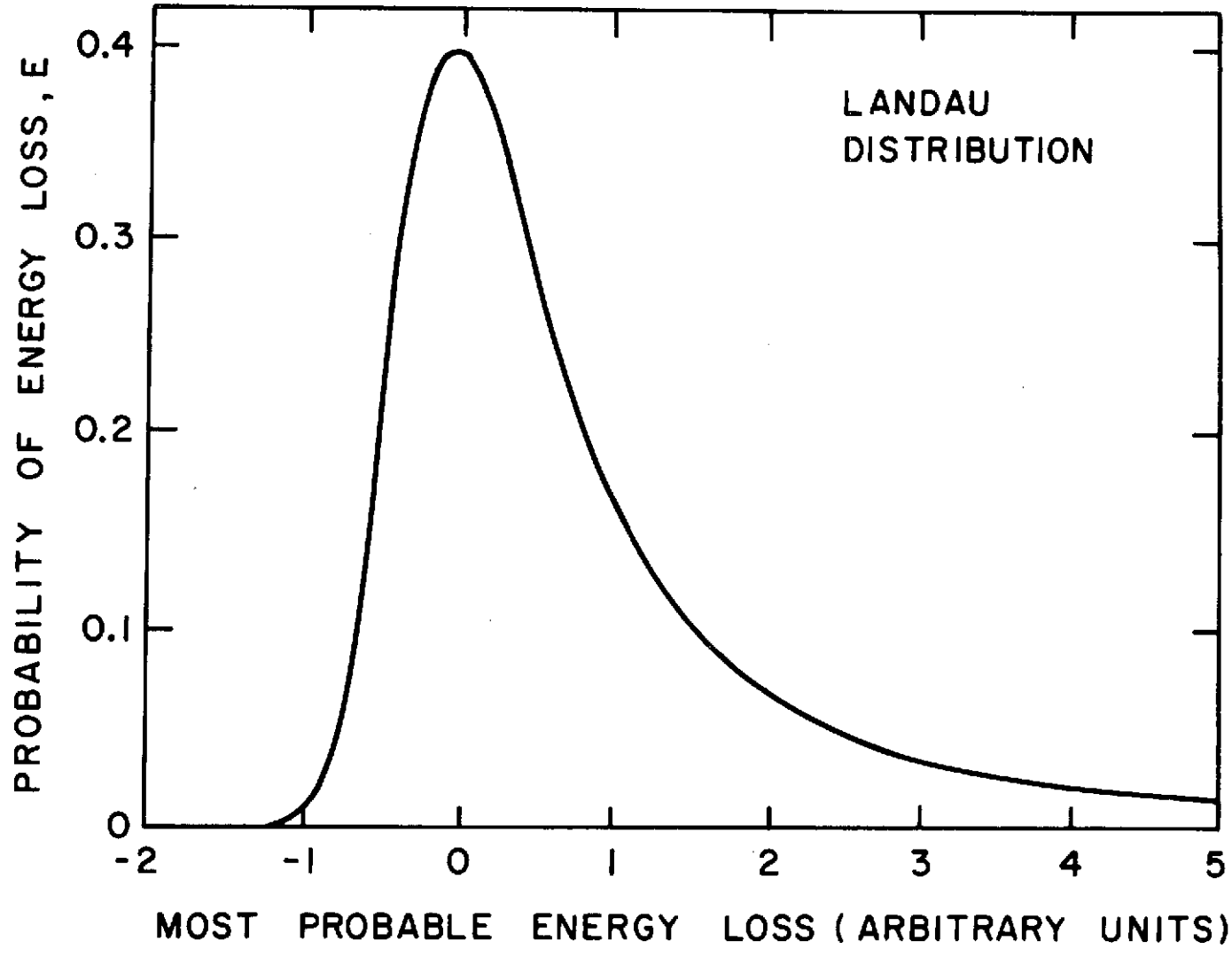

Fig. 8. Example of a Landau distribution for the most probable energy loss in a thin scintillator.

in the expression for $E_o - E_p$ are in turn determined from the parameters $G(\beta,Z)$ and β^2. Below are presented the formulae for the parameters G and Δ discussed in terms of the properties of the cosmic ray nuclei (charge Z, mass M, velocity $\beta = \frac{v}{c}$) and the detector element (average charge Z_D, average mass number A_D, thickness X).

$$G = \frac{2\,G\,m_e c^2 \times Z^2}{\beta^2 E'_m} \qquad (7)$$

$$\Delta = \frac{2\,G\,m_e c^2 \times Z^2 b}{\beta^2}$$

where $G = 0.150 \frac{Z_D}{A_D}$. The functions $j(G,\beta^2)$, $b(G,\beta^2)$, and $\lambda(G,\beta^2)$ are graphed in Rossi. The value of λ determines the amount of asymmetry of the distribution: λ is largest for small values of G which corresponds to highly relativistic particles. The quantity Δ has the dimensions of energy and is a measure of the width of the distribution.

The ultimate resolution of any detector is determined by these statistical fluctuations. Allowing for values of Z different from one, one can calculate the curve using the method outlined in Rossi. Sample calculations using the formulae presented previously generated the Landau curves shown in Figure 9 (calculated with $\beta = 0.95$ particle in a scintillator element). The Landau FWHM calculated here refers primarily to distant collisions with electrons in the scintillator and not to knock-ons from close collisions which are responsible for the Landau tail. However, the ratio of the average energy loss to most probable energy loss for minimum ionizing particles goes from approximately 1.25 for $Z = 1$ to less than 1.01 for $Z = 20$. Hence the distortion of the Landau tail also decreases significantly with increasing charge.

The dashed line in Figure 9 represents the separation between the

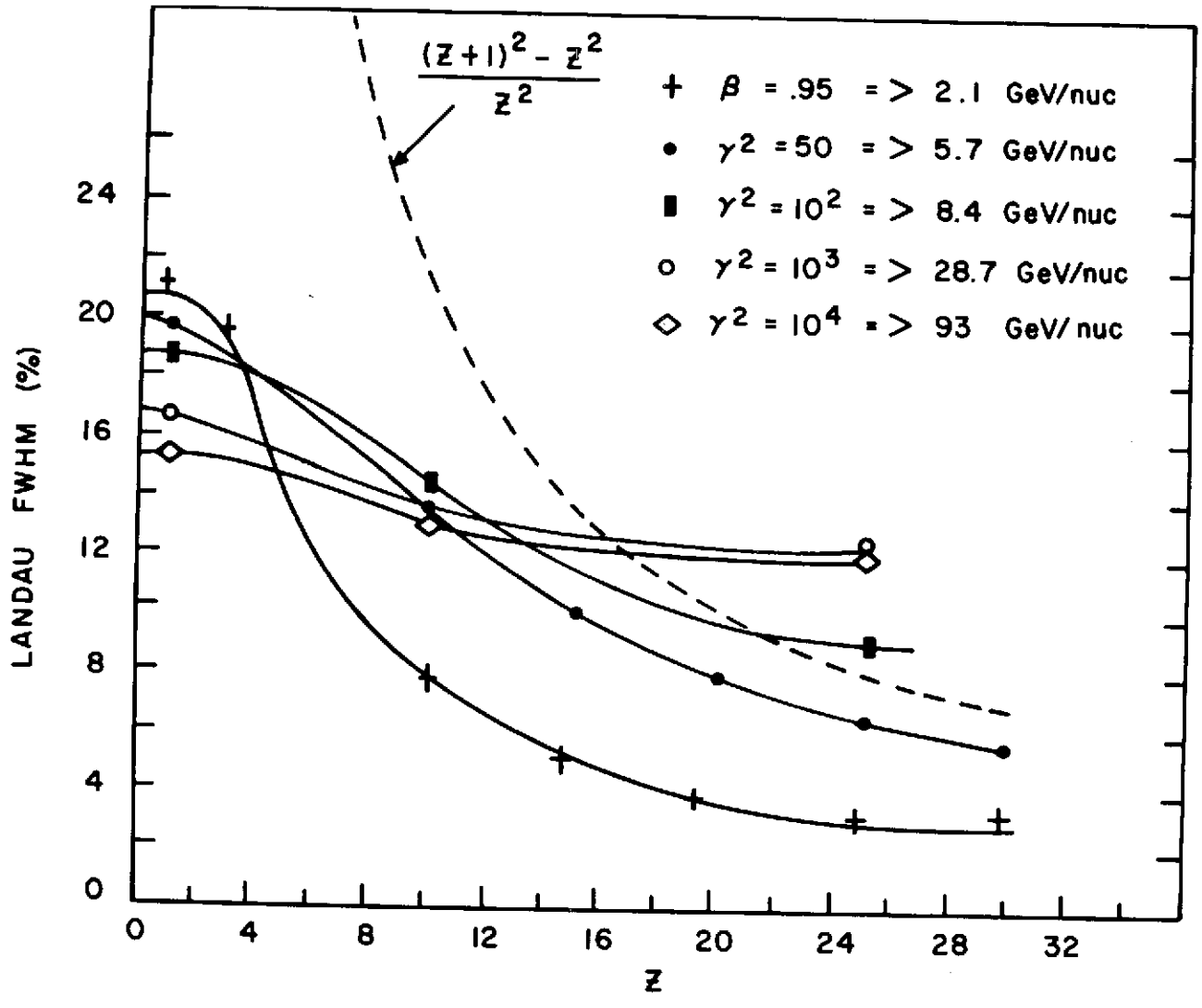

Fig. 9. The intrinsic resolution due to Landau statistical fluctuations in energy loss as a function of charge, Z, for various energies (solid curves), compared to the resolution required to separate adjacent charges (dashed curve). The curve labelled $\beta = 0.95$ is applicable to the data in this paper.

charges while the points represent the full width at half maximum calculated from Landau distribution for single detectors. Note that at 8.4 GeV/nucleon which is near the mean response for a balloon flight conducted where the cutoff is 1.36 GeV/nucleon, the FWHM exceeds the separation for $Z > 22$. At high energies this problem extends well down to $Z = 16$, and is further worsened by the skewness of the distribution becoming more extreme at higher energies. This is shown in Table 1 where the probability of a $Z = 25$ particle simulating the ionization loss of other charges is given. (For reference purposes, the energy lost by an iron nucleus of these energies is about 1.3 GeV in a 1/4" plastic scintillator). The first and second lines of the table, which roughly correspond to the mean energy under study here illustrate that the problem is not too severe at these energies. The problem arises at higher energies where the distribution becomes more skewed, making possible an error of identification of the charge of 1, 2, or even more charges.

It would appear from this table that the goal of $\pm$ 0.5 charge units of resolution is completely unachievable above a few GeV/nucleon. However the situation is not as bad as it seems at first because fluctuations which cause the skewness of the Landau distribution are caused by the production of a few very high energy knock-on electrons. Since these knock-on electrons have sufficient range to carry their energy out of the detector, the distribution of light produced will not exhibit this extreme skewness. The tails from the distributions are effectively removed and the problem of fluctuations exhibited in the table are greatly reduced. However, this gives rise to another effect. Then a significant fraction of the energy lost goes into electrons which leave the detector, so that the mean light output is reduced. The last column in the table shows this effect becomes

Table 1

STATISTICS ON LANDAU DISTRIBUTIONS FOR RELATIVISTIC Z=25 NUCLEI

Energy (GeV/nuc)	$Y = \frac{E}{mc^2}$	E_t(MeV)*	P(<24.5)	P(24.5 - 25.5)	P(25.5 - 26.5)	P(>26.5)	f_{out} **
5.7	7.1	50	0.03	0.84	0.13	0	0.8%
8.44	10	10^2	0.07	0.67	0.19	0.07	3.5%
28.7	31.6	10^3	0.08	0.48	0.22	0.22	10.4%
93	100	10^4	0.09	0.40	0.23	0.28	15.5%

*E_t is the maximum energy which can be transferred to a single knock-on electron.
**f_{out} is the fraction of energy into electrons with range greater than the detector thickness.

important for iron at energies above 25 GeV.

Because any single measurement of charge is subject to these statistical fluctuations, multiple measurements using multi-element telescopes are essential to reduce their effects. Lezniak (1969), using a multi-detector telescope on Pioneer 8, has shown that improved resolution is possible with a "minimum of three" technique. He showed that the width of the energy loss distribution for sea-level muons in solid state detectors is seen to decrease from FWHM = 30% to 22%. He concludes that the improvement results from diminishing the Landau tail in order to obtain an energy loss near the most probable energy loss.

Linsley and Herwitz (1956) have given an excellent qualitative discussion of the influence of Landau fluctuations on the possibilities of charge determination of cosmic ray particles by means of Cerenkov and scintillation counters. They find the Gaussian approximation for relativistic heavy nuclei to be good. Corydon-Petersen and Lund (1969) have performed Monte Carlo calculations which showed that poor charge resolution in such counters in general cannot arise from Landau effects. These calculations confirm that measured pulse height distributions for higher atomic numbers turn out to be Gaussian in shape, as predicted by Linsley and Herwitz with a width small compared to the distance between the mean output from neighboring Z numbers.

The method developed here utilizes four detector outputs to calculate the characteristic charge type. The most probable event type is calculated and an average over all detectors is taken. Any extreme fluctuation will appear as an anomalous pulse height value in only one of the four detectors, i.e., by demanding consistency between measurements, background events are eliminated. The methods for charge identification and background elimination are discussed more fully in the next two sections.

III.F. Four Dimensional Hyper-Ellipsoidal Charge Determination

The first step in the analysis of the data from the flight was to create a 2-D matrix of scintillator outputs for all events. One of these 2-D pulse height matrices is shown in Figure 10. The vertical position of each charged particle cell in the matrix corresponds to pulse height in one detector while the horizontal position corresponds to pulse height in any other detector. Each cell contains a number telling how many events occurred within the corresponding combination of detector outputs. The letters represent numbers greater than 9, starting with A=10, B=11, etc. These data point clumps, corresponding to particles of a particular charge value, cluster around a line which to first order is straight having a slope determined by the ratio of the response in the two detectors. Since this ratio is very closely 1, the slope is $\simeq 1$, and the line is at 45°. The matrix shown was created using programs on an IBM 360/75 computer.

Because of corrections in the data analysis to this point, each charge group stands out as an individual clump of particles in the 2-D matrix of scintillator outputs. However, due to dispersions in the detectors, the observed pulse heights are distributed around the centroids characteristic of the pulse height of the relativistic value ($\beta>0.92$) of the energy loss through ionization of each charge. (The word "relativistic" is underlined due to its importance for the Cerenkov detector centroid values. The charge determination is extremely critical because of its coupling with energy determination. Below about 2 GeV/nuc, the Cerenkov response is energy dependent and so charge analysis depends upon the energy per nucleon. However, by requiring the Cerenkov detector pulse height response to be

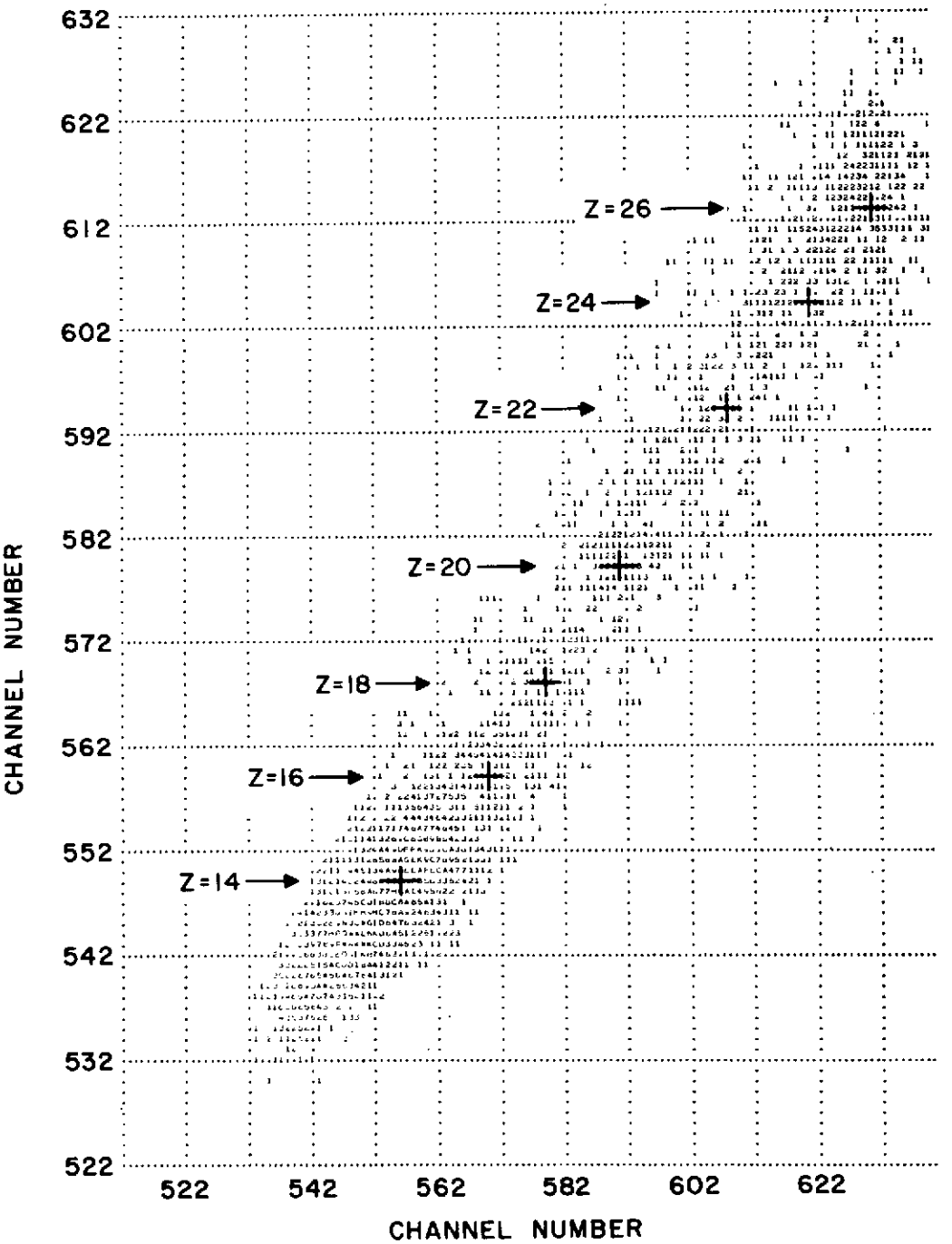

Fig. 10. Two-dimensional pulse height matrix, scintillators S1 and S2. Pulse heights have been corrected for detector dependences but background events have not been removed.

within a certain "distance" from the centroid, or relativistic value, one can be assured that the events detected are above the vertical geomagnetic cutoff and not low energy events. (See the following paragraphs for a fuller discussion). Single- and two-dimensional pulse height distributions are generated from the corrected pulse heights for each of the four detectors in the CIM, two scintillators (S1 and S2), the Cerenkov detector (C), and the cesium iodide detector (CsI), i.e. S1, S2, C, CsI, and pairs S1 vs S2, S1 vs CsI, S1 vs C, S2 vs S1, ... etc. From these the centroid of each charge in each detector and the resolution of each detector were found.

The charge determination procedure may be considered from the following point of view. An N-detector system forms an orthogonal space of N-dimensions, in which each axis is the detector output in units of the resolution of the detector, σ_{ij}, defined by

$$\sigma_{ij} = \frac{C_{ij} R_{ij}}{2.36} \tag{8}$$

where C_{ij} is the centroid and R_{ij} is the resolution for the i^{th} charge in the j^{th} detector. In this hyper-space the i^{th} centroid is located at the point $(C_{i1}/\sigma_{i1}, \ldots, C_{ij}/\sigma_{ij}, \ldots C_{iN}/\sigma_{iN})$ and a given event is located at the point $(P_{i1}/\sigma_{i1}, \ldots, P_{ij}/\sigma_{ij}, \ldots, P_{iN}/\sigma_{iN})$, P_{ij} is the observed pulse height of the i^{th} charge in the j^{th} detector and N is the total number of detectors. (For each event, the data consists of N=4 measurements.) The value of 'i' is chosen such that D_i, the total distance, is a minimum where

$$D_i^2 = \sum_j \delta_{ij}^2 = \sum_j \left(\frac{P_{ij} - C_{ij}}{\sigma_{ij}} \right)^2 \tag{9}$$

This 'i' value is then assigned to that event as the charge to which the event was closest (i = 10, ..., 28). Particles were said to have interacted, or are background, if they lay outside of the 4-D hyperellipsoid.

In order to demonstrate the selectivity of the method, a 1-dimensional charge distribution was reconstructed. The charge is determined as the minimum in the parabola formed by the distances to the three closest centroids. In this method, neither the distances nor the determined charge value are integers. The charge value is assigned to the closest integer value which the determined value approached. Both the sagitta of the parabola and the minimum of the parameter D_1 can be used as measures of the error.

Charge identification accuracy is $\sigma = \pm 0.51$ at magnesium and increases about linearly up to $\sigma = \pm 0.66$ at iron. These total errors, which are determined by the charge identification routine, may be compared to the total error calculated from the resolution of each individual detector element:

$$\frac{1}{\sigma_T^2} = \frac{1}{\sigma_{S1}^2} + \frac{1}{\sigma_{S2}^2} + \frac{1}{\sigma_{Cw}^2} + \frac{1}{\sigma_{CsI}^2} \qquad (10)$$

At charge 12 where the resolution, and hence σ, for each detector is known, this calculation yields $\sigma = 0.50$ in excellent agreement with the value given above. Reversing the calculation can yield the approximate resolution at charge 26 for detectors S1 and S2 where it is not known. First assume that the resolution improves in both detectors in about the same ratio. Using a resolution of 34% for the Cerenkov detector, 21% for the cesium iodide detector, and 6% total resolution ($\sigma = 0.66$) at charge 26 yields a resolution of 8% for S1 and 10% for S2, which is not unreasonable considering the resolution had improved by a few percent at charge 14 in both detectors. The implications of this resolution are as follows. The final resolution of a given detector d is calculated from

$$\sigma_d^2 = \sigma_L^2 + \sigma_{ph}^2 + \sigma_{sp}^2 \qquad (11)$$

where L stands for Landau statistics, ph for photoelectron statistics, and sp for the spatial resolution. The Landau resolution at charge 26 is about 3% (see Figure 9) and the resolution due to photoelectron statistics is less than 1% (at Z=1 photoelectron statistics are about 18%: they decrease as 1/Z). The spatial resolution is then deduced to be about 5-6% in agreement with sections III.B. and III.C. (angular resolution about 2%, area resolution 3-4%). This indicates detectors S1 and S2 are still dominated by spatial resolution. If this number could be reduced to 1%, the results of future flights of this detector would be significantly improved. Since the cesium iodide detector is also an ionization energy loss detector, the same analysis can be applied to it. The constant total resolution of this detector is a clue that the spatial resolution was very poor, probably due to inefficiency in the collection of light photons in the large diffusion chamber. Landau statistics are not a part of the calculation for the Cerenkov radiator since Landau fluctuations apply only to ionization energy loss processes. Photoelectron statistics can account for at most 7% of the final resolution of this detector. The Cerenkov response was determined to be such a complicated function of azimuthal and zenith angle, and position within the large area of the detector that it is felt that the limit to the resolution is reached due to uncertainties in the spatial correction rather than photoelectron statistics or other causes. Hence in every detector, it would appear that the spatial resolution limits the final resolution achieved in that detector, which in turn

limits the total resolution achieved by the multidimensional charge identification routine.

However individual charges are reasonably well resolved with background rejection quite effective as can be seen in the final charge histogram shown in Figure 11, where the peak-to-valley and charge resolution are good. It would appear from Figure 11 that odd charges have not been resolved. It must be remembered that the computer algorithm works with the pulse heights from all 4 detectors to determine a non-integer charge value for each event. The charge histogram shown in this figure is constructed from the non-integer charge values of 2 detectors, S1 and S2, only; hence the resolution does not appear to separate charges uniquely. The algorithm also assigns an integer charge value to an event based on whether the non-integer charge value lies within the hyperellipsoid defined for that charge. Using this method, there is no difficulty assigning a charge value as either odd or even. Therefore odd charges are determined usually as well as even charges over the entire charge range.

Any good events lost in this selection procedure have probably been incorrectly identified as background. Correction for the rejected good events will be discussed in the section on background that follows.

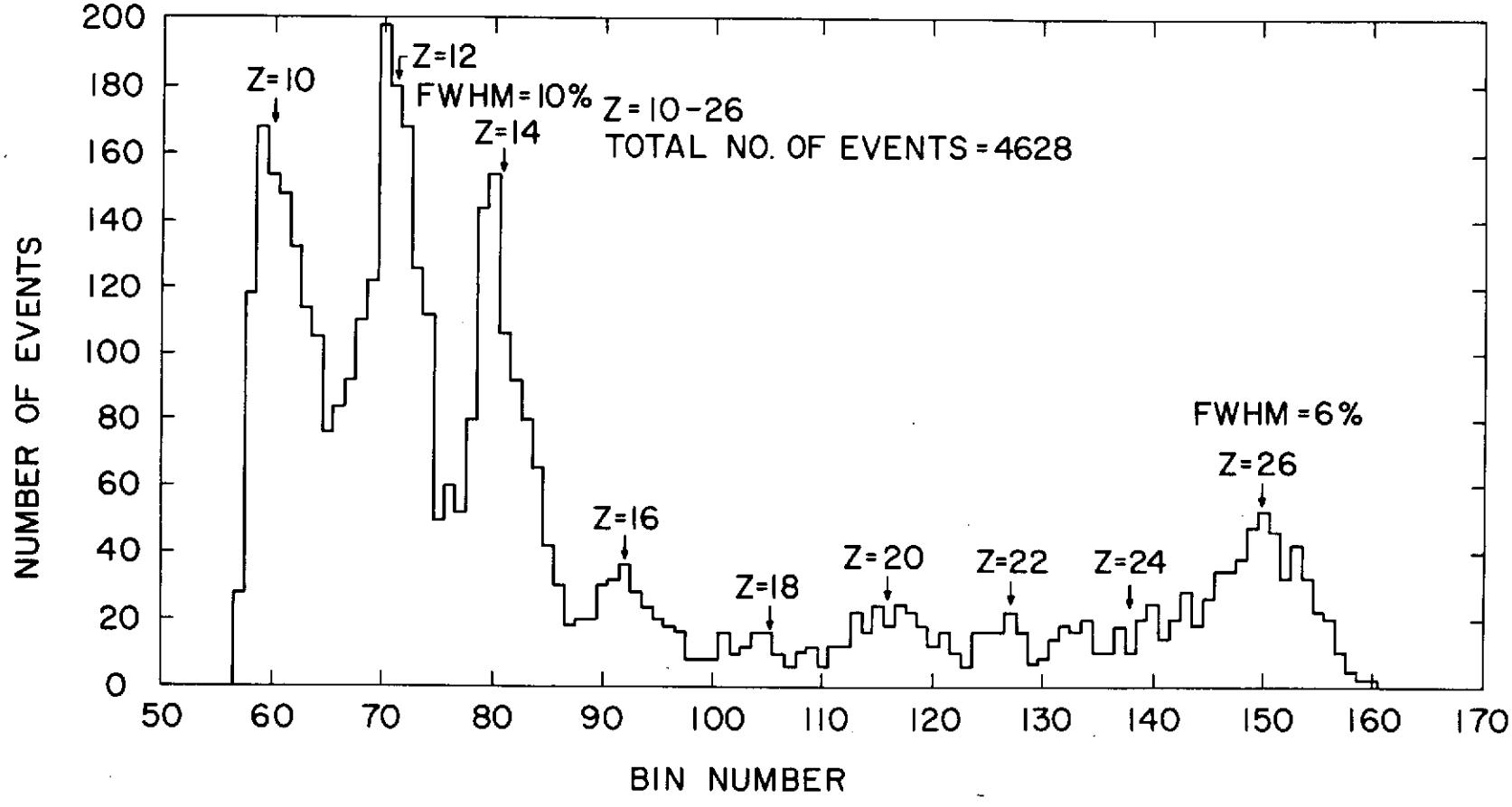

Fig. 11. Charge histogram, Z = 10-26, taken from two dimensional matrix, S1-S2, of corrected pulse heights with background removed.

III.G. Background Correction

Selection of "single" events, as determined using the criteria outlined in Appendix B on the spark chamber tracks, served to eliminate a large fraction of background events. As discussed there, the spark chamber helps to discriminate against multiple particle background events, such as atmospheric showers, since a unique track can not be found. The presence of the Cerenkov detector, with its energy threshold, makes the rejection of low energy background, both in the atmosphere and from interactions in the spectrometer, much easier.

Nuclear interactions and other anomalous events are also discarded by demanding consistency of the charge determination between the elements of the CIM. Each charge is defined in a very localized region in 4-D pulse height space. It is assumed that most background particles do not lie in the expected regions of the 4-D hyper-space, i.e., these events should be interspersed between and scattered about the clumping. Since background events are uniformly distributed over a much greater volume, background subtraction becomes straightforward by demanding consistency between the charge values determined in the 4 detector elements.

As discussed in the previous section, the charge value (non-integer) is determined as the minimum in the parabola formed by the distance to the three closest charge values. The charge is assigned to the closest integer value which the determined value approached. Another parameter is defined for all 4 detectors as the sum of the squares of the distances of the non-integer charge value from the integer charge in units of the resolution in each detector. Particles were said to have interacted, or are background, if they lay outside of the 4-D hyperellipsoid with semi-

axes defined by the value of this parameter such that applying this criterion yields an L/M ratio and individual charge composition up to Z = 10 that agrees with the published literature. Figure 12 shows the same computer matrix printout of the raw data of Figure 10 after background has been removed by applying the four dimensional hyperellipsoidal charge determination computer algorithm. (This matrix output is also used to plot the charge histogram of Figure 11).

In order to insure that background is minimized, the strict criteria on track determination, energy determination and charge determination discussed in the previous 2 paragraphs have been placed on every event. However this may mean that some good events are discarded. for example, the high efficiency of the spark chamber for singly charged particles has made the spark chamber sensitive to knock-on electrons produced by high Z nuclei and to Compton electrons from γ-rays coming from the spectrometer. As a result, the VH nuclei tracks have been confused by the presence of background. Or, for example, a good event may interact near the top of the energy spectrometer producing backscatter through the CIM. Anomalous pulse heights from the backscatter would cause the event to be rejected due to inconsistent pulse heights in the four detectors.

It is possible, and necessary, to make a correction for good events that are identified as background, and as such are removed from the charge distribution. For the charge determination procedure, events which lie outside the pulse height error range, but which have simple tracks as defined by the spark chamber, represent at most a 15% correction to the data. Background events of this type were most abundant at lithium and fell off rapidly with increasing charge so that heavy nuclei should not

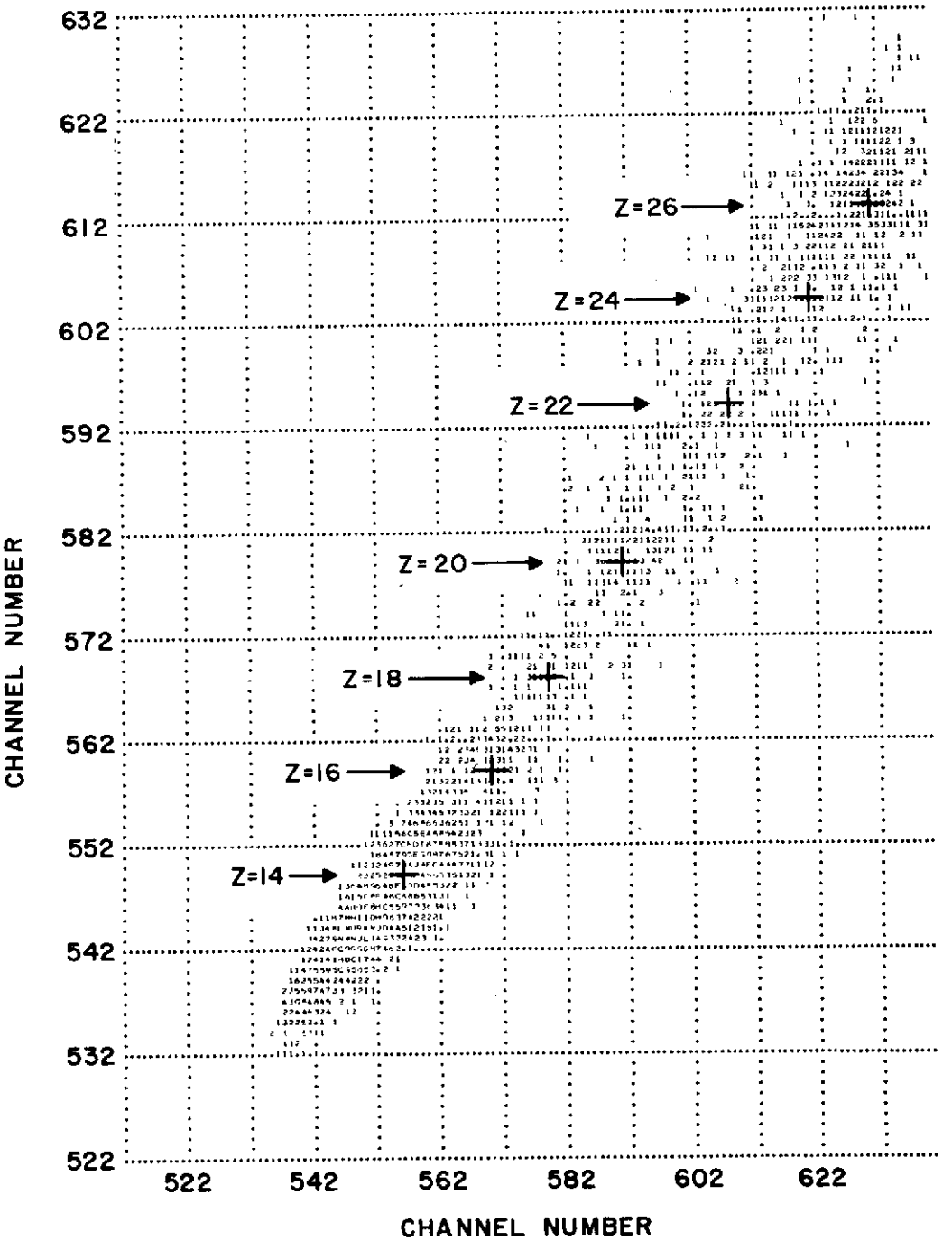

Fig. 12. Two dimensional pulse height matrix, scintillators S1 and S2, with background events removed.

have been affected much. To check that the spark chamber track classification scheme was not itself biasing the data, all complex events, i.e. those which do not satisfy the criteria in Appendix B, were subjected to the same charge determination procedure as used on simple events by assuming these complex events had trajectories at the most probable response angle of the coincidence scintillators. The data was consistent with being background. The most probable correction of 5-10% can be put on losses of well identified complex events.

The background measurement can be compared with an estimate of the fraction of events that will interact in the detector as follows. One would expect a correction factor of the form $e^{x/\Lambda}$ where x is the mean thickness of the detector in g/cm^2 and Λ is the mean free path for absorption. The interaction mean free path in a compound material, λ_{ic} is given by

$$\frac{1}{\lambda_{ic}} = \sum_j \frac{P_j}{\lambda_{ij}} \tag{12}$$

where λ_{ij} is the mean free path for an i^{th} incident nucleus on the j^{th} component nucleus with P_j the partial weight for the j^{th} nucleus. The quantity λ_{ij} is calculated from $\lambda_{ij} = \frac{\Lambda_{ij}}{n}$ where n is the number of j nuclei per gram of j element and Λ_{ij} is the black disc formula for the absorption mean free path

$$\Lambda_{ij} = \frac{m_j A_j}{\pi r_j^2 \left(A_j^{1/3} + A_i^{1/3}\right)^2} \tag{13}$$

where A_i and A_j are the atomic number of the cosmic ray and target nucleus, and m_j and r_j are the mass and radius of a nucleon. This can be simplified by considering an upper limit to the cross section for interaction $\sigma_{ij} = 1/\Lambda_{ij}$ and letting the target nucleus be hydrogen. Thus $A_j = 1$,

$m_j = 1$, $r_j = 1.45 \times 10^{-13}$cm. The mean free path then calculated will be a lower limit to the true mean free path.

The mean free paths in plastic, CsI, and aluminum have been calculated for magnesium, sulphur, calcium and iron as listed in Table 2. For the plastic calculation it is assumed that there are equal numbers of hydrogen and carbon atoms per molecule. The detector material in the telescope consisted of 2.78 g/cm^2 of plastic, 1.43 g/cm^2 of CsI, and 0.86 g/cm^2 of aluminum, a total of 5.08 g/cm^2 of material in the detector geometry.

Using these numbers, an upper limit of 32% for nuclear interactions of iron cosmic rays in the detector material is estimated. (It is interesting to note that the number of iron group nuclei identified as having complex tracks is consistent with the expected number of interactions of iron group nuclei in the CIM.) In addition background is expected from large statistical fluctuations in the pulse heights and from interactions in the matter surrounding the detector. Hence the correction factors used of 1.32 for the LH group, 1.36 for the MH group, and 1.47 for the VH group are in reasonably good agreement assuming most interactions occur in the detector material.

Table 2

INTERACTION MEAN FREE PATHS
IN PLASTIC, CESIUM IODIDE, AND ALUMINUM (g/cm^2)

	Plastic	CsI	Aluminum
Magnesium	12.64	103.43	19.61
Sulphur	11.31	96.27	17.81
Calcium	10.35	90.79	16.47
Iron	9.00	80.88	14.57

III.H. Correction for Overlying Atmosphere

Before one can interpret the measurements of the charge composition at balloon altitudes in terms of the extraterrestrial abundance of these nuclei, corrections must be made for production and loss in the atmosphere. When the primary cosmic ray beam passes through the upper layers of the atmosphere, the overlying material has a 2-fold effect on the measured intensities of the nuclei at a particular charge. Firstly, some nuclei will interact and be removed from consideration completely, and secondly, nuclei will interact and give rise to fragments of lighter charge which will still be in the charge range under consideration. The correction in general requires a complete knowledge of the fragmentation parameters of various elements into lighter nuclei. In practice measurements of the absorption of each cosmic ray element in the upper atmosphere are used to make these corrections (Webber and Ormes, 1967). For reasonably accurate results, the latter method requires large statistics for individual charges which are difficult to collect, since the flux of high energy cosmic rays is low and most balloons rise rather quickly to float altitude. Therefore the first method will be used to find the charge composition at zero depth. The second method, however, has been used to correct the integral flux measurements of charge groups since this is well within the associated errors.

The most straightforward way of making the atmospheric correction to integral fluxes of charge groups is to observe the variation of fluxes of the various nuclei as a function of depth and extrapolate that data to the top of the atmosphere. This is done by obtaining the absorption mean free paths from a plot of flux versus depth. The data on fluxes presented

here are corrected to the top of the atmosphere in just that manner: by using direct measurements of the atmospheric absorption of the various charge components.

Taking advantage of the large geometrical factor the atmospheric attenuation mfp of nuclei groups $10 \leq Z \leq 14$, $15 \leq Z \leq 19$, $20 \leq Z \leq 23$, $24 \leq Z \leq 30$, $15 \leq Z \leq 23$, and $20 \leq Z \leq 30$ have been measured with increased statistics using data from both the ascent and descent portions of the balloon flight. (This flight provided a unique opportunity for measuring the mfp in air. The experiment not only ascended slowly but, due to a failure of the experiment cut-down mechanism, descended slowly to the ground from altitude as the balloon gradually lost lift, instead of parachuting to the ground.)

From radar and barometer measurements, the altitude-time profile for both ascent and descent are known. The data is divided into 5 g/cm^2 intervals and the fluxes of the different charge components are calculated in each of 10 depth intervals over the range $5.0 \leq x \leq 55.0$ g/cm^2. The thickness of atmosphere penetrated by each incident particle is determined from its trajectory through the detector and the altitude of the balloon at the time of its arrival; thus particles penetrating any given thickness of atmosphere were observed from various zenith angles at various balloon altitudes. The effective (area) x (solid angle) x (time) factor for each depth interval is calculated by numerical integration of the detector's differential geometrical factor over the trajectories (Monte Carlo technique, see Crannell and Ormes, 1971).

Figure 13 shows the depth dependence of the fluxes of charge groups $10 \leq Z \leq 14$, $15 \leq Z \leq 19$, $20 \leq Z \leq 23$, and $24 \leq Z \leq 30$ above 1.16 GeV/nuc along with the results of a linear least squares fits. Data points have been plotted at

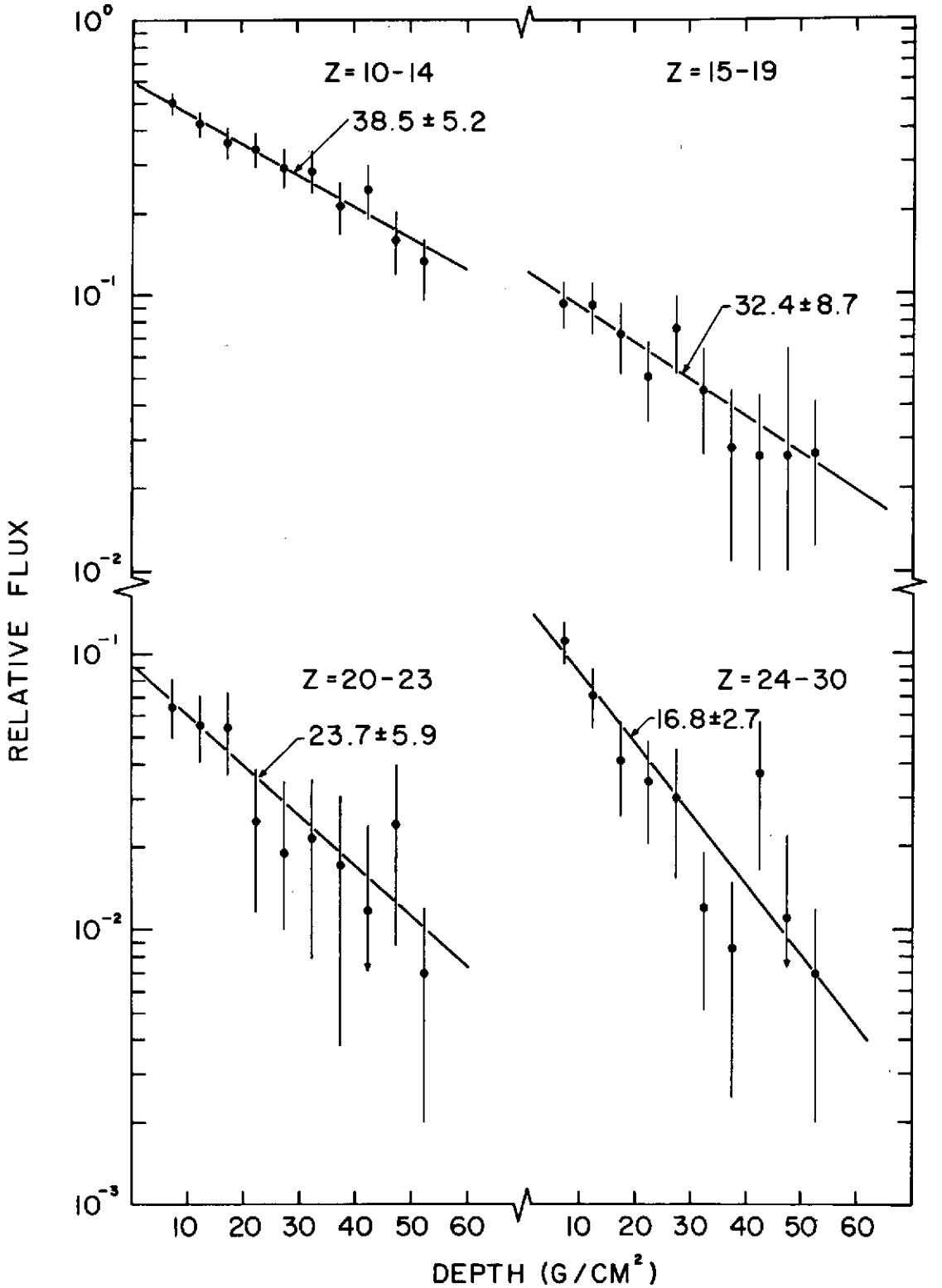

Fig. 13. Relative flux of charge groups as a function of depth in the atmosphere. The slope of the least squares fit to the data (solid line) yields the atmospheric attenuation mean free path.

the mean atmospheric depth traversed within each depth interval. Effects due to the variation of geomagnetic cutoff with incident direction are negligible because each data point represents an average over all azimuths and a wide range of zenith angles. Correction for energy loss through ionization in the atmosphere has been neglected. For example, the energy loss through ionization in air for iron nuclei is about 350 MeV/nuc in 7.4 g/cm^2.

The fit of the data yields atmospheric attenuation mfp for the different charge groups as listed in Table 3a, where they are compared to other experimental results. The values are seen to be in generally good agreement with other results. The results for charge groups $15 \leq Z \leq 19$ and $20 \leq Z \leq 23$ represent the first direct measurements of the atmospheric attenuation mfp. These values may be compared to the Webber et al. (1972) summary of the experimental data in emulsions of Cleghorn, (1967), and the direct measurements in air of Webber and Ormes (1967) and von Rosenvinge (1969). Although no error bars on the values were published by Webber in the summary paper, there still appears to be systematic differences between those values and the values measured by this experiment. The measurements of Webber and Ormes (1967) were made at lower energies where energy loss through ionization in air can not be neglected. Waddington (1969) pointed out that this correction to the mean free paths appears to have been done incorrectly. It also appears from the table as though one can not simply extrapolate the results of emulsion experiments to air. All emulsion measurements appear to be about 20% too low. The results of Mewaldt et al. (1971) are statistically the most significant so any comparison should be weighted toward these measurements. It can be seen that

Table 3a

ATMOSPHERIC ATTENUATION MEAN FREE PATHS (g/cm^2)

Charge Group	Present Experiment*	Mewaldt et al.,1971*	Webber et al.,1972+,**	Freier & Waddington, 1968c**	von Rosenvinge et al.,1969a,b**	Cleghorn, 1967**
$10 \leq Z \leq 14$	38.5 ± 5.2		28.1		30.0	
$15 \leq Z \leq 19$	32.4 ± 8.7		25.0	22.5		
$20 \leq Z \leq 23$	23.7 ± 5.9		22.1	19.1		
$24 \leq Z \leq 30$	16.8 ± 2.7		15.8			
$15 \leq Z \leq 23$	28.4 ± 5.4		22.4			
$20 \leq Z \leq 30$	19.5 ± 2.8	19.7 ± 1.6	16.1	16.2	16.5	21.9
$Z=26$		15.6 ± 2.2				

+Values calculated for groups using mfp weighted by relative abundances.
*Measured in air directly
**Extrapolated from emulsion measurements

Table 3b

ABSORPTION MEAN FREE PATHS IN AIR (g/cm^2)

Charge	MFP
26	16.8
25	17.9
24	19.1
23	20.2
22	21.4
21	22.5
20	23.7
19	25.8
18	28.0
17	30.2
16	32.4
15	34.0
14	35.5
13	37.0
12	38.5
11	40.0
10	41.5

the VH group values agree very well. The value for iron from Mewaldt agrees quite well with the value found here for the iron group, of which iron is the dominant member. In fact the value found here is somewhat larger, which it should be, since the group members, manganese and chromium, will tend to increase the value over the value for iron. (The group members Z>26 are so small in number compared to Z = 24-25 that they should not influence the mean free path value very much).

The integral fluxes of charge groups have been corrected in this manner in Table 4 in section IV. A.: the graphs of flux versus depth for each charge group were extrapolated directly to the top of the atmosphere. Correction factors from this method are given in column 3 of Table 4.

The first method for correction for the absorption-fragmentation process can be treated in terms of solving the one dimensional diffusion process. The number of nuclei at depth x, $N_i(x)$, is given by the number at the top of the atmosphere $N_i(0)$, multiplied by a function which involves all the relevant abundance and nuclear parameters. In this approach it is necessary to measure values for the abundances of nuclei, and to adopt values for the relative number of light fragments produced in each interaction of a heavier nucleus with atmospheric nuclei, i.e. the fragmentation probabilities and the interaction or absorption mean free paths (mfp). Furthermore, one must make the simplifying assumptions that no energy is lost by ionization and that fragments always maintain the direction of motion of the primary nucleus. Then the diffusion equation reads

$$\frac{dN_i(x)}{dx} = -\frac{N_i}{\Lambda_i} + \sum_{j<i} P_{ji}\ \frac{N_j}{\Lambda_j}\ ;\quad i = 1, 2, \ldots, 17 \tag{14}$$

where i = 1 corresponds to iron nuclei and i = 17 corresponds to charge 10, neon.

The number of primary nuclei with charges greater than iron is about 10^{-5} as large as that for the iron group (Fowler et al., 1967). Therefore, it is satisfactory to neglect the correction for nuclei fed into the iron peak from the SVH group ($Z \geq 30$), and to adjust for only those nuclei which leave the iron peak. (Hence the sum in the equation runs for $j<i$). Then for the iron nuclei, the number N(0) at depth x = 0 (top of atmosphere) is given by

$$N_1(0) = N_1(x) \exp(+x/\Lambda_1) \tag{15}$$

where Λ_1 is the absorption mfp of iron nuclei. For those nuclei of the next lighter charge, the solution to the diffusion equation becomes

$$N_2(0) = \left\{ N_2(x) - \frac{P_{12}\Lambda_2 N_1(0)}{\Lambda_2 - \Lambda_1}\left[\exp(-x/\Lambda_2) - \exp(-x/\Lambda_1)\right] \right\} \Big/ \exp(-x/\Lambda_2) \tag{16}$$

A similar solution must also be generated for each succeeding nucleus, solutions which become even more complex in analytic form.

These equations show that in order to calculate primary abundances it is necessary to know the mean free paths (mfp) and fragmentation probabilities applicable to the atmosphere. These values are not well known and appear subject to some controversy. Interaction mfp and fragmentation probabilities may be measured directly in media such as carbon, Teflon, or nuclear emulsion that resemble air in their nuclear makeup. From these measurements estimates of the appropriate mfp in air may be made. (See, for example, Judek and van Heerden, 1966; Cleghorn, 1967; Cleghorn et al., 1968; and Long, 1968). These authors found that the fragmentation probabilities are constant with energy in photographic emulsions, and have

assumed the same to be true for interactions in air. Direct experimental determinations of the fragmentation cross sections using protons incident on high Z material targets have shown that cross sections are constant to ±10% beyond about 1 GeV/nuc. Though all fragmentation interactions have not been studied completely, variations of cross section with energy above 1 GeV/nuc. seem unlikely. For a summary of results and discussion, see Shapiro et al. (1971).

The absorption mean free paths (mfp) for individual nuclei were created from the measured group absorption mean free paths by assuming that the measured value corresponds to the most abundant charge in that group and linearly interpolating between measured values for the amfp to get the amfp for each individual charge in that group. This method yields the absorption mean free paths in air for charges 10-26 as shown in Table 3b. Constructing the individual amfp from the group amfp in this manner does not increase the error in the final results since each individual amfp is within the 20% error bar of the amfp for the group to which it belongs. These errors are included in errors for the final results.

The fragmentation probabilities for air have been created from the Silberberg and Tsao (1973) nuclear interaction cross sections in hydrogen (see Table 7) using a correction factor for air based on the latest results of heavy ion experiment performed on the Lawrence Berkeley Laboratory accelerator by Heckman and Greiner. (See Heckman et al., 1972; D. E. Greiner 1973; H. H. Heckman, 1973; and H. H. Heckman, private communication*).

*The author wishes to thank Dr. H. H. Heckman for providing his valuable results to this author prior to publication.

The correction is calculated as follows. Heckman et al. have found that at high energy the cross section for production of element X from projectile C with target B fits the functional form

$$\sigma_{CB}^{X} = \gamma_{C}^{X} \gamma_{B} \tag{17}$$

where σ_{CB}^{X} is the cross section, which is separable (factorization) into a part that depends on the projectile and product γ_{C}^{X}, and γ_{B}, a part which depends exclusively on the target. From their experiments, $\gamma_{B} = A_{B}^{.256}$, a result which is somewhat less than considering the target's cross section to vary as the geometric area, in which case the cross section would vary as $A^{2/3}$, and also surprisingly less than considering the cross section to vary as the circumference, in which case the cross section would vary as $A^{1/3}$. (This latter case implies the interaction occurs with only an annular ring of nucleons in the target). Knowing the hydrogen cross sections, H, to a reasonable accuracy of 10-20%, it is then a simple matter to correct these for interactions in air. For simplicity of demonstration, assume air is pure nitrogen, N. Then

$$\frac{\sigma_{CN}^{X}}{\sigma_{CH}^{X}} = \frac{\gamma_{C}^{X}}{\gamma_{C}^{X}} \frac{\gamma_{N}}{\gamma_{H}} = \frac{(A_N)^{.256}}{(A_H)^{.256}} = \frac{(14)^{.256}}{(1)^{.256}} = (14)^{.256} \tag{18}$$

so $\sigma_{CN}^{X} = (14)^{.256}\ \sigma_{CH}^{X}$. That is, the cross sections for hydrogen are multiplied by $(14)^{.256}$. In actual fact the calculated correction factor was based on an air mixture of 80% -N and 20% -O.

This paper utilizes these new results to extrapolate individual charge composition data collected at balloon depth to the top of the atmosphere. Previous investigators claiming individual charge resolution at balloon depth and again at the top of the atmosphere have nonetheless extrapolated

their individual charge composition results to the top of the atmosphere by lumping their individually measured charges into groups, using group fragmentation parameters, and redistributing the growth or diminution of that group back to individual elements.

The results of the present method are given in column 5 of Table 6.

III.I. Correction for Solar Modulation

Solar modulation introduces another complication to the data analysis. Its influence on intensity measurements is considerable since the data under study here was collected at solar maximum conditions. This influence will be eliminated as much as possible by using the method outlined in Appendix C.

The charge intensities presented in column 2 of Table 4 represent those that would be measured at the top of the atmosphere. The force field solution is used to correct these intensity measurements:

$$\frac{j_t(r,E)}{j_0(\infty, E+\Phi)} = \frac{E^2 - E_0^2}{(E+\Phi)^2 - E_0^2} \qquad (19)$$

where j_t (r,E) is the intensity measured at Earth at time t, j_0 (∞, E+Φ) is the intensity in interstellar space, E is the total energy of the particle, E_0 is the particle rest energy, and Φ is the mean energy loss due to adiabatic deceleration.

Previous attempts to correct for solar modulation adjusted the measured intensities to the solar minimum of 1965 using regression curves because the amount of modulation at solar minimum was unknown (Mewaldt, 1971; von Rosenvinge, 1969). In order to more reasonably compare the present data to these past results, this author will also correct the data presented here to the solar minimum of 1965, but using values given below for the parameters. Hence, the correction factors, given by the quantity in square brackets in the equation below, for R=4.9 GV and R=3.25 GV are calculated using the appropriate parameters from

$$j_{1965}(E) = j_{1970}(E) \left[\frac{(E+\Phi)^2_{1970} - E_0^2}{(E+\Phi)^2_{1965} - E_0^2} \right] \qquad (20)$$

Urch and Gleeson (1972) have determined the values of Φ for the years 1965-1970 for various values of kinetic energies of helium cosmic rays. For 1970: Φ = 0.445 GeV/nuc. at T = 1.58 GeV/nuc. (4.9GV); Φ = 0.425 GeV/nuc. at T = 0.870 GeV/nuc. (3.25GV). For 1965: Φ = 0.175 GeV/nuc. for both T = 1.58 GeV/nuc. and T = 0.870 GeV/nuc. (See Figure 7 in that paper). The solar modulation correction factors are given in column 3 of Table 4.

An important point to remember is that the charge composition, which is the main thrust of this paper, is <u>not</u> affected by solar modulation: solar modulation depends on the Z/A ratio, as indicated in Appendix C, which is approximately 2 for all heavy cosmic ray nuclei. The Z/A ratio enters the theory through the quantity Φ which is defined by

$$\Phi = \frac{Z}{A}\varphi \qquad (21)$$

where φ represents the force field potential. Approximating the Z/A ratio to 2 introduces a small error of about 4% in the relative charge composition, an error which is much smaller than other errors associated with the charge composition measurements. This error will be neglected in the charge composition results. Any interpretations about the relative charge composition are not altered by this approximation. See Appendix C for a more complete discussion.

IV. RESULTS

IV.A. Fluxes at Top of Atmosphere

Table 4 summarizes the results of this experiment regarding the integral fluxes measured above the vertical cutoff rigidity at the regions of ascent and descent of the balloon and the correction factor calculated from the discussion in sections III.A. to III.I. This table presents the data for charge groups Z=10 - 14 (LH), Z=15 - 19 (MH), Z=20 - 30 (VH), and groups Z=15 - 23, Z=20 - 23, and Z=24 - 30 (Fe).

The resulting fluxes are compared with those reported by other workers in Table 5. The data chosen for comparison in Table 5 have been chosen because they represent the most statistically significant data in the present charge and energy range published to date. [Some workers have reported their results for integral rigidity spectra and others for integral kinetic energy spectra. For comparison, using A/Z = 2.10 for charges Z=10 - 30, a rigidity of 3.25 GV equals 0.870 GeV/nuc. and a rigidity of 4.9 GV equals 1.58 GeV/nuc.] It can be seen from the many data of other workers that is missing that this survey represents one of the most complete surveys available.

To give the reader an idea of the statistical significance of the results reported here, the results of Webber and Ormes (1967) are reported on about 300 nuclei with $Z \geq 10$, the results of Bhatia et al. (1970) on 440 nuclei with Z = 10 - 28, the results of Freier and Waddington (1968a) on 315 nuclei with $Z \geq 20$, and the results of von Rosenvinge (1969) on about 600 nuclei Z = 10 - 28.

The surveys that are statistically comparable are those of Smith et al. (1973) with about 1800 total events $Z \geq 10$, Mewaldt et al. (1971) with about 16000 events for $Z \geq 20$, Webber et al. (1973) with about 4000 events $10 \leq Z \leq 28$, and Balasubrahmanyan and Ormes (1973a) on about 770 nuclei

$10 \leq Z \leq 28$. (The integral values quoted for this experiment differ from the Balasubrahmanyan and Ormes results even though the results are taken from the same flight of the same experiment. This can be explained as follows. The integral flux values quoted here are taken from ascent which occurred at 4.9 GV rigidity: 4.9 GV is the vertical geomagnetic cutoff. The Balasubrahmanyan and Ormes result is taken from an energy measurement in the ionization spectrometer and converted to rigidity. The results do agree within errors.) The total number of events detected by this experiment was about 5000 for $Z \geq 10$. It can be seen that discrepancies exist among these published results, the value from this experiment being in general about 20-30% lower where they can be compared.

There are several possible systematic errors which might explain the discrepancies. In this experiment there is some uncertainty in the correction for events that are lost due to strict criteria on charge identification. The systematic effects of uncertainty in collection time or geometrical factor, or the systematic effects of inefficiency of operation of the spark chamber for higher charges influence the results quoted here.

Difficulties in comparison of various results may be due to the various levels of solar modulation prevailing at the time of each experimenter's measurements. Both charge resolution and statistics of total number of events measured by the experiments span a wide range. Some small difficulties in comparison arise due to non-uniformity in the definition of the various charge groups. For example, some experimenters define LH nuclei as charges 10 to 15 while others define this charge group as 10 to 14. Difficulties in comparison also arise due to the variety of energy or rigidity cutoffs quoted by other experimenters. And lastly, the various experiments all have flown under different amounts of atmosphere,

from 2 to 7.4 $g.cm^2$ of air, requiring different atmospheric corrections to be applied to the data. In view of all these differences, the agreement of the flux values amongst various experimenters is generally good. The discussion of the charge composition data, presented in the next section, should not be adversely affected by these systematic flux problems.

Table 4a

INTEGRAL FLUXES** (particles/m^2 ster sec)

Charge Group	Observed Flux (>3.25 GV)	Correction factors *			Corrected Flux (>3.25 GV)
10-14 (LH)	$7.58 \pm 0.65 \times 10^{-1}$	(1.15)	(1.32)	(1.34)	$1.54 \pm 0.13 \times 10^{0}$
15-19 (MH)	$1.59 \pm 0.32 \times 10^{-1}$	(1.0)	(1.36)	(1.34)	$2.90 \pm 0.58 \times 10^{-1}$
20-23	$1.15 \pm 0.28 \times 10^{-1}$	(1.0)	(1.36)	(1.34)	$2.10 \pm 0.51 \times 10^{-1}$
24-28 (Fe Group)	$1.83 \pm 0.38 \times 10^{-1}$	(1.0)	(1.47)	(1.34)	$3.60 \pm 0.75 \times 10^{-1}$
15-23	$2.64 \pm 0.41 \times 10^{-1}$	(1.0)	(1.36)	(1.34)	$4.81 \pm 0.75 \times 10^{-1}$
20-28 (VH)	$2.93 \pm 0.46 \times 10^{-1}$	(1.0)	(1.47)	(1.34)	$5.77 \pm 0.91 \times 10^{-1}$

** The fluxes presented here have been corrected to the top of the atmosphere using extrapolation of the atmospheric attenuation curves.

* (correction for events outside identification) (correction for interactions in CIM) (correction for solar modulation+)

+ This correction factor normalizes the flux values to solar minimum, 1965, Mt. Washington neutron monitor = 2400 for easier comparison to other published results.

Table 4b

INTEGRAL FLUXES** (particles/m^2 ster sec)

Charge Group	Observed Flux (>4.9 GV)	Correction factors *			Corrected Flux (>4.9 GV)
10-14 (LH)	$5.09 \pm 0.37 \times 10^{-1}$	(1.15)	(1.32)	(1.24)	$9.58 \pm 0.70 \times 10^{-1}$
15-19 (MH)	$1.07 \pm 0.17 \times 10^{-1}$	(1.0)	(1.36)	(1.24)	$1.80 \pm 0.29 \times 10^{-1}$
20-23	$6.84 \pm 1.54 \times 10^{-2}$	(1.0)	(1.36)	(1.24)	$1.15 \pm 0.26 \times 10^{-1}$
24-28 (Fe Group)	$1.30 \pm 0.24 \times 10^{-1}$	(1.0)	(1.47)	(1.24)	$2.37 \pm 0.44 \times 10^{-1}$
15-23	$1.70 \pm 0.22 \times 10^{-1}$	(1.0)	(1.36)	(1.24)	$2.87 \pm 0.37 \times 10^{-1}$
20-28 (VH)	$1.92 \pm 0.27 \times 10^{-1}$	(1.0)	(1.47)	(1.24)	$3.50 \pm 0.49 \times 10^{-1}$

** The fluxes presented here have been corrected to the top of the atmosphere using extrapolation of the atmospheric attenuation curves.

* (correction for events outside identification) (correction for interactions in CIM) (correction for solar modulation+)

+ This correction factor normalizes the flux values to solar minimum, 1965, Mt. Washington neutron monitor = 2400 for easier comparison to other published results.

Table 5a

INTEGRAL FLUXES (particles/m^2 ster sec)

Charge Group	Present Experiment (>3.25 GV)	Webber et al., 1973 (>0.85 GeV/nuc)	Bhatia et al., 1970 (>1.0 GeV/nuc)	Webber & Ormes, 1967 (>3.25 GV)
$10 \leq Z \leq 14$ (LH)	1.54 ± 0.13		2.0 ± 0.2 ($10 \leq Z \leq 15$)	1.84 ± 0.20
$15 \leq Z \leq 19$ (MH)	0.290 ± 0.058		0.45 ± 0.10 ($16 \leq Z \leq 19$)	0.250 ± 0.045
$20 \leq Z \leq 23$	0.210 ± 0.051			
$24 \leq Z \leq 30$ (Fe Group)	0.360 ± 0.075	0.352 ± 0.018		
$15 \leq Z \leq 23$	0.481 ± 0.075	0.345 ± 0.019 ($17 \leq Z \leq 25$)		
$20 \leq Z \leq 28$ (VH)	0.577 ± 0.091		0.6 ± 0.10	0.69 ± 0.09

Table 5b
INTEGRAL FLUXES (particles/m^2 ster sec)

Charge Group	Present Experiment (>4.9 GV)	Smith et al., 1973 (>5 GV)	Juliusson et al., 1972 (>1.6 GeV/nuc)
$10 \leq Z \leq 14$ (LH)	0.958 ± 0.070	1.50 ± 0.03	1.067 ± 0.028
$15 \leq Z \leq 19$ (MH)	0.180 ± 0.029		0.127 ± 0.023
$20 \leq Z \leq 23$	0.115 ± 0.026		0.112 ± 0.011
$24 \leq Z \leq 30$ (Fe Group)	0.237 ± 0.044	0.30 ± 0.03	0.275 ± 0.014
$15 \leq Z \leq 23$	0.287 ± 0.037	0.36 ± 0.03	0.239 ± 0.033
$20 \leq Z \leq 28$ (VH)	0.350 ± 0.049		0.387 ± 0.037

Table 5b (continued)
INTEGRAL FLUXES (particles/m^2 ster sec)

Charge Group	Balasubrahmanyan & Ormes, 1973 (>4.5 GV)	Webber et al., 1973 (>5.0 GV)	Mewaldt et al., 1971 (>4.9 GV)
$10 \leq Z \leq 14$ (LH)	1.08 ± 0.20		
$15 \leq Z \leq 19$ (MH)			0.14 ± 0.03 ($16 \leq Z \leq 19$)
$20 \leq Z \leq 23$			
$24 \leq Z \leq 30$ (Fe Group)		0.207 ± 0.014	
$15 \leq Z \leq 23$	0.30 ± 0.06	0.228 ± 0.014 ($17 \leq Z \leq 25$)	
$20 \leq Z \leq 28$ (VH)	0.44 ± 0.09		0.470 ± 0.034

Table 5b (continued)
INTEGRAL FLUXES (particles/m^2 ster sec)

Charge Group	Webber & Ormes 1967 (>4.9 GV)	Freier & Waddington, 1968 (>4.9 GV)	von Rosenvinge, 1969 (>4.9 GV)
$10 \leq Z \leq 14$ (LH)	1.2 ± 0.1		1.086 ± 0.051
$15 \leq Z \leq 19$ (MH)	0.12 ± 0.04	0.086 ± 0.010 ($16 \leq Z \leq 19$)	0.160 ± 0.020
$20 \leq Z \leq 23$			
$24 \leq Z \leq 30$ (Fe Group)			
$15 \leq Z \leq 23$			
$20 \leq Z \leq 28$ (VH)	0.36 ± 0.06	0.403 ± 0.023	0.377 ± 0.040

IV.B. Charge Composition, $10 \leq Z \leq 28$

IV.B. 1. Present Experiment

The results of the charge composition study of this experiment for charges ten through twenty eight are listed in Table 6. This table lists the actual number of nuclei of each charge observed along with correction factors as calculated in the previous chapter of this paper. The last column shows the number of each charge, $10 \leq Z \leq 28$, that would have been observed at the top of the atmosphere by extrapolating the corrected number of events observed back through 7.4 g/cm^2 of air using the attenuation mean free paths in air as directly determined in this experiment and the latest set of fragmentation parameters in air as presented in Table 3. The errors shown in column 4 are the cumulative effects of statistics, errors in correction for misidentification of charges, and correction for interactions in the detector. Errors given in column 5 reflect these errors plus the additional error involved in extrapolating to the top of the atmosphere, i.e. it reflects the uncertainties of about 20% in the fragmentation parameters and about 20% in the absorption mean free paths.

The abundances at the top of the atmosphere of the charges Z = 10 - 28, normalized to iron, are shown in Figure 14.

Table 6

CHARGE COMPOSITION, $10 \leq Z \leq 28$

Charge	Number Observed	Correction Factors*	Number Observed (Corrected for Losses)	Number Incident at Top of Atmosphere
10	997 ± 32		1513 ± 140	1620 ± 154
11	192 ± 14		291 ± 33	275 ± 35
12	1035 ± 32	(1.15 ±0.09) (1.32 ±0.05)	1571 ± 145	1764 ± 169
13	164 ± 13		249 ± 29	254 ± 31
14	776 ± 28		1178 ± 111	1376 ± 137
15	57 ± 8		78 ± 13	69 ± 14
16	249 ± 16		339 ± 39	350 ± 42
17	47 ± 7	(1.00 ±0.08) (1.36 ±0.05)	64 ± 11	42 ± 12
18	137 ± 12		186 ± 24	165 ± 27
19	42 ± 6		57 ± 10	26 ± 15
20	158 ± 13		221 ± 26	229 ± 30
21	34 ± 6	(1.00 ±0.07) (1.40 ±0.05)	48 ± 9	44 ± 11
22	113 ± 10		158 ± 20	117 ± 28
23	66 ± 8		92 ± 14	61 ± 22
24	103 ± 10		151 ± 19	117 ± 31
25	46 ± 7		68 ± 12	70 ± 22
26	412 ± 20	(1.00 ±0.04) (1.47 ±0.06)	606 ± 54	941 ± 122
27	14 ± 4		21 ± 6	33 ± 10
28	24 ± 5		35 ± 7	54 ± 19

*(Correction for events outside identification limit)
(Correction for interactions in charge module)

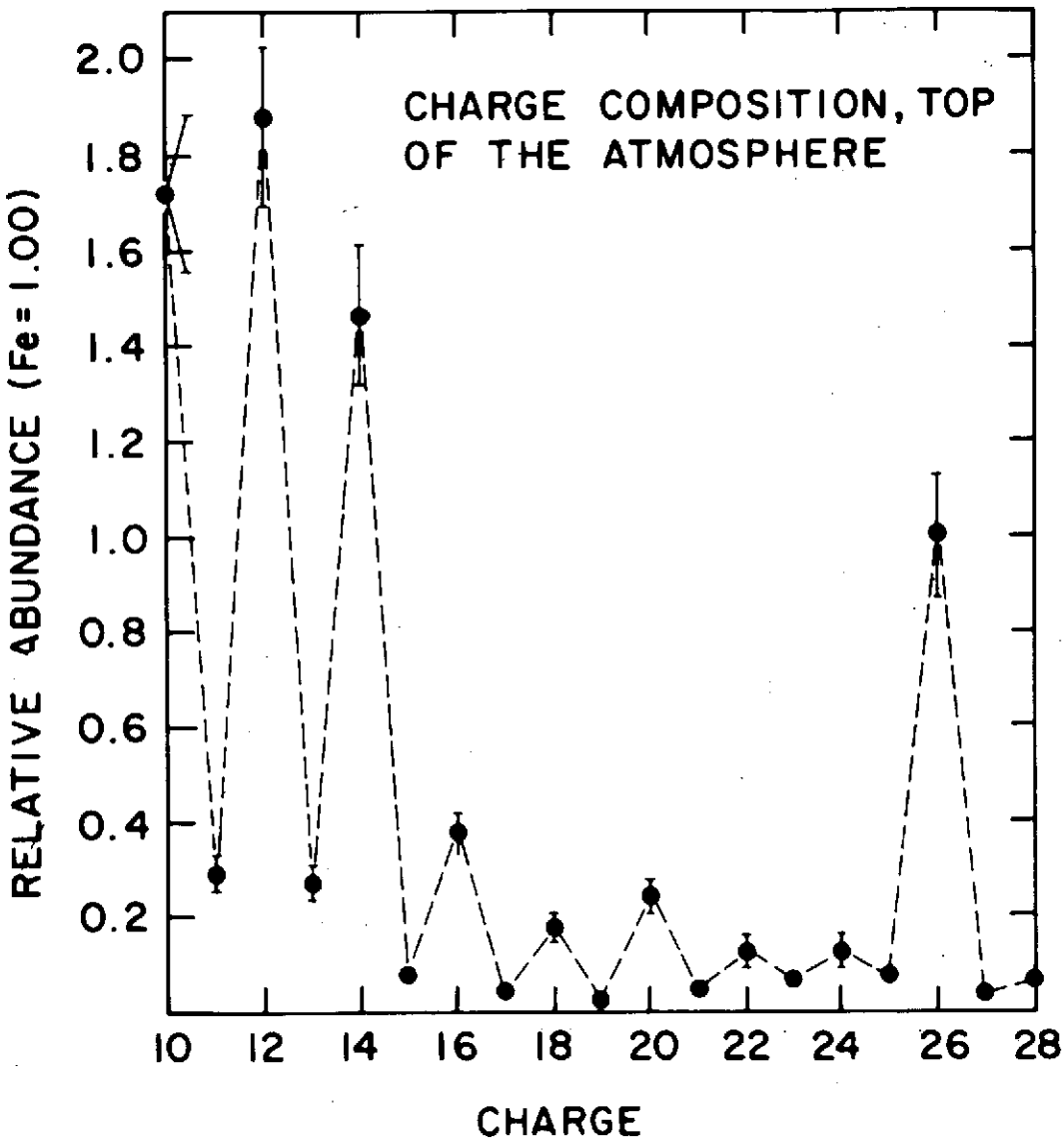

Fig. 14. Charge composition, Z = 10–28, at the top of the atmosphere, normalized to the iron abundance.

IV.B. 2. Comparison With Other Measurements

In Figures 15-16, and Table 7 the results of the relative abundances of this experiment are compared to those of other workers. The comparison between the work of various authors is sometimes difficult since groups of elements are not always chosen in the same way. However, recently several groups have published results on abundances of individual charges. (Webber et al., 1972; Juliusson et al., 1972; Casse et al., 1971). The present results are compared to these works. Also for comparison is one set of low energy results (Cartwright et al., 1973) and one satellite measurement (Lezniak et al., 1970, Pioneer 8) which is included since it is free of atmospheric corrections.

Figure 15 compares the results of the present experiment to two recent review papers, one by Tsao et al. (1973) and one by Webber (1972). These two papers have summarized the results published to date. Both sets of authors have weighted the summary to those results which have the greatest statistics and best charge resolution. The greatest disagreement exists at charges 10, 12, and 14 where the results differ by almost 15%, a seemingly not large error. But since these charges are believed to be present at the source, the discrepancies affect the predictions of the mechanism for nucleosynthesis. (See Chapter V). A factor of two difference in the potassium abundance is noted but due to the large statistical error in this measurement, it is not considered serious.

Table 7 compares the results of 3 recent charge composition surveys to the results obtained by this author (Webber et al., 1972; Casse et al., 1971; Juliusson et al., 1972). These results were chosen for comparison because they demonstrate charge composition as measured by several different

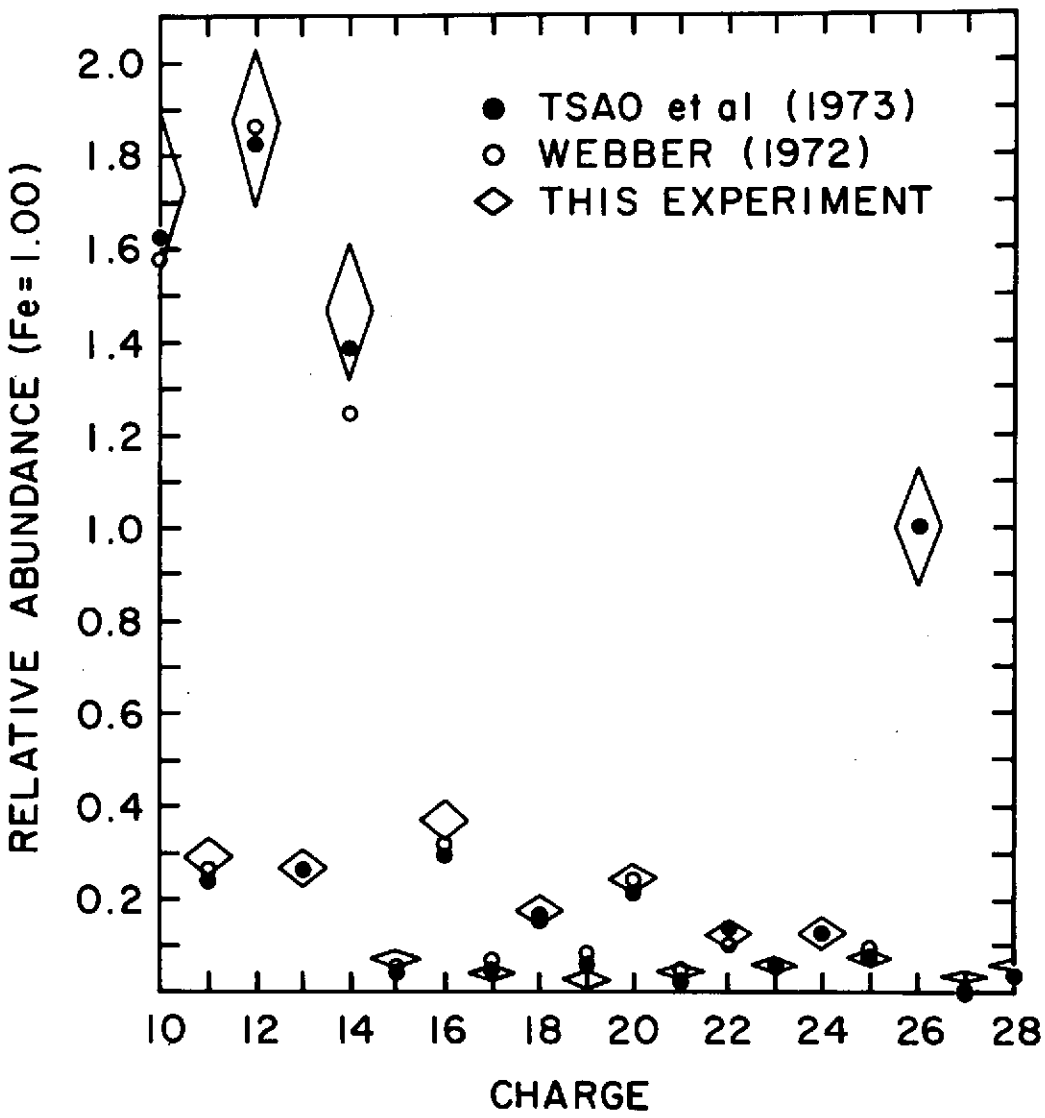

Fig. 15. Charge composition, Z = 10-28, at the top of the atmosphere compared to the review article summaries of Webber (1972) and Tsao et al. (1973), normalized to the iron abundance.

Table 7

CHARGE COMPOSITION MEASURED IN THIS EXPERIMENT
COMPARED TO OTHER RESULTS

Charge	This Experiment	Tsao et al., 1973	Webber, 1972	Webber et al., 1972	Casse et al., 1971
10	1.722 ± 0.164	1.625 ± 0.185	1.582 ± 0.106	1.695 ± 0.055	1.691 ± 0.229
11	0.292 ± 0.037	0.249 ± 0.037	0.264 ± 0.035	0.276 ± 0.018	0.323 ± 0.105
12	1.875 ± 0.180	1.825 ± 0.093	1.864 ± 0.070	1.962 ± 0.045	1.981 ± 0.248
13	0.270 ± 0.033	0.269 ± 0.093	0.264 ± 0.049	0.248 ± 0.018	0.543 ± 0.133
14	1.462 ± 0.146	1.386 ± 0.185	1.245 ± 0.070	1.295 ± 0.036	1.669 ± 0.229
15	0.073 ± 0.015	0.050 ± 0.019	0.052 ± 0.014	0.043 ± 0.009	0.090 ± 0.048
16	0.372 ± 0.045	0.299 ± 0.037	0.318 ± 0.042	0.333 ± 0.018	0.230 ± 0.040
17	0.045 ± 0.013	0.060 ± 0.019	0.063 ± 0.007	0.053 ± 0.009	0.060 ± 0.020
18	0.175 ± 0.029	0.160 ± 0.028	0.155 ± 0.014	0.124 ± 0.018	0.090 ± 0.030
19	0.028 ± 0.016	0.070 ± 0.019	0.085 ± 0.021	0.114 ± 0.009	0.140 ± 0.030
20	0.243 ± 0.032	0.210 ± 0.046	0.236 ± 0.021	0.248 ± 0.018	0.140 ± 0.030
21	0.047 ± 0.012	0.030 ± 0.019	0.045 ± 0.007	0.038 ± 0.006	0.070 ± 0.020
22	0.124 ± 0.030	0.132 ± 0.028	0.109 ± 0.021	0.133 ± 0.009	0.170 ± 0.030
23	0.065 ± 0.023	0.070 ± 0.028	0.059 ± 0.007	0.048 ± 0.009	0.050 ± 0.020
24	0.124 ± 0.033	0.126 ± 0.037	0.127 ± 0.014	0.102 ± 0.009	0.090 ± 0.020
25	0.074 ± 0.023	0.070 ± 0.019	0.091 ± 0.021	0.081 ± 0.009	0.120 ± 0.030
26	1.000 ± 0.130	1.000 ± 0.130	1.000 ± 0.070	1.000 ± 0.036	1.000 ± 0.190
27	0.035 ± 0.011	0.002 ± 0.004		0.037 ± 0.009	
28	0.057 ± 0.020	0.042 ± 0.009	0.045 ± 0.014	0.042 ± 0.009	

Table 7 (continued)

CHARGE COMPOSITION MEASURED IN THIS EXPERIMENT
COMPARED TO OTHER RESULTS

Charge	Juliusson et al., 1972	Lezniak et al., 1971	Cartwright et al., 1973
10	1.292 ± 0.033	2.665 ± 0.110	
11	0.218 ± 0.006	0.526 ± 0.048	
12	1.700 ± 0.042	2.751 ± 0.110	
13	0.348 ± 0.015	0.593 ± 0.059	
14	1.383 ± 0.033	1.986 ± 0.091	1.176 ± 0.118
15	0.054 ± 0.030	0.254 ± 0.050	0.078 ± 0.020
16	0.269 ± 0.013	0.268 ± 0.060	0.196 ± 0.029
17	0.068 ± 0.026	0.134 ± 0.030	0.029 ± 0.009
18	0.105 ± 0.028	0.196 ± 0.040	0.108 ± 0.029
19	0.092 ± 0.008	0.153 ± 0.040	0.039 ± 0.009
20	0.213 ± 0.011	0.306 ± 0.060	0.127 ± 0.029
21	0.066 ± 0.018	0.077 ± 0.020	0.020 ± 0.009
22	0.152 ± 0.015	0.100 ± 0.030	0.027 ± 0.039
23	0.089 ± 0.007	0.120 ± 0.030	0.039 ± 0.020
24	0.167 ± 0.008	0.290 ± 0.060	0.118 ± 0.049
25	0.043 ± 0.025	0.200 ± 0.040	0.142 ± 0.074
26	1.000 ± 0.010	1.000 ± 0.069	1.000 ± 0.108
27	0.017 ± 0.016		
28	0.046 ± 0.020		

methods: Webber et al. (1972) use a combination scintillator - Cerenkov counter detector but compensate for differences in path length using curved detector elements; Casse et al. (1971) use as the prime measuring element the Cerenkov detectors with spark chamber plates and photography for trajectory determination; the Juliusson et al. (1972) experiment makes use of gas Cerenkov counters for high energy charge composition measurements. A comparison of the results in more detail follows.

The only discrepancy that exists between the Webber et al. (1972) results and the results presented here occurs at charge 19. This is certainly not a serious discrepancy. The error bar is large on potassium due to its low absolute abundance. In addition, potassium is difficult to separate from its much more abundant neighbor, calcium. The relative abundance for silicon differs by about 15% between the 2 experiments. However the error bars do overlap, bringing the values into reasonable agreement (less than 1σ).

The results of Casse et al. (1971) differ in many minor respects from the results obtained here. Statistically their results are about a factor of 3 poorer, which could explain these differences. In most cases in fact, the large statistical error bars on their measurements bring their results into agreement with those reported here.

Less neon relative to iron is detected by Juliusson et al. (1972) than the present results and when compared to other authors. However, this discrepancy is only 1σ in most cases. Charge 23 has a large statistical error bar due to its low absolute abundance and also agrees to within 1σ of these results.

The satellite results (Pioneer 8) of Lezniak et al. (1970) and the low

energy (40-450 MeV/nuc) data of Cartwright et al. (1973) are included for completeness. Satellite results of course are not subject to atmospheric corrections. However, the results of Pioneer 8 do not agree very well at all with the bulk of balloon launched experiments. As can be seen from Figure 16, all charges relative to iron are overabundant when compared to atmospheric experiments. In particular chromium and manganese are overabundant by factors of 2 and 3 respectively relative to balloon borne experiments, leading this author to believe that some iron has been misidentified as these lower charges, thus reducing the iron abundance and increasing the relative abundances. There are no serious discrepancies between the present results and those at low energy (Cartwright et al., 1973) when account is taken of the large statistical error in their measurements, although there appears to be a systematic underabundance of even nuclei relative to iron when compared to the present experiment. This results however, from the fact that their data lumps charges 25-27 together as iron, resulting in a larger iron abundance than is present. Another interpretation of this data has come to light in recent measurements of the charge composition at various energies (Webber et al., 1973; Balasubrahmanyan and Ormes, 1973; Smith et al., 1973; Juliusson et al., 1972; Casse et al., 1971). Results of these experiments indicate that the energy spectrum of iron group nuclei is not as steep as the energy spectra of other groups of nuclei. Therefore the ratio relative to iron of these other elements decreases with increasing energy. The results of Lezniak et al. and Cartwright et al. were taken at low energies where the ratio (Z=10-14)/(Z=24-28) would be higher than in the present experiment which is taken at high energies.

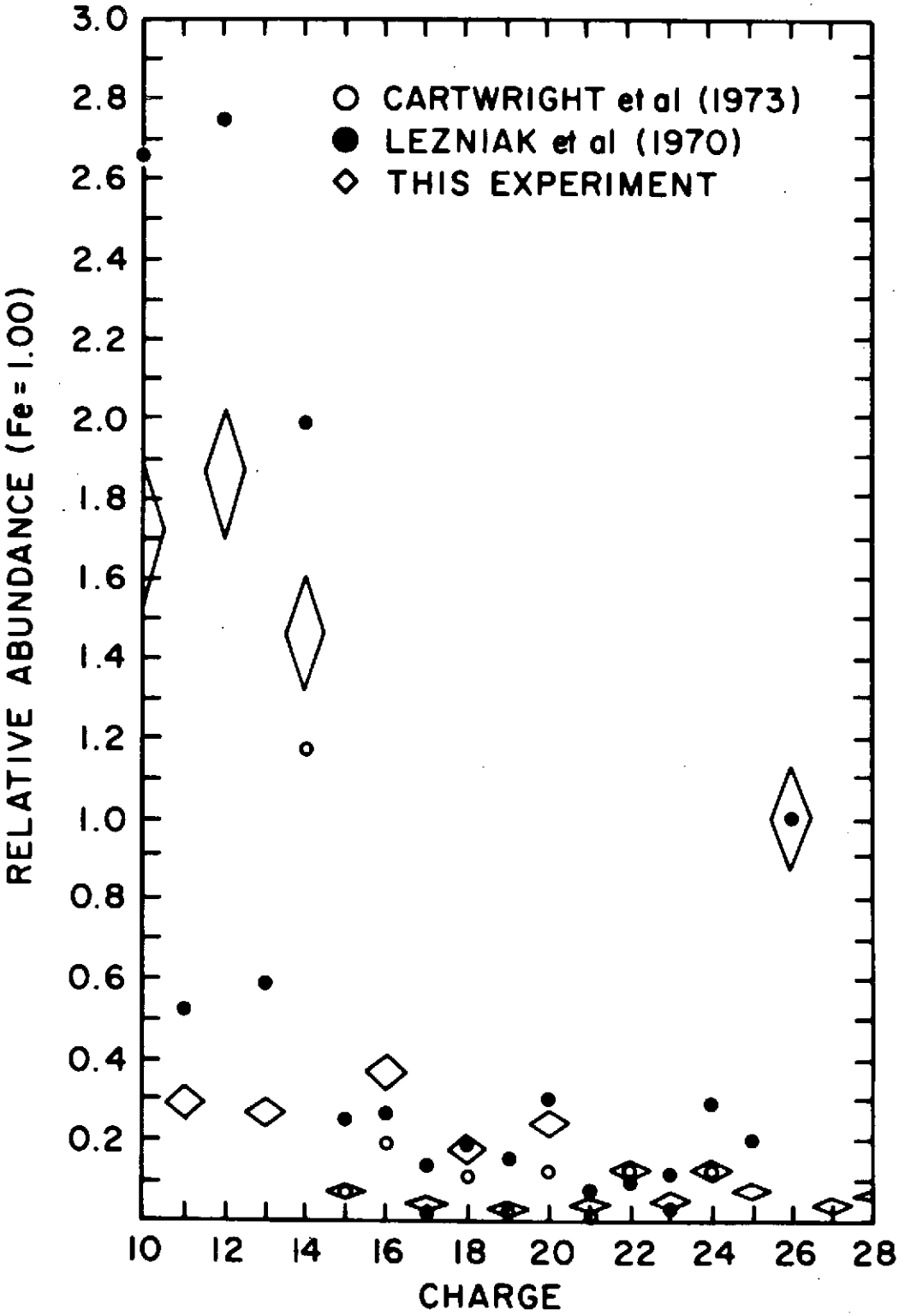

Fig. 16. Charge composition, Z = 10-28, at the top of the atmosphere compared to the low energy results of Cartwright et al. (1973) and Lezniak et al. (1970), normalized to iron.

Mentioned in passing are two other experiments: the pioneer work in this field by von Rosenvinge (1969) and the large exposure factor experiment of Mewaldt et al. (1973). von Rosenvinge's results, although statistically extremely poor, nevertheless agree within errors with the results of the present experiment and the bulk of larger, more sophisticated experiments. Mewaldt et al. have published the most significant statistical survey to date. However, their experimental charge resolution is so poor that they could identify only even charges with certainty. Therefore, their results were not included for comparison.

V. INTERPRETATION OF EXPERIMENTAL RESULTS

V.A. Extrapolation Back to Source

After leaving their source region, cosmic rays diffuse through interstellar space. During the propagation of these charged nuclei through interstellar matter, the nuclei will be subject to the effects of the matter and the magnetic fields traversed. The matter affects the primary cosmic radiation through energy loss due to ionization processes and charge alteration due to nuclear interactions. The magnetic fields isotropize the arrival direction of the nuclei and may affect the energy of individual nuclei through acceleration and/or deceleration. The magnitude of the effect of matter depends both on the nature and on the amount of matter traversed, which in turn depends on the configuration and strength of the magnetic fields experienced by nuclei during their traversal of the medium.

Charge ratios outside the solar cavity depend importantly on the characteristics of the propagation of the primary cosmic radiation in interstellar space, and on the injection spectra which may not be identical from charge to charge. Cosmic ray nuclei arriving at the boundary of the solar cavity then would not be expected to have the same relative charge abundance that they have at the source, due to the effects of the propagation. One may ask: what is the initial distribution (source distribution) of elements which, enroute to the solar cavity, would be transformed to the observed distribution, and how does one find this source distribution?

In the previous section, the charge distribution outside the solar cavity is presented. The final step in the analysis is to reverse the process outlined in the previous paragraph and "propagate" the data back

to the source. This source composition can then be examined for its possible meaning. In this section then, by assuming various propagation parameters such as fragmentation probabilities, interaction mean free paths, an exponential distribution of path lengths, and the experimentally observed charge composition, restrictions can be placed on the source composition.

In any attempt to discuss the propagation of cosmic ray nuclei through interstellar material and the consequent distortion of the charge composition, it is first of all necessary to make some general assumptions regarding the model of the Galaxy and the source model to be used in the calculations. Regarding the source model: it will be assumed that the source spectra of all multiply charged nuclei have the same shape, and further that it is to be a power law in total energy. Another assumption that must be made is that the light nuclei, Li-Be-B, are absent at the source, i.e. they are all secondary, but this assumption is of no consequence here since the results are confined to $10 \leq Z \leq 28$. (These elements are known to be absent in the solar system abundances, a fact which can be explained by their high nuclear reaction rates at the temperatures obtained in the solar interior: nuclear reactions proceed quickly enough to consume them completely. Extrapolation of this result to stellar interiors, which have as high or higher temperatures, is therefore not unreasonable.)

The leaky box model (Gloeckler and Jokipii, 1969) of the Galaxy will be used in the following analysis. This model assumes the cosmic ray sources are uniformly distributed in a spherical volume in space with the Sun at the center, that particle emission is constant in time, and that

equilibrium is established between creation and loss. Cosmic rays then diffuse through and are confined to this region which is bounded, although there is a finite probability for escape which can be characterized by a mean life against escape, T, commonly referred to as the leakage lifetime. This model is probably most realistic from the point of view of the current understanding of the cosmic ray origin-propagation problem and magnetic field structure of the Galaxy. It is mathematically equivalent to an exponential path length distribution first suggested by Davis (1960). The exponential path length is smooth, is strongly weighted toward short path lengths but also contains very long path lengths, and is assumed to be independent of the energy/nucleon of the particle.

It is assumed that particle propagation is the same for all charges apart from the effects of interactions. It is assumed cosmic rays are not accelerated or decelerated in interstellar space. The effects of energy loss through ionization are also excluded. Parker shows that these effects are negligible for particles above 4.5 GV rigidity (Parker, 1966). Cowsik et al. (1967) showed that for steady state propagation, the effect of ionization loss is not very drastic for heavy nuclei even at the lowest energies of several hundred MeV/nucleon. Gloeckler and Jokipii (1969) find ionization energy loss only significant below about 200 MeV/nucleon. The energy losses for all nuclei under consideration here are less than 20%, as found by Beck and Yiou (1968), e.g. at 1.5 GeV/nucleon the energy losses along a generally accepted cosmic ray path of 5 g/cm^2 are about 250 MeV for an iron nucleus, which is only 15%. Error due to neglect of energy loss processes is further minimized since only charge ratios of integral fluxes over a limited region are treated. Further, it is assumed that at high

energy, (relativistic) comsic ray transport is independent of energy.

Lastly, it is assumed that the interstellar medium is composed of pure hydrogen. This assumption is not of much consequence since the effects of ionization energy loss have been excluded already. However even with ionization energy loss, this assumption is still valid. Durgaprasad considered propagation in an ionized medium of pure (~89%) and ionized (~4%) hydrogen, and pure (~6%) and ionized (~1%) helium (Durgaprasad, 1968). He showed there was no significant difference between the rate of energy loss in the pure hydrogen medium and the "combination" medium which approximated interstellar space.

With the previously mentioned assumptions, one can determine how the cosmic ray charge distribution is altered by fragmentation as the particles propagate from sources to the observer by solving the following system of differential equations, which describe the collisional breakup of parent nuclides, and the production and loss of secondary ones in successive increments of path length:

$$\frac{dN_i(x)}{dx} = -\frac{N_i}{\Lambda_i} - \frac{N_i(x)}{\Lambda_i} + \sum_{j<i} \frac{N_j(x)}{\Lambda_j} P_{ji} \qquad (22)$$

Here $N_i(x)$ is the number of nuclei of the i^{th} charge component at a distance x g/cm^2 from the source. The first term on the right is the loss due to nuclear interactions which alter the identity of a nucleus, the second term is the loss due to leakage, the third term is production of secondary nuclei due to nuclei of greater Z. The first and second terms can be combined together to form an effective absorption mean free path:

$$\frac{1}{\Lambda} = \frac{1}{\Lambda_1} + \frac{1}{\Lambda_1} . \qquad (23)$$

In order to solve this set of equations which extrapolates the observed charge spectrum back to the hypothetical source region, one needs to know:

1. the nuclear interaction cross sections for each isotope passing through interstellar space, from which are calculated the fragmentation probabilities, (i.e. the probability that a particular fragment will be produced in a nuclear interaction), and the absorption mean free paths in hydrogen,
2. the path length distribution of nuclei during their diffusive travel from source to detector.

Most of the nuclear parameters of k. are not well known experimentally. These parameters have been calculated from the semi-empirical cross section formula of Silberberg and Tsao (1973) rather than Rudstam (1966). They derive their formula using Rudstam's formula as a basis but using new experimental values for cross sections not available to Rudstam. The errors calculated from their formula are much smaller, with standard deviations of about 10-20%, than Rudstam's formula, with factors of 2-4, when compared to experimentally known values. The parameters have been obtained from Silberberg and Tsao (private communication, 1973) with the aid of their computer algorithm that gives values for energies $\geq$2.3 GeV/nucleon, at which energy they become constant, for the most abundant isotopes between iron and neon. (The errors involved in using the parameters down to 1.5 GeV/nucleon are small, $\approx$ 5%). The values of the fragmentation parameters used are given in Table 8. Since the interactions occur in a low density medium where the nuclei spend a long time, all radioactive nuclei produced have been assumed to decay to stable end products, except those whose sole mode of decay is K-capture and those with half-lives greater than 10^6 years. The fragmentation probabilities, given

Table 8

FRAGMENTATION PROBABILITIES FOR COLLISIONS
WITH HYDROGEN (Silberberg and Tsao, 1973)

Target Product	26	25	24	23	22	21	20	19	18	17	16	15	14	13	12	11	10
26																	
25	.0490																
24	.1212	.1179															
23	.0712	.0766	.0787														
22	.0955	.1026	.1197	.1361													
21	.0182	.0184	.0236	.0243	.0270												
20	.0545	.0567	.0661	.0762	.0894	.1084											
19	.0303	.0322	.0362	.0421	.0506	.0612	.0628										
18	.0500	.0521	.0567	.0697	.0809	.0962	.0646	.0914									
17	.0212	.0245	.0268	.0324	.0388	.0437	.0305	.0436	.0537								
16	.0424	.0444	.0488	.0551	.0675	.0804	.0503	.0705	.0875	.1132							
15	.0136	.0153	.0142	.0178	.0219	.0227	.0144	.0210	.0239	.0288	.0280						
14	.0318	.0337	.0378	.0438	.0523	.0612	.0359	.0514	.0616	.0741	.0862	.1287					
13	.0136	.0138	.0142	.0178	.0202	.0227	.0108	.0171	.0199	.0226	.0216	.0345	.0411				
12	.0273	.0291	.0315	.0357	.0422	.0490	.0287	.0438	.0457	.0535	.0625	.0897	.1111	.1476			
11	.0106	.0123	.0126	.0146	.0169	.0192	.0090	.0133	.0159	.0185	.0172	.0253	.0290	.0356	.0485		
10	.0212	.0230	.0252	.0376	.0337	.0385	.0233	.0305	.0358	.0391	.0453	.0598	.0725	.0891	.1078	.1552	

in Table 8, are calculated from

$$P_{ji} = P(Z_t, A_t; Z_p, A_p) \tag{24}$$

$$= \sum_{A_p} \sigma (Z_t, A_t; Z_p, A_p)/\sigma_t$$

where $\sigma (Z_t, A_t; Z_p, A_p)$ is the nuclear interaction cross section for the production of element (Z_p, A_p) from element (Z_t, A_t) and σ_t is the total inelastic cross section of element (Z_t, A_t) with

$$\sigma_t = 10\pi (1.25)^2 [A^{2/3} - 1] \tag{25}$$

(Silberberg and Tsao, private communication, 1973). The absorption mean free paths in hydrogen, given in Table 9, have been calculated from $\Lambda_i = m_p/\sigma_i$ where m_p = mass of the proton.

The problem of what form of distribution of path lengths goes to make up the average amount of interstellar matter traversed is not well understood, and deserves a few more remarks than given in the introductory paragraphs of this section. Models used have ranged from a distribution that is a δ-function (simple slab approximation) in which all particles traverse the same amount of matter, to a Gaussian distribution centered on some mean value, which arises from considering a point source in a homogeneous isotropic diffusive medium (Balasubrahmanyan et al., 1965), to an exponential distribution $\Phi(x)\, dx = a\, e^{-ax}$ which arises from considering propagation in a bounded medium (Cowsik et al., 1967). The slab model is used for atmospheric corrections but is physically artificial for interstellar propagation. The Gaussian distribution, although physically more realistic, does not fit experimental evidence and can also be rejected. (Shapiro et al.,

Table 9

ABSORPTION MEAN FREE PATHS IN HYDROGEN

Charge	MFP (g/cm^2)
10	5.14
11	4.80
12	4.50
13	4.25
14	4.03
15	3.84
16	3.60
17	3.44
18	3.32
19	3.18
20	3.00
21	2.92
22	2.82
23	2.71
24	2.63
25	2.56
26	2.53

1970b) Calculations done by several authors indicate that not only is the exponential distribution the most physically realistic[/], but it fits the existing data most accurately. Shapiro et al. (1970a, b) found the slab model could not reproduce the observed abundance of L-nuclei given the observed abundance of $17 \leq Z \leq 25$ which are produced from iron nuclei. They found the exponential vacuum path length with exp (-016 ± 0.04) x fit the observed charge ratios at high energies ($E > 1.5$ GeV/nucleon) best. Cowsik et al. (1967) conclude that the generally used matter-slab approximation for interstellar matter traversed by cosmic radiation leads to an erroneous interpretation of the experimental data. They find that the matter slab is inconsistent with low energy data and show that propagation of cosmic rays must involve a wide distribution of path lengths (Cowsik et al., 1970). The data collected by von Rosenvinge and his analysis (von Rosenvinge, 1969) is also consistent with an exponential path length. Mewaldt et al. (1971) also conclude that the simple slab model does not fit their data but an exponential does. Using new measurements for production cross sections, Shapiro et al. (1971) still find the observed L/M ratio and $(17 \leq Z \leq 25)$/Fe ratio can be reproduced best by a pure exponential distribution of path lengths of the form exp $(-0.23\ x)$ for $x > 1$ and a linear increase from zero to 1 g/cm^2.

The treatment here then will be limited to the pure exponential vacuum path length distribution of the form:

$$\frac{dN}{dx} \approx \exp\ (-x/x_o) \tag{26}$$

[/]The exponential path length distribution arises from a uniform spherical distribution of sources in a bounded medium with the Sun at the center. Fichtel and Reames (1966), however, have deduced strictly from diffusion theory an exponential-like distribution so similar to a pure exponential that its application to existing data can not differentiate between them.

where x is the mean path length traversed by cosmic rays, or age since $x_o = \beta c n m_p \tau$ where τ is cosmic ray age; The exponential distribution used here is $dN/dx \propto e^{-0.20x}$ as shown in Figure 17.

Using the values given for the propagation parameters and an exponential path length distribution in the differential equations indicated previously, it is relatively easy to calculate from the observed charge spectrum what the equivalent spectrum should have been before passage through some assumed mean amount of matter. One starts with the heaviest element, iron, and assumes there is no fragmentation into the iron group from heavier nuclei (the ratio $[Z \geq 30]/Fe$ is $< 10^{-5}$). The calculations have been performed according to the matrix solution method outlined in von Rosenvinge (1969). The method calculates the source abundance of each element in turn beginning with iron nuclei by extrapolating the abundance of each element back through an exponential path length distribution of matter, before calculating the source abundance of the next lower element. This allows the abundance of any one element to increase or decrease as secondaries, tertiaries, quaternaries, etc. enter its abundance and secondaries, tertiaries, quaternaries, etc. leave the abundance. This procedure can result in negative abundances of certain elements before the extrapolation is complete. Each charge is considered to have contributed to fragmentation only so long as the abundance of that element is positive. When the abundance of an element reaches zero or goes negative, that abundance is "frozen" at zero in the calculation so that it can not contribute further to secondary production during the calculations of succeeding lower elements. This fragmentation would produce "negative" secondaries which would incorrectly decrease the abundance of lower elements. Clearly a

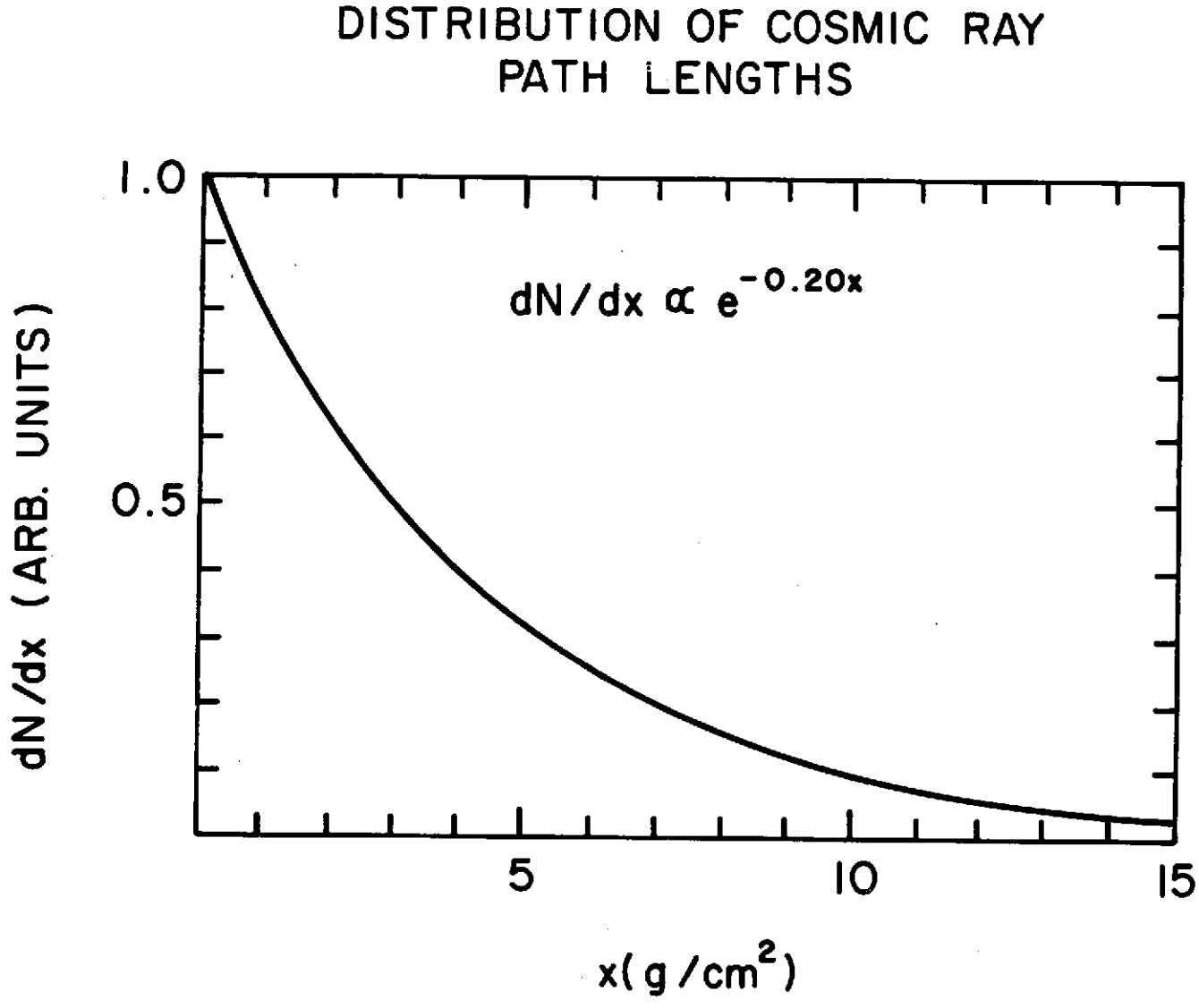

Fig. 17. Exponential distribution of cosmic ray path lengths, $dN/dx \propto e^{-0.20x}$.

limit is set on such an extrapolation if many of the deduced abundances become negative. If these negative abundances reach significant values, this implies it is physically unreasonable to postulate propagation through as much matter as assumed. This sets an upper limit on the amount of matter traversed. (However it is not possible to set a lower limit from heavy nuclei alone since the primary spectrum has a variable path length distribution. To establish a lower limit, an independent piece of information, such as the L/M ratio, must be used). Slight negative abundances of a few individual elements also may be used to test the assumption that these nuclei are absent in the sources.

The detailed predictions of these calculated extrapolations lead to the source composition shown in Figure 18. Numbers for the source abundances relative to iron and the error bars are given in column 3 of Table 11 where they are also compared to solar system abundances. Errors on the relative abundances are due to the effects of errors in the composition at the top of the atmosphere and uncertainties of about 20% in the fragmentation probabilities and absorption mean free paths. Errors due to composition uncertainty range from less than 1% at sodium to 60% at chlorine and vanadium. Errors due to uncertainty of the fragmentation parameters range from 1% at silicon to about 60% at chlorine, titanium, and vanadium. Errors due to uncertainties in the mean free paths range from less than 1% at silicon to about 60% at chlorine, titanium, and vanadium. Generally, for a given element, the fragmentation probability contributed the largest portion of the cumulative error, it being a factor of 2 larger than other errors. In all cases, errors in the absorption mean free paths were the smallest contributors to the cumulative error.

Various forms of an exponential distribution of path lengths were tried.

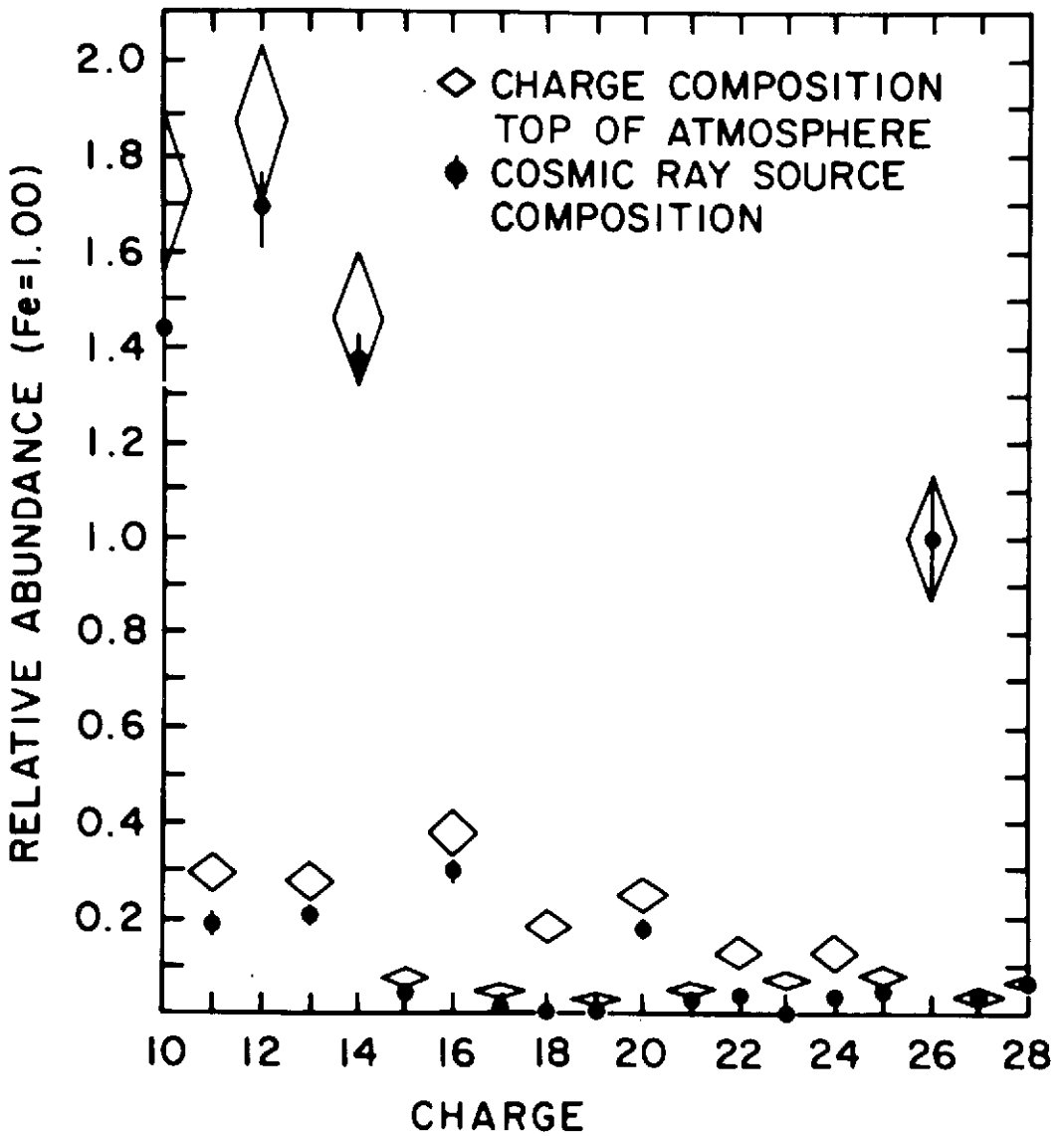

Fig. 18. Comparison of cosmic ray source composition to the cosmic ray charge composition at the top of the atmosphere.

Limits on the distribution were established as exp(-0.16x) to exp(-0.24x) which correspond to mean amounts of matter of 6.3 g/cm^2 and 4.2 g/cm^2 respectively. The lower limit is established at the thickness of matter where the first element reaches zero or goes negative. This occurred for potassium after about 4.2 g/cm^2. After this amount of matter however, most other secondary elements such as chlorine, scandium, and vanadium still had positive abundances. The upper limit is established by requiring the abundances of all charges 21-25 to reach zero or go negative. Of course, after this amount of matter, elements such as chlorine, argon, and potassium had large negative abundances. After a mean amount of matter of 5.0 g/cm^2, the abundances of argon and potassium were only slightly negative, chlorine and vanadium were zero, and scandium, titanium, chromium, and manganese were only slightly positive. This was chosen as the optimum value: $5^{+1}_{-0.8}$ g/cm^2 for the mean amount of matter cosmic rays have traversed.

From Figure 18 it can be seen that by x = 5 g/cm^2 the average abundance of the elements 15 and 17 to 19 is zero. The abundances of nuclei $21 \leq Z \leq 25$ are also nearly zero at about 5 g/cm^2. These nuclei are thought to be due to the interstellar fragmentation of iron since their abundances are very low in the solar system, only about 0.02 that of iron (Cameron, 1973). Hence one must conclude that heavy nuclei in cosmic radiation cannot have traversed much more than 5 g/cm^2 of interstellar matter, although they could have traversed less, if one assumes these nuclei are present at the source.

There appear to be finite abundances of S and Ca at the source. The source ratios of these elements are: Ca/Fe = 0.18 $\pm$0.01, S/Fe = 0.29 $\pm$0.02. The data is therefore consistent with a source consisting predominantly of

iron, silicon, magnesium, and neon with small percentage admixtures of S and Ca. The mean matter length $x = 5^{+1.3}_{-0.8}$ g/cm^2 resulting from an exponential path length distribution is also consistent with values found to fit the L/M ratio and VVH nuclei. (Gloeckler and Jokipii, 1969, find a value of 4.0 $\pm$0.8 g/cm^2 using the L/M ratio; Cowsik et al., 1970, find a value of 5.3 to 8.6 g.cm^2 using VVH data; Shapiro et al., 1970, find a value of $6.26^{+2.08}_{-1.25}$ using the L/M ratio and letting the abundance of Z = 17-25 go to zero; Fowler et al., 1970, find a value of 4.0 $\pm$2.0 g/cm^2 using their VVH data).

V.B. Cosmic Ray Age - Amount of Matter in Interstellar Space

Nuclei in the charge range Z = 17-25, in particular odd charges 17 and 19, and all charges 21-25, are believed to be produced mostly by spallation reactions of iron and its passage thorugh interstellar matter (Lezniak et al., 1970). This implies their source composition is zero.

If one assumes that the mean amount of matter traversed is that which is found by extrapolating the observed composition back through sufficient material such that these abundances become zero, as done in the previous section, then this estimate of the mean amount of matter through which cosmic rays have passed leads to an estimate of the age of cosmic rays. The mean density of matter in interstellar space traversed by cosmic ray nuclei is related to x, the total amount of matter traversed in g/cm^2 by the relation

$$x = \bar{\rho}\, \beta c\, \tau \qquad (27)$$

Here βc is the mean velocity of nuclei. For this experiment $\beta = 1$ (relativistic cosmic rays). The quantity x as determined in the previous section is 5.0 g/cm^2. With the generally accepted assumption of the average density of interstellar space in the disc of one hydrogen atom per cubic centimeter (if cosmic rays are confined to the disc), this leads to a time $\tau = 3.2 \,^{+0.8}_{-0.5} \times 10^6$ years which cosmic rays must spend in the disc.

Another method exists for the determination of the age of cosmic rays: using as the measuring device the time dilated decay of Be^{10} moving with relativistic velocity. This isotope has a half-life at rest of 1.5×10^6 years and is suitable for the measurement of ages in the range $10^6 - 10^8$ years. This method consists of measuring the isotopic abundance of beryllium or the variation with energy of the ratio of beryllium to boron. The age is then estimated from the ratio

Be^{10}/Be^{7+9+10}

which depends on the amount of time Be^{10} has had to decay; or the age is estimated from the ratio

Be/B

which should vary with energy due to the time dilation of the decay of Be^{10} to B^{10} via the reaction

$$Be^{10} \rightarrow B^{10} + e + \nu.$$

These two ratios measure cosmic ray age directly. They give $\tau \simeq 3.4 \times 10^6$ years (Webber et al., 1973), a value which is in good agreement with the value obtained here (nb: the estimate of cosmic ray age using beryllium and boron abundances depends on x, the mean amount of matter through which cosmic rays have passed, but is independent of $\bar{\rho}$, the average interstellar density. However the mean amount of matter can be estimated by other means such as the L/M ratio, and does not depend on the value found here for heavy particles. Hence these 2 estimates of cosmic ray age can be considered to be independent of each other).

V.C. Comparison to Solar System Abundances

Before comparing the cosmic ray source composition to solar system abundances, the cosmic ray source composition obtained in this paper will be compared to results obtained by other authors. Several authors have recently published possible source abundances of cosmic ray nuclei in the charge range $10 \leq Z \leq 30$, including von Rosenvinge (1969), Shapiro and Silberberg (1970b), Ramaty and Lingenfelter (1971), Shapiro et al. (1971), Cartwright et al. (1971), Webber et al. (1972), and Shapiro et al. (1973), using a variety of forms of an exponential distribution of path lengths and fragmentation parameters from Rudstam's equations and from Silberberg and Tsao's equations. Table 10 lists the cosmic ray source composition deduced by several authors (Webber et al., 1972; Ramaty and Lingenfelter, 1971; Shapiro et al., 1973) including the results calculated here. This paper uses an exponential distribution exp(-0.20x) with the Silberberg and Tsao parameters, Shapiro et al. (1973) use an exponential distribution exp(-0.24x) for $x > 1$ g/cm^2 and a linear rise from $x = 0$ to $x = 1$ g/cm^2 with the Silberberg and Tsao parameters, Ramaty and Lingenfelter (1971) use an exponential distribution exp(-0.20x) with the Rudstam parameters, and Webber et al. (1972) use an exponential distribution exp(-0.20x) with an earlier form of the Silberberg and Tsao parameters (Shapiro and Silberberg, 1970a).

Upon comparison of this work to these authors, one concludes that there are still wide variations in the deduced cosmic ray source composition. The wide variations are not completely explained as due to the different exponential forms for path length distribution and Rudstam's parameters or Silberberg and Tsao's parameters used by the various authors. Factors of

Table 10

COMPARISON OF DEDUCED COSMIC RAY SOURCE COMPOSITION OF SEVERAL AUTHORS

Charge	This Calculation	Shapiro et al. (1973)	Ramaty and Lingenfelter (1971)	Webber et al. (1972)
10	1.443 ± 0.121	0.780 ± 0.098	0.850	0.868 ± 0.029
11	0.185 ± 0.024	0.039 ± 0.020	0.040	0.067 ± 0.020
12	1.684 ± 0.077	1.122 ± 0.098	1.110	1.200 ± 0.035
13	0.205 ± 0.015	0.098 ± 0.049	0.051	0.110 ± 0.022
14	1.375 ± 0.052	0.995 ± 0.146	0.890	0.890 ± 0.030
15	0.042 ± 0.007	0.010 ± 0.010	0.002	0.010 ± 0.010
16	0.294 ± 0.021	0.146 ± 0.029	0.130	0.175 ± 0.025
17	0.005 ± 0.005	0.0	0.0	0.010 ± 0.010
18	0.0 ± 0.010	0.034 ± 0.024	0.032	0.015 ± 0.015
19	0.0 ± 0.010	0.0	0.0	0.019 ± 0.012
20	0.180 ± 0.010	0.107 ± 0.039	0.0	0.130 ± 0.020
21	0.027 ± 0.007	0.0	0.0	0.015 ± 0.015
22	0.035 ± 0.035	0.0	0.0	0.035 ± 0.022
23	0.005 ± 0.005	0.0	0.0	0.010 ± 0.010
24	0.036 ± 0.024	0.015 ± 0.015	0.20	0.030 ± 0.030
25	0.047 ± 0.015	0.010 ± 0.010	0.045	0.025 ± 0.015
26	1.000 ± 0.130	1.000 ± 0.146	1.000	1.000 ± 0.033
27	0.035 ± 0.007	0.0		0.0
28	0.057 ± 0.007	0.039 ± 0.010		0.035 ± 0.007

4 and 5 differences occur between the Rudstam, and Silberberg and Tsao parameters which could explain the variations between the Webber et al. results, the Ramaty and Lingenfelter results, and those reported here. A 20% error in the fragmentation parameters accounts for about 1/2 of the errors on the deduced source abundances quoted here. This would not explain the variation between the Shapiro et al. results and those reported here since the same fragmentation parameters were used. It is not believed that the variation in source composition is due to the exponential distribution of path length chosen: Ramaty and Lingenfelter (1971), using several propagation models, conclude that the source abundances are not strongly model-dependent, a conclusion also reached by this author. Rather it is suggested that the wide disparity between the deduced source composition of various authors is due to compositional uncertainties at the top of the atmosphere. Errors in the composition at the top of the atmosphere account for the remaining 1/2 of the error in the deduced source abundance of most elements quoted here. In the last few years, subtle but significant changes have occurred in the cosmic ray composition at the top of the atmosphere, for example the chromium abundance mentioned in the next paragraph. These changes are probably responsible for the variations in the deduced cosmic ray source composition since the results reported here begin with the Ramaty and Lingenfelter work in 1971 up through to the present work in 1973.

The results of this investigation reveal that the elements neon, magnesium, silicon, and iron dominate the distribution. Sulfur must also be present at the source in large amounts relative to iron. Calcium is definitely present in cosmic ray sources but there is probably no source

abundance of argon in agreement with Shapiro et al. (1973) and Webber et al. (1972). Earlier experimental measurements showed a sizable Cr/Fe ratio at both high and low energies (Mathieson et al., 1968; Waddington et al., 1970; Lezniak et al., 1970; Dayton et al., 1970; Price et al., 1970; Garcia-Munoz and Simpson, 1970), forcing the conclusion that substantial chromium existed at the source (Shapiro and Silberberg, 1970b; von Rosenvinge, 1969; Ramaty and Lingenfelter, 1971). More recent measurements with better resolution and greater statistics show a lower flux of chromium (Binns et al., 1971; Webber et al., 1971; Casse et al., 1971; Mewaldt et al., 1973). The chromium abundance observed in this experiment is low enough to conclude that it is principally secondary in origin, in agreement with the conclusions of Shapiro et al. (1973) and Webber et al. (1972).

If one somewhat arbitrarily states that a source abundance is "real" if less than 25% of the abundance at the top of the atmosphere were due to secondaries, then one can conclude that the trend of the most recent experimental and theoretical work favors finite source abundances in this charge range of neon, magnesium, silicon, sulfur, calcium, and iron. If $> 50\%$ of the abundance of an element observed at the top of the atmosphere is due to spallation, then these elements probably do not exist in the sources. Elements in this group are Cr, V, Ti, Sc, K, Ar, Cl, and P. The region from 25-50% secondary production is nebulous and probably indicates some source abundance. The source abundances are probably ≤ 0.20 of iron, with large uncertainties attached. Elements in this group are Mn, Al, and Na.

After extrapolation back to the cosmic ray source region, the cosmic ray source abundances (CRS), although similar in general features, are different from the solar system abundances when examined for fine points of

detail. Table 11 and Figure 19 compare the deduced cosmic ray source composition to the solar system composition as reported by Cameron (Cameron, 1973), both relative abundances normalized to iron, Z = 26. The abundances given by Cameron in this paper are intended to represent the typical values in the solar system, or for normal main sequence stars. These solar system abundances (SS) are derived from meteorites, solar photosphere and chromosphere spectroscopic measurements, with some input from measurements of energetic solar particle abundances, and a few interpolated values values based on nucleosynthesis theory. The following discussion examines in more detail the finer points of the table and figure where the CRS and SS abundances differ.

In general, there is a relative richness of heavy nuclei in the cosmic rays with a strongly peaked iron group and a large even-odd effect, when compared to the SS abundance. Neon, magnesium, silicon, and sulfur are clearly present in cosmic rays. The presence of these elements in cosmic rays, however, indicates a somewhat different evolution than the solar system. Although neon is underabundant in CRS relative to SS, the value for neon in the SS comes from solar cosmic ray observations which come from solar flare events, and hence may not be representative of the "universal" SS abundance. The ratios CRS/SS for magnesium and silicon are very close to 1. There is a large uncertainty in the SS abundance of sulfur. Cameron chose 0.6 because this amount can be produced by nucleosynthesis under hydrostatic equilibrium conditions which is the process believed to be responsible for the elemental abundances in the sun.

The odd elements, sodium and aluminum, have ratios CRS/SS which are still close to 1 suggesting they might have a common origin.

Table 11

COMPARISON OF SOLAR SYSTEM ABUNDANCES
TO COSMIC RAY SOURCE ABUNDANCES (NORMALIZED TO IRON)

Charge	SS (Cameron, 1973)	CRS	CR (Top of Atmosphere)
10-Ne	4.14	1.443 ± 0.121	1.722 ± 0.164
11-Na	0.072	0.185 ± 0.024	0.292 ± 0.037
12-Mg	1.278	1.684 ± 0.077	1.875 ± 0.180
13-Al	0.102	0.205 ± 0.015	0.270 ± 0.033
14-Si	1.205	1.375 ± 0.052	1.462 ± 0.146
15-P	0.012	0.042 ± 0.007	0.073 ± 0.015
16-S	0.602	0.294 ± 0.021	0.372 ± 0.045
17-Cl	6.867×10^{-3}	0.005 ± 0.005	0.045 ± 0.013
18-Ar	0.141	0.0 ± 0.010	0.175 ± 0.029
19-K	$5.060 \times^{-3}$	0.0 ± 0.010	0.028 ± 0.016
20-Ca	0.087	0.180 ± 0.010	0.243 ± 0.032
21-Sc	4.217×10^{-5}	0.027 ± 0.007	0.047 ± 0.012
22-Ti	3.343×10^{-3}	0.035 ± 0.035	0.124 ± 0.030
23-V	3.157×10^{-4}	0.005 ± 0.005	0.065 ± 0.023
24-Cr	0.015	0.036 ± 0.024	0.124 ± 0.033
25-Mn	0.011	0.047 ± 0.015	0.074 ± 0.023
26-Fe	1.000	1.000 ± 0.130	1.000 ± 0.130
27-Co	2.663×10^{-3}	0.034 ± 0.005	0.035 ± 0.011
28-Ni	0.058	0.060 ± 0.007	0.057 ± 0.020

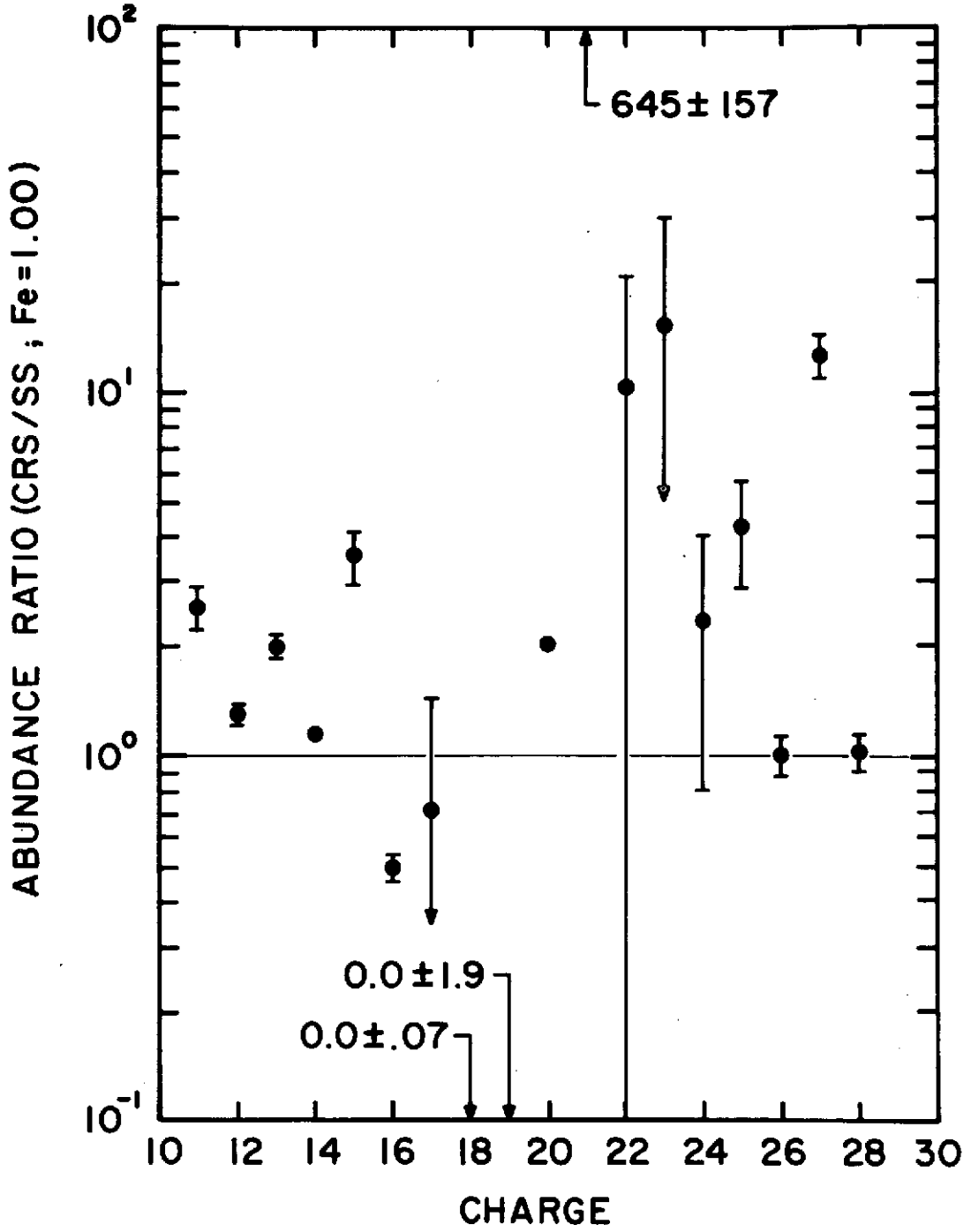

Fig. 19. Comparison of cosmic ray source composition to solar system abundances, normalized to iron.

Examination of Table 11 reveals the relative rarity in the SS of elements of chlorine to manganese, which is also true of CR source abundances. The argon abundance is an anomaly: there is no argon in cosmic ray source regions. This is a significant disagreement with the SS where some argon appears to exist. However, it should be noted that the SS argon value is poorly known. Cameron's abundance value for A^{36} is simply an interpolation between the observed abundances of S^{32} and Ca^{40}.

Table 11 and Figure 19 indicate a cosmic ray excess at calcium, and the heavier elements around the iron peak, chromium, and manganese. Only about one quarter of the calcium has resulted from fragmentation, implying that this element had to be present at the source. In the Z = 21-25 region, the overabundance of chromium and manganese in the CRS relative to SS abundances is apparent, along with possible overabundances of titanium and vanadium.

Although cobalt and nickel were not extrapolated back to the source region, the source abundance should be about the same as that detected at the top of the atmosphere since the spallation contribution to these two elements from elements $Z \geq 30$ is negligible and loss processes should be identical to iron.

The differences in the CRS and SS abundances examined in the preceding discussion are not as regular as might be expected if cosmic rays were preferentially accelerated from a sample of solar-like material. If the CRS/SS ratios are the same (equal to 1) then cosmic rays must have been formed by the same mechanism that produces elements in the Sun, but if the ratios are not equal, the abundances may be compared to other models in an attempt to determine the formation process for their origin. Knowledge

of the relative abundances of cosmic rays when compared to solar system abundances places boundary conditions on models for cosmic ray production.

The differences in the relative abundances of CRS and SS suggest some form of systematic nuclear evolution of the cosmic ray abundances beyond that observed in solar matter.

V.D. Possible Source of Primary Cosmic Radiation

The endpoint of the study undertaken here should be to relate the results obtained in this study on the cosmic ray source composition to the abundance distribution that might be expected to exist in cosmic ray sources based on the predictions of nucleosynthesis theories. In this manner, one can identify, or at least place restrictions on, the cosmic ray source and/or mechanisms responsible for the production of primary cosmic radiation. For example, if cosmic radiation has its origin in the late stages of supernova evolution, then the relative abundances should reflect the abundances of energetic supernova ejecta.

The idea that the bulk of primary radiation is ejected during supernova explosions is not new (Burbidge et al., 1957; Ginsburg and Syrovatskii, 1964). Theoretical models of supernovae predict such violent explosions as to imply significant element synthesis up through iron by the thermonuclear reactions that occur under these extreme conditions. The explosion itself ejects material from the outer regions of the star, this same material which has been processed to the iron peak by explosive burning. If this highly energetic ejected material becomes primary cosmic radiation, then cosmic rays should reflect the source composition of explosive nucleosynthesis, after the effects of interstellar propagation are removed, as stated by Arnett (1973):

> "With improving data, better known fragmentation cross sections, and a better understanding of the process of cosmic ray propagation, the cosmic radiation may be a powerful tool for exploring explosive events."

This author feels these conditions are now reasonably well satisfied, and

wishes to undertake just such a study as further suggested by Arnett in that same review article.

> "A detailed quantitative comparison of cosmic ray source abundances with predictions of explosive nucleosynthesis may soon be possible."

Up to this time, most of the predictions of the theory of explosive nucleosynthesis have been compared to solar system abundances (cf. Arnett, 1969; Truran and Arnett, 1970; Michaud and Fowler, 1972; Arnett and Clayton, 1970; Arnett et al., 1971). The features of solar system abundance distribution of elements can be reproduced with a good degree of success by calculating the nucleosynthesis that takes place when massive stars burn their evolved cores and outer layers violently and quickly on a hydrodynamic timescale. This excellent agreement suggests that supernovae can produce the heavy element abundances through explosive nucleosynthesis. However, the results of the predictions agree mostly with the solar system abundances, but as pointed out in section V.C. cosmic ray composition differs in some important respects from solar system abundances. Only three very brief studies have attempted to compare cosmic ray relative abundances to solar system relative abundances: Kozlovsky and Ramaty (1973) who compared only Mg, Si and Fe; Arnett and Schramm (1973) who compared Ne, Mg, Si, and Fe; and Mewaldt (1971) who compared only the even elements in the charge range $16 \geq Z \geq 26$.

An attempt will not be made here to go into the intricacies of explosive nucleosynthesis. It is a topic unto itself. Only the results of the predictions of the theory of explosive nucleosynthesis through carbon burning, oxygen burning, and silicon burning will be presented and compared to cosmic ray source abundances. The reader is referred to the detailed

papers of combinations of authors such as Arnett, Clayton, Truran, and Woosley (cf papers referenced in the previous paragraph: Arnett (1969) and Arnett et al. (1971) for explosive carbon burning; Truran and Arnett (1970) for explosive oxygen burning; Clayton and Peters (1970) and Michaud and Fowler (1972) for explosive silicon burning.)

Briefly, however, the elements neon to aluminum can only be produced by carbon burning, silicon to calcium by oxygen burning, and the higher Z elements by silicon burning. These various forms of explosive nucleosynthesis can occur in several different mass zones of a star where boundary conditions of density and temperature are satisfied for each form of nucleosynthesis. None of these forms of nucleosynthesis can produce the relative abundances of all the elements from charge 10 to 28 due to "freeze-out" of nuclear reactions as expansion occurs after the explosion. But if it can be assumed that conditions in different mass zones are satisfied for each form of explosive nucleosynthesis as the explosion proceeds outward through the star, then the results of each form of nucleosynthesis can be added: high Z elements would be formed in inner zones, intermediate Z elements in intermediate mass zones, and low Z elements in outer mass zones.

The abundances in column 5 of Table 12 represent the integrated matter ejected from explosive nucleosynthesis of the supernova model, i.e. it represents an integration over the products of explosive carbon burning, explosive oxygen burning, and explosive silicon burning (cf previously referenced papers in this section).

Can the abundances of elements in groups one and three, designated previously as those which are known with reasonable certainty to be primary, be produced by explosive nucleosynthesis as would occur in supernovae?

Table 12

COMPARISON OF DEDUCED COSMIC RAY SOURCE COMPOSITION TO EXPLOSIVE NUCLEOSYNTHESIS PREDICTIONS

Charge	Composition (Top of Atmosphere)	Secondary Production	Cosmic Ray Source	Explosive Nucleosynthesis Predictions/
Ni	0.057	0.0	0.057 ± 0.007	0.066
Co	0.035	0.0	0.035 ± 0.005	0.001
Fe	1.000	0.0	1.000 ± 0.130	1.000
Mn	0.074	0.027	0.047 ± 0.015	0.005
Cr	0.124	0.088	0.036 ± 0.024	0.015
V	0.065	0.060	0.005 ± 0.005	0.001
Ti	0.124	0.090	0.035 ± 0.035	0.004
Sc	0.047	0.020	0.027 ± 0.007	0.0
Ca	0.243	0.063	0.180 ± 0.010	0.173
K	0.028	0.028	0.0 ± 0.010	0.003
Ar	0.175	0.175	0.0 ± 0.010	0.126
Cl	0.045	0.040	0.005 ± 0.005	0.002
S	0.372	0.078	0.294 ± 0.021	0.663
P	0.073	0.031	0.042 ± 0.007	0.001
Si	1.462	0.087	1.375 ± 0.052	1.389
Al	0.270	0.065	0.205 ± 0.015	0.109
Mg	1.875	0.191	1.684 ± 0.077	1.037
Na	0.292	0.107	0.185 ± 0.024	0.080
Ne	1.722	0.279	1.443 ± 0.121	2.565

/Taken from Arnett and Clayton (1970), Michaud & Fowler (1972), Arnett (1969), and Truran and Arnett (1970).

Figure 20 compares the predictions of explosive nucleosynthesis for the abundances of elements to the cosmic ray source composition found here for those elements in groups 1 and 3 - Ne, Na, Mg, Al, Si, S, Ca, Mn, Fe, and Ni. This integrated model leads to abundance predictions which are in good agreement within a factor of 2 or 3 with the cosmic ray source distribution found here. Magnesium and silicon are believed to be products of explosive nucleosynthesis. If these elements in CRS abundances have explosive nucleosynthesis as their common origin, then the ratio (CRS/EN) should be close to 1. The ratio close to 1 calculated here is consistent with this viewpoint. Since argon is believed to be the product of nucleosynthesis of silicon with subsequent α-particle capture, its low value at the cosmic ray source may be an important clue to the nature of nucleosynthesis at the source, i.e. whether it is hydrostatic burning as in main sequence stars or explosive nucleosynthesis, as in supernovae. However, the abundance value of argon is not known well enough to include it for comparison at this time. The previously noted overabundances of cosmic ray sources relative to the solar system of Cr and Mn, and possible Ti and V, is a clue which reveals that nucleosynthesis must have proceeded further in cosmic ray sources than in the solar system. The ratio (CRS/EN) of Mn substantiates this conclusion. (The source abundances of Cr, Ti, and V are also not known well enough to include for comparison to models of explosive nucleosynthesis). However this ratio is large enough to suggest that the abundance of manganese, or extrapolation of manganese back to the source is in error. The presence of nickel in cosmic ray sources with an abundance of 5% of iron indicates that nucleosynthesis processes which terminate at iron must not completely dominate the production of cosmic rays at the sources.

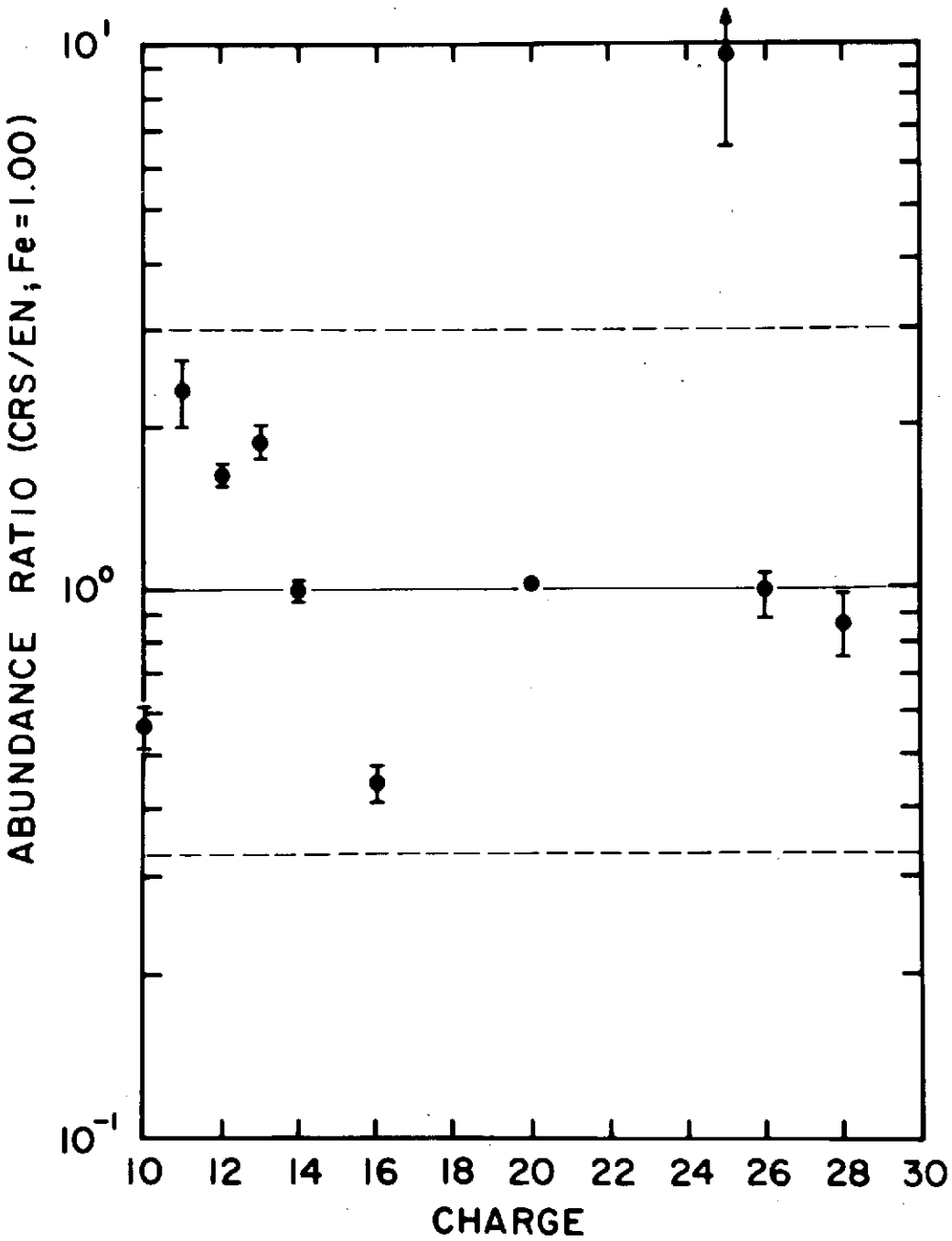

Fig. 20. Comparison of deduced cosmic ray source composition to the predictions of explosive nucleosynthesis, normalized to iron.

In fact, the presence of this level of nickel begins to open up the possibility of choosing between alternate source nucleosynthesis models, such as "extensive" and "complete" silicon burning predictions of Arnett and Clayton (1970).

This author finds that the cosmic ray source abundances from neon to iron calculated in this paper are consistent with the predictions of different forms of explosive nucleosynthesis as would occur in different mass zones during the supernova explosion of an ordinary highly evolved massive star, $8 \leq M/M_{\odot} \leq 70$. It is suggested that these stars may be the source of primary cosmic radiation. It should be pointed out however that there are factors of 2 and 3 involved in the predictions of the theory of explosive nucleosynthesis due to uncertainties in the theory. For example, it is not yet clear to physicists studying nucleosynthesis whether the supernova model can produce all the elements $10 \leq Z \leq 28$ in their proper relative abundances in a single event. Can the highly evolved core of a massive star implode, releasing an outgoing pressure wave which will trigger explosive nucleosynthesis of overlying non-central mass zones? If the relative abundances can not be reproduced in a single event, can the relative abundances still be produced by integrating over many events of different types of supernovae? Can the explosion itself, or a remnant of the explosion such as a pulsar or rotating neutron star, accelerate the material to the high energies observed in cosmic rays? Lastly several important isotopes known to be present in the solar system are not produced by explosive nucleosynthesis, and must be produced under other circumstances. Cosmic ray isotope measurements are awaited to clarify this discrepancy.

VI. Summary/Conclusions

It is appropriate at this point to summarize the results of this paper. About 5000 events of relativistic cosmic ray nuclei with $10 \leq Z \leq 28$ with energies greater than 1.16 Gev/nuc have been observed by the High Energy Cosmic Ray Experiment, an ionization spectrometer type detector. These data have been analyzed for their possible meaning.

Absolute fluxes of various charge groups at various rigidities, which have also been extrapolated to the top of the atmosphere using atmospheric growth curves measured on ascent and descent portions of the flight, have been presented. Integral flux values of $10 \leq Z \leq 14 = 9.58 \pm 0.70 \times 10^{-1}$, $15 \leq Z \leq 19 = 1.80 \pm 0.29 \times 10^{-1}$, $20 \leq Z \leq 23 = 1.15 \pm 0.26 \times 10^{-1}$, and $24 \leq Z \leq 28 = 2.37 \pm 0.44 \times 10^{-1}$ particles/m^2-sec-ster for rigidity greater than 4.9 GV and $10 \leq Z \leq 14 = 1.54 \pm 0.13 \times 10^{0}$, $15 \leq Z \leq 19 = 2.90 \pm 0.58 \times 10^{-1}$ and $24 \leq Z \leq 28 = 3.60 \pm 0.75 \times 10^{-1}$ particles/m^2-sec-ster for rigidity greater than 3.25 GV are reported. These results are compared to other recent measurements at similar geomagnetic latitude. The fluxes measured are generally consistent but systematically seem to be lower than those measured by other workers

Measurements of the relative abundances of these elements are in general agreement with previous results although the results presented here differ in fine detail. It is felt that the results reported in this paper represent an advancement over previous results due to the combination of the large statistical nature of the survey and good charge resolution. The results at the top of the atmosphere reported here for the more abundant elements relative to iron are: Ne/Fe = 1.722 ± 0.164, Mg/Fe = 1.875 ± 0.180, Si/Fe = 1.462 ± 0.146, Ca/Fe = 0.243 ± 0.032. Agreement amongst various

workers (Cartwright et al., 1973; Webber et al., 1972; Casse et al., 1971; Juliusson et al., 1972) in the field of cosmic radiation is now within 1σ for these more abundant elements. Agreement for the less abundant elements is not as good, probably as a result of poor collection statistics and difficulties is separating these elements from their more abundant neighbors. For example, results reported here for potassium and vanadium are: K/Fe = 0.028 ± 0.016 and V/Fe = 0.065 ± 0.023. These results differ from those of other workers mentioned above by factors of 2 and 3 in some cases, although error bars are so large that the measurements can be said to agree due to overlap of data. This charge composition observed at balloon depth has been extrapolated to the top of the atmosphere, using attenuation mean free paths measured directly by the experiment combined with the very latest data on cross sections, i.e. fragmentation probabilities, not available to previous investigators. New values of 38.5 ± 5.2, 32.4 ± 8.7, 23.7 ± 5.9, and 16.8 ± 2.7 g/cm^2 for the attenuation mean free paths in air for these same charge groups are reported. These data represent one of the most complete sets of attenuation mean free paths in air reported to date.

Propagation calculations for $10 \leq Z \leq 28$ nuclei indicate that the observed abundances are consistent with a source composition having Ne/Fe = 1.44 ± 0.12, Mg/Fe = 1.68 ± 0.08, Si/Fe = 1.38 ± 0.05, S/Fe = 0.29 ± 0.02, and Ca/Fe = 0.18 ± 0.01, with all other abundances $16 \leq Z \leq 28$, which are generally agreed to be secondary, ≤ 0.04. The abundances also have been found to be consistent with an exponential path length distribution with a mean amount of matter of $5^{+1.3}_{-0.8}$ g/cm^2.

The source composition is deficient in sulfur and argon relative to the solar system, pointing to the conclusion that cosmic rays are synthesized

under different conditions than solar system elements. It is unlikely these abundance differences are the result of propagational effects. More likely the deficiencies can be explained by differences in the environmental conditions under which the elements are synthesized. With most cosmic ray nuclei abundances in the charge range Z = 10-28 known to an accuracy comparable to solar system abundances, it can be tentatively concluded that these nuclei originated during the explosive nucleosynthesis stage of highly evolved massive stars, i.e. a supernova origin for energetic heavy cosmic rays.

Where should the study of cosmic ray physics proceed to from here? First of all, future work should concentrate somewhat on the less abundant elements between charges 10 and 28 where more definitive measurements are still needed. In particular, the abundances of chlorine, potassium, vanadium, manganese, and nickel need to be measured more accurately. Errors in composition at the top of the atmosphere are the cause of a significant part of the error in the deduced source composition. Reducing these errors will help to pin down the type of explosive nucleosynthesis responsible for the elements in this charge range. This measurement would not require an instrument any more sophisticated than the one described in this paper, a multiple scintillator - Cerenkov radiator combination; it requires more collection time at higher altitudes with improved resolution, possibly on a satellite. A suggestion for low, medium, and high energy accelerator experiments is the improved measurement of existing cross sections for interactions of charges 10 to 28 in hydrogen and air-like materials, and the filling-in of the gaps in existing cross sections. Argon is a specific case where there appears to be a discrepancy between its deduced source

abundance and the solar system abundance. This discrepancy may be due to incorrect cross sections for interaction of argon, or incorrect secondary production of argon from other elements.

One of the more promising informational studies includes a measurement of the isotopic composition of cosmic ray nuclei in this same charge region. The results of a determination of the isotopic composition of iron bears heavily on the question of how these nuclei were synthesized. For example, if the Fe^{56} isotope dominates over the Fe^{54} isotope in the iron peak, then these isotopes must have been produced during silicon burning nucleosynthesis in supernovae as opposed to other types of nucleosynthesis in which Fe^{54} would be the dominant isotope. To go one step further: the relative isotope abundance of Fe^{56}/Fe^{58} determines whether partial or complete silicon burning has occurred. This gives some indications as to conditions of temperature and neutron excess existing during the explosion, and also indicates whether the explosion was fast on a hydrodynamic time scale. For if the explosion were quick on a hydrodynamic time scale, then the material contributing to nucleosynthesis expands and cools faster than silicon burning can be completed, in which case Fe^{58} is not built up and Fe^{56} dominates the distribution. Isotopic measurements require an experiment that features mass resolution as well as considerably improved charge resolution. Some such experiments are just now coming into their own (Webber et al., 1973; Fisher et al., 1973).

An even more sensitive test of path length distribution can be made by supplementing the meager data that exists on the relative abundances of VVH and SVH nuclei, $Z \geq 30$, with more experimental results. Iron nuclei have an interaction mean free path of about 2.5 g/cm^2; lead nuclei (Z=82)

have an interaction mean free path of about 1 g/cm^2. Lead nuclei traverse about 4 or 5 mean free paths in 5 g/cm^2 of interstellar material as opposed to 2 mfp for iron. Mewaldt et al. (1971) have begun a series of measurements of $Z \geq 30$ nuclei using a multiple ionization counter detector system. Due to the low fluxes of these elements, their results have not yet provided a definitive test of the path length distribution but they are consistent with a leakage length of 5 g/cm^2.

It is important to point out that differential energy spectra measurements of cosmic rays should be made at many energies, particularly very high energies of 100 GeV/nuc. or more where recent results (Webber et al., 1973; Balasubrahmanyan and Ormes, 1973; Smith et al., 1972) indicate the relative abundances are not constant with energy, an assumption that has been made by all cosmic ray physicists in the past for analyzing data. Intercomparison of low, high, and very high energy results should aid even more in contributing to an understanding of interstellar propagation and delineating source regions. The change in slope of the spectrum of iron group nuclei detected by Ormes et al. (1972) can lead to the conclusion of 2 possible sources of cosmic ray iron nuclei, as pointed out by Ramaty et al. (1973). Changes in composition with energy detected by several groups mentioned above, i.e. the decreasing ratio of daughter nuclei to parent nuclei with increasing energy, can lead to the conclusion that confinement of cosmic rays in the galaxy is energy dependent. Many experiments can be used to make these energy spectra measurements: gas Cerenkov counters, superconducting magnets, ionization spectrometers, most of which are already in use by the groups mentioned above.

The preceding paragraphs have pointed out some experimental discrep-

ancies still existing in the field of cosmic radiation and some experiments which can be performed to resolve these discrepancies and test the various hypotheses.

It is hoped that in the near future a satellite version of this experiment can be flown so that data collected, away from atmospheric and other terrestrial effects and with much greater statistics, can be analyzed to answer these remaining questions, but which, at the same time, will probably raise many new questions.

APPENDIX A

ELECTRONICS AND THRESHOLD SETTINGS

A.1. Detector Electronics

The electronics system for this experiment can be divided into four major subsystems. The following paragraphs will describe each of these subsystems in turn. Block diagrams for the detector electronics and data handling system are presented in Figures A1 and A2.

The coincidence trigger subsystem produces the fast pulse for triggering the spark chamber and also provides the signal to initiate data handling. Its associated electronics search for coincidences between scintillator S1 and scintillator S2. As has been mentioned previously, the plastic scintillators are used to provide a coincidence event because they produce a fast pulse as opposed to the CsI scintillator which produces a slow rise-time pulse. A fast pulse is needed to initiate the spark chamber so that ionization produced by the charged particle will not diffuse too far from the particle's path. The gates for pulse height analysis of the charged particle detectors are also derived from this subsystem.

Using gates from the coincidence trigger subsystem, the charge identification electronics subsystem analyzes the pulse height distribution of the incident cosmic ray particles. Pulse height analysis is performed on all 3 scintillators and the Cerenkov radiator whenever the S1 - S2 coincidence occurs. Each pulse height analyzer is of the same design and operated over three ranges of gain. This "3-slope" analyzer then effectively has a dynamic range of 10^3 so that it could detect VH nuclei as well as protons. The basic analyzer is 256 channels and con-

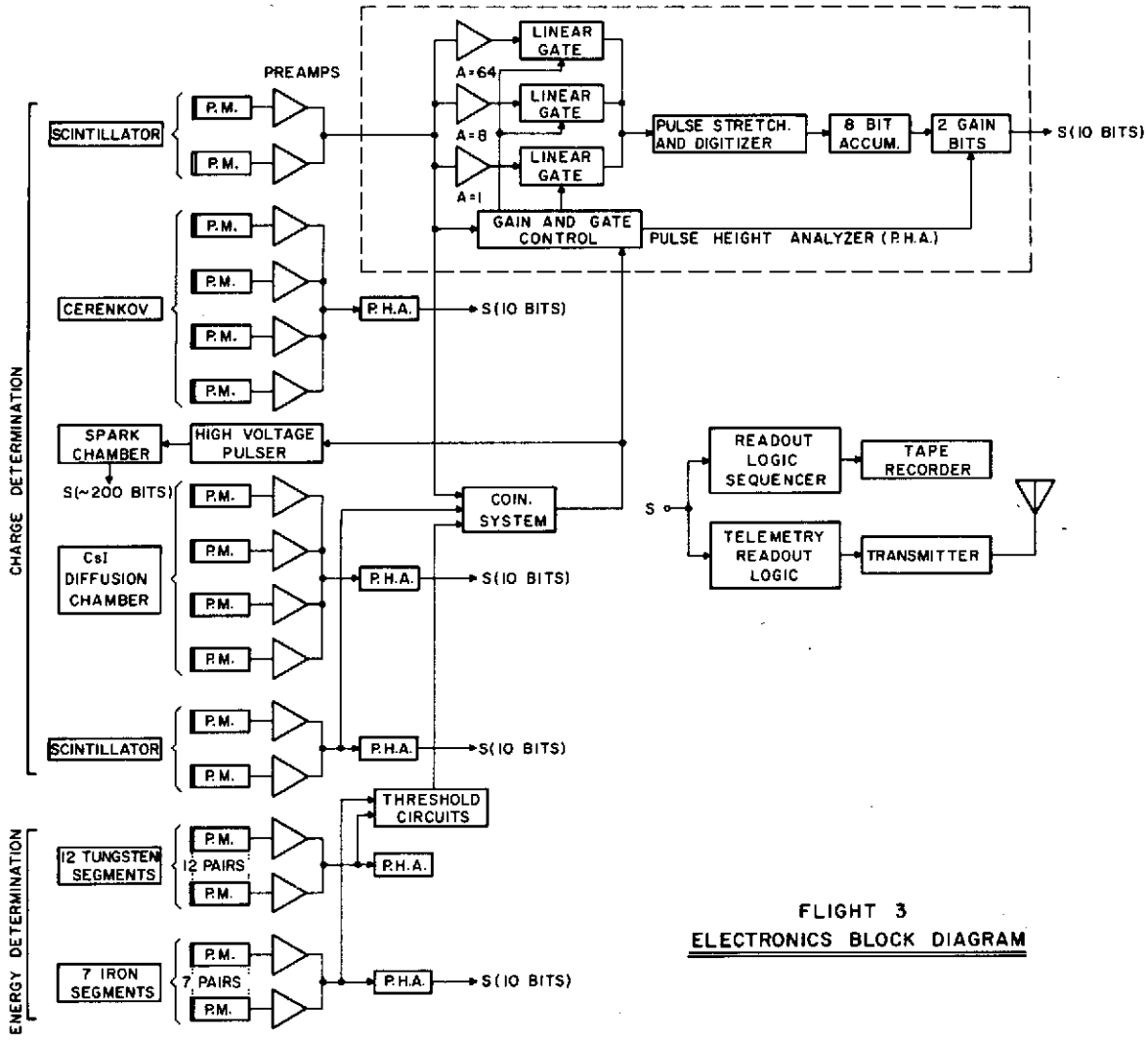

Fig. A1. Electronics block diagram.

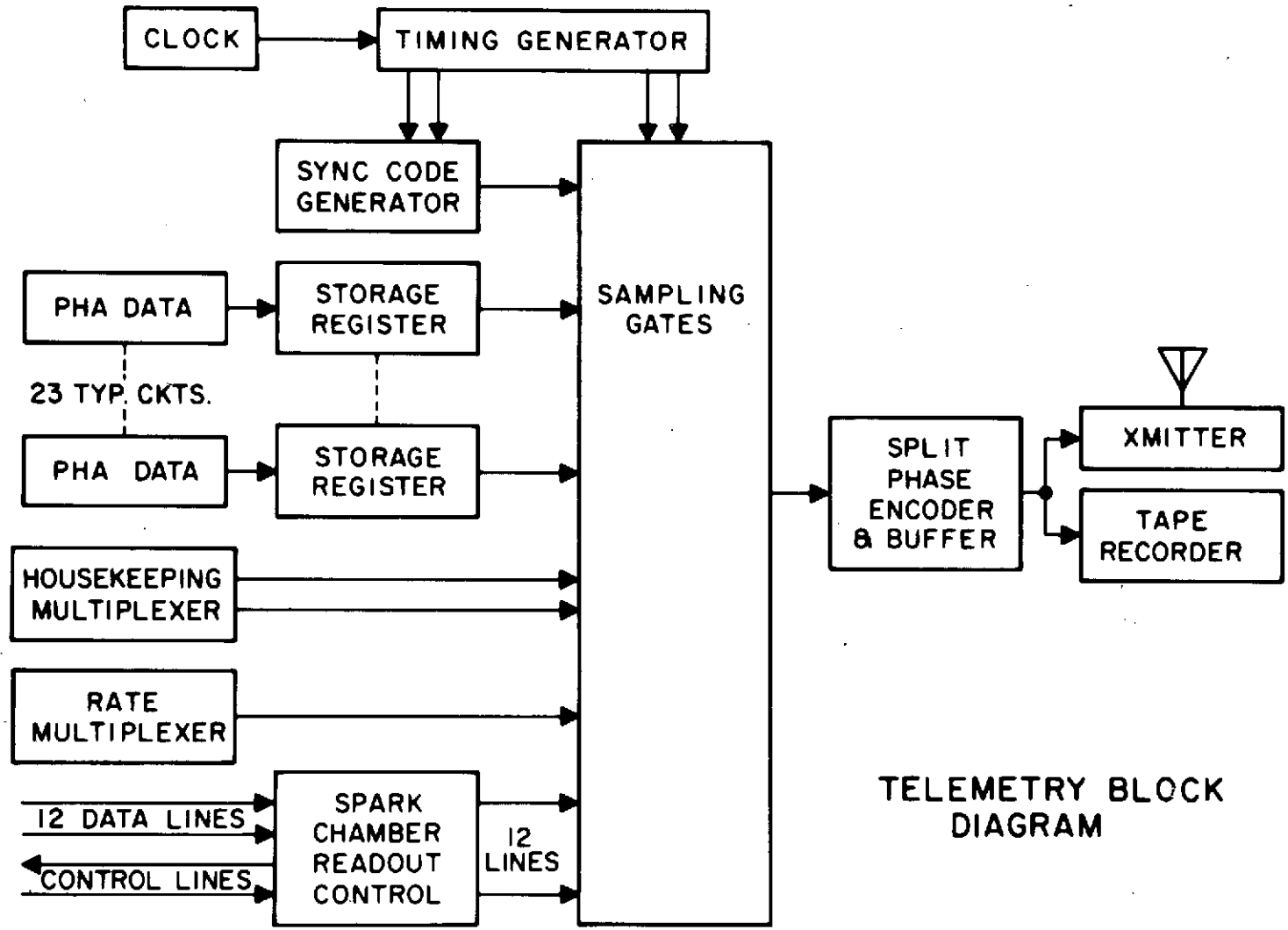

Fig. A2. Data handling and telemetry block diagram.

verted pulse analog data to digital data for readout. The threshold selection ensures that a pulse height from an event is routed to the correct range of the analyzer. Each range has an amplifier of gain ≃ 8 over the previous range. Besides the digital data for the actual pulse height value, a gain bit is also set in each data word to determine in which range the pulse height event occurred.

The gains of the four scintillators are adjusted in the laboratory by first locating the Z = 1 peak corresponding to minimum ionizing muons at sea level. (The gain of the phototubes used should easily cover the 10^4 dynamic range of pulse height values needed to record events for all charges.) The trigger levels are then set at approximately 1.5 times minimum to decrease not only background but also inhibit the large flux of protons known to be present in primary cosmic radiation. This trigger criterion then would accept all nuclei with $Z \geq 2$.

The spark chamber subsystem is capable of identifying the trajectory of the incident particles and of distinguishing whether the event is due to a single particle or multiple particles. The spark chamber readout time limited the speed of the CIM to 10 events/sec.

The data handling subsystem, or encoder, arranges all information of interest during the balloon flight into the proper format for telemetry and for recording by balloon-borne tape recorders. (Redundancy of data handling was provided in this crucial area for increased reliability.) The data was handled as a fixed format telemetry frame consisting of sync pulses, housekeeping data on temperature, external pressures, etc., and then a series of words filled by the experiment data. Whenever an event occurs, the experiment data words are filled by data in a known format. The first word is the time tag to identify

an event. The second group of words contains data from the CIM (48 bits). Data from the ionization spectrometer modules then follows (160 bits). These three fixed-length blocks of words are followed by a variable number of words of spark chamber data ($\approx$ 200 bits), and finally an end-of-event word. This results in 420 bits/event or 4200 bits/sec for events of interest which was transmitted at a 12.0 kbit/sec rate from balloon to ground via FM/FM telemetry. Twelve hours of recording time on serial PCM balloon tape recorders was allowed for this flight.

The PMTs, PHAs and readout logic operate on 45 watts of battery power. The telemetry and on-board recorder require another 5 watts, for a total power of 50 watts.

In addition to the features discussed previously, Figures A1 and A2 also emphasize the redundancy which has been built into the experiment to avoid a catastrophic failure. For example, there are two PMTs looking at each detection element, and there are two complete and independent data readout systems.

A. 2. Event Selection: Triggering Modes

The High Energy Cosmic Ray Experiment is designed to look at all of the various components of the cosmic rays above an energy 10^9 eV: the electrons, protons and multiply-charged nuclei. Because of this and the large area of the detector, complex triggering requirements have been set up to select events of interest. Were this not done, the experiment would trigger on the much more plentiful low energy proton and alpha events. By electronically selecting only those events of particular interest, the data transmission rate and spark chamber repetition rate have been reduced to an acceptable level.

To convert pulse height values to charge of particles, the one particle normalization point must be known. The background flux of muons at sea level provides a convenient means of calibrating the detectors in units of single relativistic particles, i.e., a minimum ionizing particle. The peak in the muon distribution gives the most probable ionization loss. Using this value as the calibration point for the analog electronics, the channels of the pulse height analyzers were set such that protons and electrons, both charge 1, were set at 0.3 x minimum.

There were four modes: electron or e mode, proton or p mode, nuclei or Z mode, and calibrate or c mode. Only the Z mode is of interest here so this mode will be described in the following paragraph.

Whenever the experiment is not in the calibrate mode, it is considered to be in the experiment mode: any event in the e, p, or Z mode is classified as experiment mode. However, the experiment mode is allowed to trigger in the calibrate mode once every 32nd event, i.e.,

the coincidence requirements for the experiment mode are relaxed and the first particle which passes through the S1 - S2 scintillator geometry is recorded by the detector.

The Z mode, divided into a low Z mode and a high Z mode, is designed to be sensitive to any charged nucleus with Z > 2. For the flight data under examination, the requirements on the scintillators were simply:

$$20 \times \text{min} > S1 > 7 \times \text{minimum}$$

$$20 \times \text{min} > S2 > 7 \times \text{minimum}$$

$$C > 6 \times \text{minimum} .$$

For the low Z mode (Charges 3 and 4 which are not of interest here) there were no other requirements. For the high Z mode consistency between the S1 - S2 pulses is required as follows:

$$S1 \text{ or } S2 > 20 \times \text{minimum}$$

$$S1 > 15 \times \text{minimum}$$

$$S2 > 15 \times \text{minimum}$$

$$C > 6 \times \text{minimum}$$

The requirements for accepting an event and pulsing the spark chamber in the Z mode are shown in Figure A3.

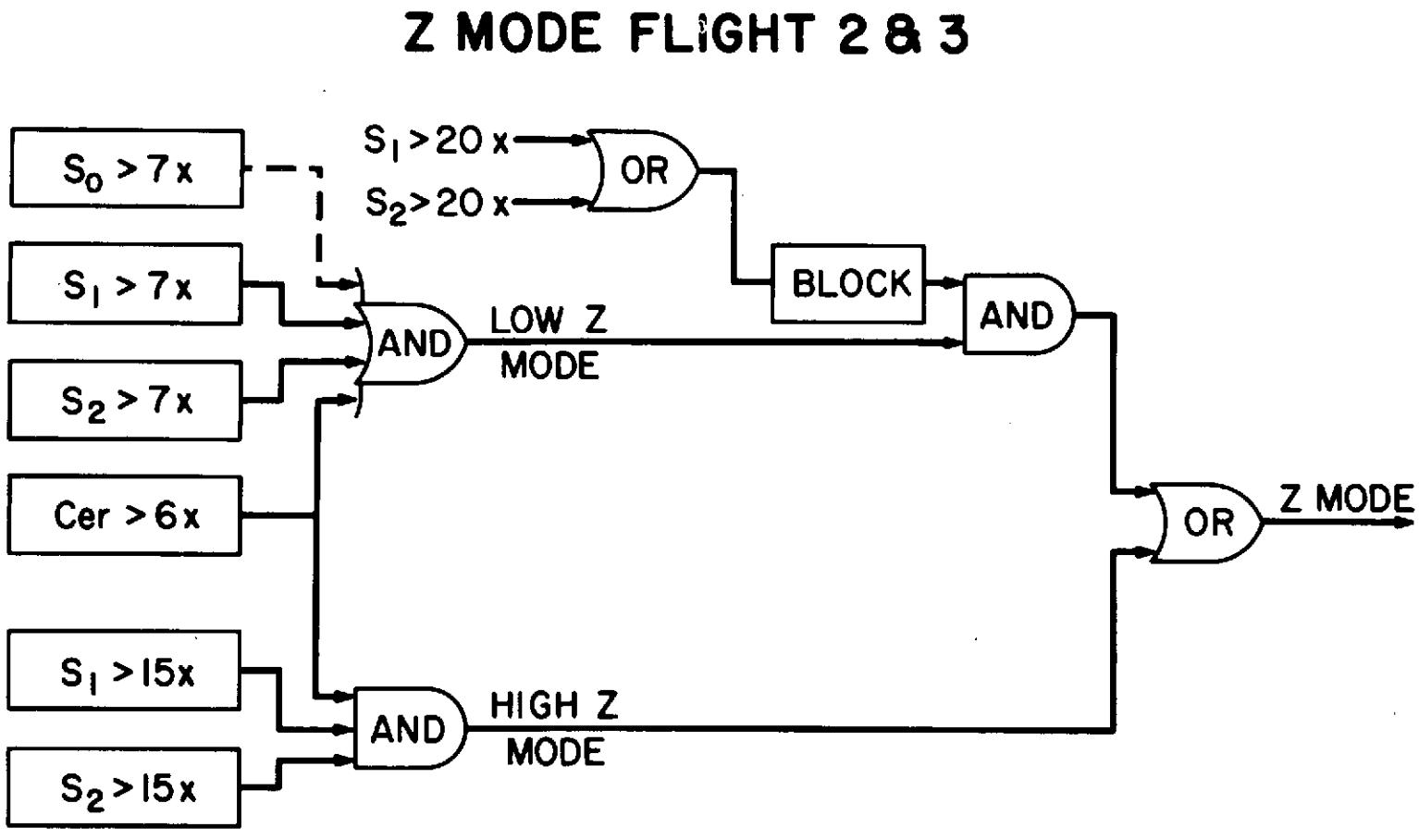

Fig. A3. Logic diagram showing event acceptance criteria and triggering requirements.

APPENDIX B

DEFINITION OF A "GOOD EVENT" IN SPARK CHAMBER

The Master Analysis Tape program reads and unpacks the cosmic ray data tapes. Included in this data are spark chamber coordinates describing the incident direction of the charged particles. From this, an attempt is made, using the criteria specified later in this section, to determine a trajectory for each event. Determination of a unique trajectory is impossible for a high percentage of events due to multiple coordinates in one or more planes or the absence of coordinates in one or more planes. When a trajectory cannot be determined for an event, that event is labelled as complex and classified into one of seven different types. For each of these types more criteria are established and another attempt is made at determining the path of the cosmic ray particle through the detector.

Ideally, a particle passing through the spark chamber would cause a single wire to be set in each plane, thereby resulting in 4 pairs of (X, Y) coordinates. Unfortunately, in actual operation each spark chamber plane may have from zero to about seven adjacent or nearly adjacent wires set by an incident particle. Consequently, the arithmetic average

$$C_{avg} = \left(\sum_{i=1}^{n} C_i\right)/n \qquad \text{(B1)}$$

is used to determine a single coordinate value. Specifically set wires immediately adjacent, or set wires separated by one or two unset wires are averaged using this averaging technique. Up to seven set wires are averaged as long as the two extreme set wires are not separated by more

than six wires. The following examples in which a + indicates a set wire and an 0 an unset wire would be averaged:

++; +0+; +++++; +00+0+.

The following examples would not be averaged due to separations of greater than six wires between the extreme set wires and would be assigned to one of the classifications of complex events:

++++++; +00+0+0++.

Even after averaging there are frequently multiple coordinates in several spark chamber planes. These cases are given critical consideration in the following paragraphs.

The zero level XY plane of the rectangular coordinate system in which the trajectory is computed is the Y_4 spark chamber plane. The Z axis is perpendicular to the Y_4 plane. The trajectory is computed in terms of the slopes and intercepts of the projections of the trajectory onto the XZ and YZ planes.

The projection of the trajectory onto the XZ plane is computed from the averaged spark chamber coordinates in the X_1, X_2, X_3 and X_4 spark chamber planes and the fixed distances between the X planes along the Z axis. The projection of the trajectory onto the YZ plane is similarly computed using the Y spark chamber planes. The following paragraphs state the methods used to compute the slope and intercept of each projection for events with various combinations of coordinates.

Case 1. One coordinate per plane is the simplest case. It is also the ideal event. The slope and intercept are obtained by performing a straight line fit on the four coordinates. This same method is applied

to three coordinates if one of the four planes has no coordinates. The root mean square deviation of the fit is also calculated. If this value exceeds an input acceptance criterion, the event is classified as complex.

Case 2. An event in which more than two planes had no coordinates would immediately be classified as complex.

Case 3. To analyze an event producing multiple coordinates in one plane, at least two of the three remaining planes must have only one coordinate. The other plane could have one or no coordinates. A trajectory is determined by performing a least squares fit with each coordinate in the plane with multiple coordinates in combination with the single coordinates of the other planes. The fit with the smallest rms is chosen if that rms is less than the acceptance criterion, the event is classified as complex.

Case 4. When the case of multiple coordinates in more than one plane occurs, the best fit is calculated using each spark chamber plane, provided each plane has at least one coordinate. If the rms of the best fit does not satisfy the acceptance criterion, the event is classified as complex. If each spark chamber plane does not have at least one coordinate the event is also classified as complex.

Each event is assigned a simplification level which is a measure of the degree of difficulty involved in computing a trajectory. There are 5 simplification levels numbered 0 to 4 with levels 2 to 4 being sublevels of level 1. Cases 1 to 4 discussed previously are assigned level 0. Events which are not assigned level 0 but which satisfy either of the following criteria are assigned level 1:

1. There exists one coordinate in each plane after averaging and the least squares fit acceptance criterion is satisfied if one coordinate is ignored.
2. There exist multiple coordinates after averaging in one plane, and single coordinates in the remaining three planes. In this case all coordinates in the plane with multiple coordinates are ignored except for that coordinate which results in the best least squares fit. If this least squares fit does not satisfy the least squares fit acceptance criterion but a satisfactory least squares fit is obtained by ignoring one of the remaining four coordinates, then level 1 is assigned.

Level 2 is assigned to an event if a trajectory satisfying the least squares fit acceptance criterion can be computed subject to the following conditions:

1. A coordinate from each of the four planes is used to compute the trajectory.
2. At least two of the four coordinates used to compute the trajectory are averaged coordinates.

A least squares fit through every combination of two averaged coordinates is performed. The remaining two coordinates used in the fit are those closest to a straight line passing directly through the averaged coordinates. These two may or may not be averaged.

If two fits satisfy the acceptance criterion, their rms deviations are compared to an internally-defined criterion of 0.05 inches. If both deviations are less than this criterion then the event is again classified as complex.

If the smallest rms deviation computed as described in the previous paragraph does not satisfy the least squares fit acceptance criterion, or if there are not two planes containing averaged coordinates, then level 3 or level 4 is assigned.

A least squares fit through every combination of coordinates not tried for level 2 is performed. If a satisfactory trajectory is found using one averaged coordinate the event is assigned level 3. If a satisfactory trajectory is not found using one averaged coordinate but is found using no averaged coordinates, the event is assigned level 4.

An example of a well-defined trajectory, in which case the event is acceptable and is classified as "good," is shown in Figure B1. A spark chamber track for a carbon nucleus is illustrated in this figure. The chamber is separated into an (X, Z) view (upper 4 lines) and a (Y, Z) view. Every 7th line is shown as a dot and each set core is denoted by a vertical line.

If an acceptable trajectory cannot be found by any of the methods discussed in previous paragraphs, the event is classified as complex and must be discarded.

These events fall into one of seven complex event types recognized by the computer algorithm. They are:

1. The particle path does not intersect the coincidence scintillators, S1-S2.
2. There are no spark chamber coordinates.
3. Three spark chamber planes have no coordinates.
4. The width of a coordinate set requiring averaging is greater than seven wires.

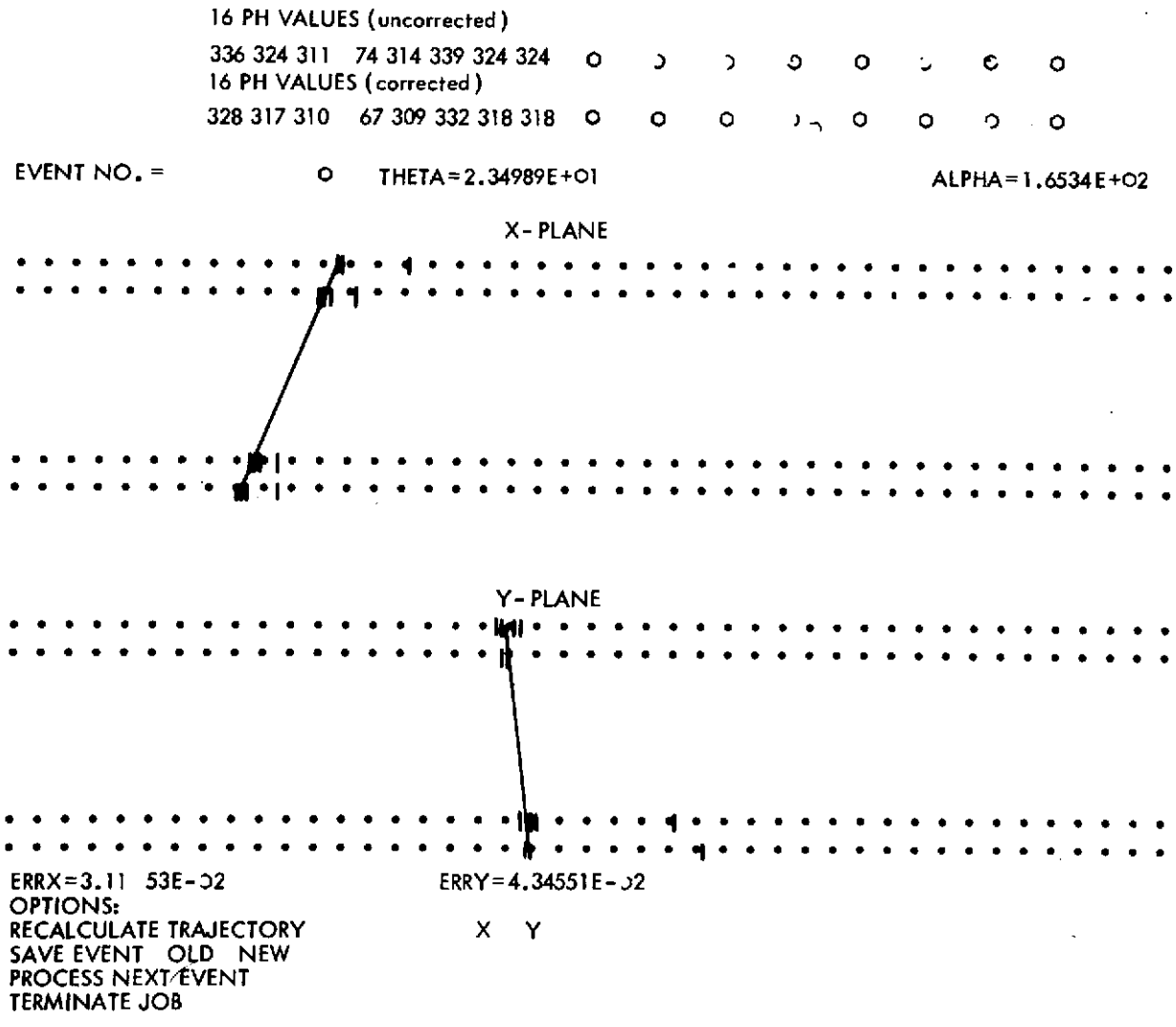

Fig. B1. Example of a well defined trajectory through the spark chamber for a carbon nucleus event. Note the satellite sparks near the trajectory which are presumably due to knock on electrons. This figure has been created from a slide taken of a graphic display unit which can be used to look at individual events.

5. The least squares fit acceptance criterion is not satisfied.
6. There are multiple coordinates in more than one plane, and none of the acceptance criteria mentioned previously are satisfied.
7. There exists more than one trajectory satisfying the least squares fit acceptance criterion for multiple trajectories.

APPENDIX C

SOLAR MODULATION

In general, the cosmic ray intensity detected near the earth is depressed below that which would be measured outside the solar system in interstellar space. The magnitude of the solar modulation depends on the level of solar activity; it is probably both rigidity and velocity dependent, and also reduces the energy of the particles. A completely adequate theory of solar modulation that will permit the intensities to be demodulated to obtain the intensities in interstellar space does not exist. This is due to the considerable amount of uncertainty that exists regarding the amount and form of the solar modulation even at times of minimum solar activity where there may be some residual modulation.

To summarize, two aspects of solar modulation are of importance in the demodulation of the intensities measured at Earth to those existing in interstellar space: the functional form of the modulation, and the magnitude of the residual modulation existing at solar minimum.

Numerous theories have been put forth in an attempt to explain solar modulation. Several papers now exist which review and analyze the models in sufficient detail such that it is not necessary to do so here. Thus only a general discussion of the problem will be presented with specific details given only as necessary to the development of the discussion.

The current state of understanding of these aspects may be reviewed in the following papers: (1) Diffusion Convection Theory, Parker, 1958, 1961, 1963; Dorman, 1960; (2) Adiabatic Deceleration

Energy Loss Process, Fisk and Axford, 1969; Gleeson and Axford, 1967, 1968 (this model leads to the force field solution at high energies, $E \geq 1$ GeV/nuc); (3) Statistical Treatments of Magnetic Field Power Spectrum, Roelof, 1966; Jokipii, 1966. Difficulties with the latter theory have been pointed out recently by Fisk et al., 1973. The reader is also referred to several excellent review articles: Quenby, 1967; Webber, 1967a; Jokipii, 1967; Cleghorn, 1970.

Several important conclusions of the previously mentioned theories are important to the correction factor calculated in Section III. I. There are good theoretical reasons for believing that nuclei having similar charge-to-mass ratios will be equally affected by the solar modulation process. When evaluating solar modulation effects, it is usually considered that all charges with $Z \geq 3$ have $A/Z \simeq 2$; therefore, changes in the intensities of heavier nuclei brought about by solar modulation are the same for all such nuclei. More importantly it allows the results of the more numerous studies of the modulation of helium nuclei, where also $A/Z \simeq 2$, to be applied directly to the modulation of heavy nuclei. (For helium nuclei, $A/Z = 1.95$, due to a 10% admixture of He^3. For iron nuclei, where $A/Z = 2.15$, the error introduced in the correction factor using $A/Z = 2.0$ is about 4% at the energies under consideration here. This is well within the error on the estimate of the amount of energy loss of helium nuclei, with $A/Z = 1.95$, due to solar modulation in 1970 which is about 15%.) The only study of the modulation of VH nuclei substantiates this approximation.

Cleghorn (1970) reviewed the existing theories and concluded that charge-dependent modulation is not predicted by any of them. He found the solar modulation of VH nuclei to be identical to that of helium

nuclei to within the statistical accuracy of his experiment. In another study (Garcia - Munoz and Simpson, 1970), IMP-4 data at solar maximum is compared to OGO-1 data at solar minimum of Comstock (1969). They find the relative abundances versus energy per nucleon are not dependent on solar modulation, i.e. all heavy nuclei are modulated the same. These satellite results are more substantial since they are not subject to atmospheric problems. An earlier review paper (Freier and Waddington, 1964) suggested the modulation is the same for heavy nuclei as for helium nuclei, or at least that the process is not strongly charge dependent.

The extent to which particles lose energy as they penetrate the solar wind on their way to Earth is not accurately known. At solar minimum the total loss may be 100 MeV/nuc.; at solar maximum it may be several hundred MeV/nucleon (Freier and Waddington, 1965; Gleeson and Axford, 1968). This ionization energy loss has only a small effect on the shape of the energy spectrum. Its only effect on the charge composition would be to shift the energy threshold of the observed intensities to a higher energy outside the solar cavity.

The most complete theory available for the study of solar modulation of cosmic rays is the theory which includes diffusion-convection and adiabatic deceleration energy loss. This problem has no analytic solution but can be solved by numerical techniques (see Fisk, 1971; Fisk et al., 1970; Fisk and Axford, 1969). However, simplifying assumptions result in several analytic solutions: separable diffusion coefficients of different forms result in analytic solutions (Urch and Gleeson, 1972; Jokipii, 1971). These authors compared the results of the numerical solution to the solutions reached from other theories. The conclude that above about 1 GeV/nuc. the theories produce

essentially similar results: Cleghorn (1970) concludes that the diffusion-convection model and force field model solutions are essentially similar above 1 GeV/nuc., Fisk and Axford (1969), and Gleeson and Axford (1968) concluded that the diffusion-convection model and adiabatic deceleration are essentially the same to within $\pm$ 10%. But more importantly, Gleeson and Axford (1968), Fisk and Axford (1969), Fisk et al. (1970), Fisk (1971), Gleeson and Urch (1971), and Urch and Gleeson (1972), show that above several hundred MeV/nuc the force field solution and complete numerical solution are very nearly the same. Since the force field solution is easiest to use, it will be used by this author to calculate a solar modulation correction factor to the data presented here.

The force field solution:

$$\frac{j_t(r,E)}{j_0(\infty, E+\bar{\Phi})} = \frac{E^2 - E_0^2}{(E+\bar{\Phi})^2 - E_0^2} \tag{C1}$$

where $j_t(r,E)$ is the intensity measured at Earth at time t, $j_0(\infty,E+\Phi)$ is the intensity in interstellar space, E is the total energy of the particle, E_0 is the particle rest energy, and $\bar{\Phi}$ is the mean energy loss due to adiabatic deceleration, will not be derived here. The reader is referred to papers where it is derived from Liouville's theorem (Freier and Waddington, 1965)

$$D = \frac{\delta N}{\delta x\, \delta y\, \delta z\, \delta p_x\, \delta p_y\, \delta p_z} = \text{constant} \tag{C2}$$

or by assuming the cosmic ray streaming is zero (Gleeson and Axford, 1968).

$$S = VU - K \frac{\partial U}{\partial r} - \frac{V}{3} \frac{\partial}{\partial T} (\alpha \, TU) \equiv o \qquad (C3)$$

Fisk and Axford (1969) have shown that these two starting points are mutually consistent by reducing the $S \equiv o$ equation to Liouville's theorem for conservative force fields.

The force field solution directly relates the local intensity to the unmodulated interstellar intensity. The intensity behaves as though the modulation were due to a conservative force field that it dependent on particle energy. Once a value of Φ is determined from experimental data, the modulation correction factor can be calculated.

An interesting sidelight is to compare the calculations from the detailed theory to the old method of using a regression curve. The regression curve method is detailed in the following paragraph.

A convenient way to represent the variation of the cosmic ray intensity is to construct a regression curve between the nuclei intensity above some rigidity threshold and the sea level cosmic ray intensity as measured by a particular neutron monitor. On such a regression plot, the data points should be distributed about a unique curve within the statistical deviations. The regression curve can then be used to predict the value of the nuclei intensity at any particular counting rate of the neutron monitor. Regression curves of the intensities of helium nuclei as a function of modulation as measured by neutron monitors have been presented by several workers (Freier and Waddington, 1965; Webber, 1967; Freier and Waddington, 1968; Rygg, 1970). Figures in these papers show the modulation of the primary intensity as a function of the Mt. Washington neutron monitor counting rate at various

energies, normalized to zero modulation when the counting rate is 2400, the solar minimum counting rate. The average neutron monitor rate of 2108 for this flight has been found by averaging the neutron monitor hourly counting rate over the duration of the balloon flight (J.A. Lockwood, private communication).

Using the results of figures from Webber (1967) and/or Freier and Waddington (1968) (their results are essentially the same since the figure of Freier and Waddington is derived from the figure of Webber), one calculates correction factors of 1.38 for $R \geq 3.25$ GV and 1.17 for $R \geq 4.9$ GV.

Since there is little difference between the correction factors calculated here and those resulting from the regression plot, the author concludes that no systematic differences should arise in comparing the present experimental data to previously published data which used the regression plot method.

One final remark is in order. It will be assumed here that there is no residual solar modulation at solar minimum, even though the theory predicts some small amount. It is, therefore, assumed that the values given in Column 3 of Table 4 are those existing in interstellar space outside the solar modulation cavity.

Justification for this assumption rests in the fact that this part of the theory is yet to be substantiated by experiment. In addition, interpretation of the data on charge composition depends on the relative abundances, not on the absolute intensities.

Bibliography

1. Anand, K. C., R. R. Daniel, and S. A. Stephens, Phys. Rev. Letters, 20, 764, 1968.

2. Arnett, W. D., Astrophys. J., 157, 1369, 1969.

3. Arnett, W. D. and D. D. Clayton, Nature, 227, 780, 1970.

4. Arnett, W. D., J. W. Truran, and S. E. Woosley, Astrophys. J., 165, 87, 1971.

5. Arnett, W. D., Ann. Rev. Astron. & Astrophys., 11, 73, 1973.

6. Arnett, W. D. and D. N. Schramm, Astrophys. J. Letters, 184, L47, 1973.

7. Audouze, J. M. and C. J. Cesarsky, Nature, 241, 98, 1973.

8. Badhwar, G. D., C. L. Deney, B. R. Dennis, and M. F. Kaplon, Nucl. Instr. & Meth. 57, 116, 1967.

9. Balasubrahmanyan, V. K., E. Boldt, and R. A. R. Palmiera, Phys. Rev., 140B, 1157, 1965.

10. Balasubrahmanyan, V. K., F. B. McDonald, and J. F. Ormes, NASA/GSFC document X-661-67-468, 1967.

11. Balasubrahmanyan, V. K., and J. F. Ormes, Astrophys. J., 186, 109, 1973.

12. Beck, F., and F. Yiou, Astrophys. Letters,1, 75, 1968.

13. Bhatia, V. S., V. S. Chohan, S. D. Pabbi, and S. Biswas, Can. J. Phys., 46, S588, 1968.

14. Bhatia, V. S., S. Biswas, V. S. Chohan, P. S. Kainth, and S. D. Pabbi, Acta Physica Hung.,29, Suppl. 1, 337, 1970.

15. Binns, W. R., J. I. Fernandez, M. H. Israel, J. Klarmann, and R. A. Mewaldt, Proc. 12th Inter. Conf. Cosmic Rays, Hobart, Tasmania, 1, 260, 1971.

16. Bradt, H. L., and B. Peters, Phys. Rev.,74, 1828, 1948.

17. Burbidge, E. M., G. R. Burbidge, W. A. Fowler, and F. Hoyle, Rev. Mod. Phys.,29, 547, 1957.

18. Cameron, A. G. W., Conf. on Explosive Nucleosynthesis, Austin, Texas, 1973.

19. Cartwright, B. G., M. Garcia-Munoz, and J. A. Simpson, Proc. 12th Inter. Conf. Cosmic Rays, Hobart, Tasmania, 1, 215, 1971.

20. Cartwright, B., M. Garcia-Munoz, and J. A. Simpson, Proc. 13th Inter. Conf. Cosmic Rays, Denver, 1, 232, 1973.

21. Casse, M. L., L. Koch, N. Lund, J. P. Meyer, B. Peters, A. Soutoul, and S. N. Tandon, Proc. 12th Inter. Conf. Cosmic Rays, Hobart, Tasmania, 1, 241, 1971.

22. Clayton, D.D. and J. G. Peters, Acta Physica Hung., 29, Suppl. 1, 381, 1970.

23. Cleghorn, T.S., M. S. Thesis, University of Minnesota, 1967.

24. Cleghorn, T. S., P. S. Freier, and C. J. Waddington, Can. J. Phys., 46, S572, 1968.

25. Cleghorn, T. S., Ph.D. Thesis, University of Minnesota, 1970.

26. Colgate, S.A. and H. J. Johnson, Phys. Rev. Letters, 5, 235, 1960.

27. Comstock, G. M., C. Y. Fan, and J. A. Simpson, Astrophys. J., 146, 51, 1966.

28. Comstock, G. M., Astrophys. J., 155, 619, 1969.

29. Comstock, G. M., C. Y. Fan, and J. A. Simpson, Astrophys. J., 155, 609, 1969.

30. Corydon-Petersen, O., and N. Lund, Danish Space Research Institute, internal technical report, 1969.

31. Cowsik, R., Y. Pal, S. N. Tandon, and R. P. Verma, Phys. Rev., 158, 1238, 1967.

32. Cowsik, R., Y. Pal, S. N. Tandon, and R. P. Verma, Can. J. Phys., 46, S646, 1968.

33. Cowsik, R., Y. Pal, S. N. Tandon, and R. P. Verma, Acta Physica Hung., 29, Suppl. 1, 439, 1970.

34. Cowsik, R., Proc. 12th Inter. Conf. Cosmic Rays, Hobart, Tasmania, 1, 329, 1971.

35. Crannell, C. J., and J. F. Ormes, Nucl. Instr. & Meth., 94, 179, 1971.

36. Crannell, C. J., R. A. Gearhart, F. A. Hagen, W. V. Jones, R. J. Kurz, J. F. Ormes, R. D. Price, R. F. Silverberg, and G. M. Simnett, Nucl. Inst. & Meth., 108, 445, 1973.

37. Davis, L., Jr., Proc. Moscow Conf. Cosmic Rays, 3, 220, 1960.

38. Dayton, B., N. Lund and R. Risbo, Acta Physica Hung., 29, Suppl. 1, 385, 1970.

39. Dorman, L. I., Proc. Moscow Conf. Cosmic Rays, 4, 320, 1960.

40. Durgaprasad, N., J. Geophys. Res., 72, 965, 1967.

41. Durgaprasad, N., J. Geophys. Res., 73, 1583, 1968.

42. Durgaprasad, N., C. E. Fichtel, D.E. Guss, D. V. Reames, F. W. O'Dell, M. M. Shapiro, R. Silberberg, B. Stiller, and C. H. Tsao, Phys. Rev. D, 1, 1021, 1970.

43. Ehmert, A., Proc. Moscow Conf. on Cosmic Rays, 4, 142, 1960.

44. Fan, C. Y., G. Gloeckler, and J. A. Simpson, Can. J. Phys., 46, S549, 1968.

45. Fichtel, C. E., and D. V. Reames, Phys. Rev., 149, 995, 1966.

46. Fichtel, C. E., and D. V. Reames, Phys. Rev., 175, 1564, 1968.

47. Fisher, A. J., J. F. Ormes, and F. A. Hagen, Proc. 13th Inter. Conf. Cosmic Rays, Denver, 4, 2895, 1973.

48. Fisk, L. A. and W. I. Axford, J. Geophys., 74, 4973, 1969.

49. Fisk, L. A., L. J. Gleeson, and W. I. Axford, Acta Physica Hung., 29, 2, 5, 1970.

50. Fisk, L. A., J. Geophys. Res., 76, 221, 1971.

51. Fisk, L. A., M. L. Goldstein, A. J. Klimas, and G. Sandri, to be submitted to Astrophys. J., 1973.

52. Fleischer, R. L., P. B. Price, R. M. Walker, and M. Maurette, J. Geophys. Res., 72, 331, 1967a.

53. Fleischer, R. L., P. B. Price, R. M. Walker, M. Maurette, and G. Morgan, J. Geophys. Res., 72, 355, 1967b.

54. Fowler, P. H., R. A. Adams, V. G. Cowen, and T. J. Kidd, Proc. Roy. Soc. A301, 39, 1967.

55. Fowler, P. H., V. M. Clapham, V. G. Cowen, T. J. Kidd, and R. T. Moses, Proc. Roy. Soc. A318, 1, 1970.

56. Freier, P. S., E. J. Lofgren, E. P. Ney, F. Oppenheimer, H. L. Bradt, and B. Peters, Phys. Rev., 74, 213, 1948a.

57. Freier, P. S., E. J. Lofgren, E. P. Ney, and F. Oppenheimer, Phys. Rev., 74, 1818, 1948b.

58. Freier, P. S., and C. J. Waddington, Phys. Rev. B, 135, 724, 1964.

59. Freier, P. S., and C. J. Waddington, Space Sci. Rev., 4, 313, 1965.

60. Freier, P. S., and C. J. Waddington, Phys. Rev. 175, 1641, 1968a.

61. Freier, P. S., and C. J. Waddington, Phys. Rev. 175, 1649, 1968b.

62. Freier, P. S., and C. J. Waddington, Can. J. Phys.,46, S578, 1968c.

63. Garcia-Munoz, M. and J. A. Simpson, Acta Physica Hung.,29, 1, 317, 1970.

64. Ginzburg, V. L., and S. I. Syrovatskii, Origin of Cosmic Rays, Pergamon Press, New York, 1964.

65. Gleeson, L. J., and W. I. Axford, Astrophys. J. Letters, 149, L115, 1967.

66. Gleeson, L. J., and W. I. Axford, Astrophys. J., 154, 1011, 1968.

67. Gleeson, L. J., and I. H. Urch, Astrophys. & Space Sci., 11, 288, 1971.

68. Gloeckler, G., and J. R. Jokipii, Phys. Rev. Letters, 22, 1448, 1969.

69. Gold, T., Nature, 221, 25, 1969.

70. Greiner, D. E., Seminar talk, Univ. of Calif. Berkeley, 1973.

71. Grigorov, N. L., V. Murzin, and I. Rapoport, Soviet Phys. J.E.T.P., 7, 348, 1958.

72. Heckman, H. H., D. E. Greiner, P. J. Lundstrom, and F. S. Bieser, Phys. Rev. Letters, 28, 926, 1972.

73. Heckman, H. H., Proc. 5th Inter. Conf. High Energy Physics & Nuclear Structure, Sweden, 1973.

74. Jokipii, J. R., Astrophys. J., 146, 480, 1966.

75. Jokipii, J. R., Astrophys. J., 149, 405, 1967.

76. Jokipii, J. R., Rev. Geophys. and Space Physics, 9, 27, 1971.

77. Judek, B., and I. J. van Heerden, Can. J. Phys., 44, 1121, 1966.

78. Juliusson, E., P. Meyer, and D. Muller, Phys. Rev. Letters, 29, 445, 1972.

79. Juliusson, E., Proc. 13th Inter. Conf. Cosmic Rays, Denver, 1, 178, 1973.

80. Kozlovsky, B. Z. and R. Ramaty, NASA doc. X-660-73-237, 1973.

81. Kulsrud, R. M., J. P. Ostriker, and J. E. Gunn, Phys. Rev. Letters, 28, 636, 1972.

82. Landau, L., J. of Physics, U.S.S.R., 8, 201, 1944.

83. Lezniak, J. A., Ph.D. Thesis, Univ. of Minnesota, 1969.

84. Lezniak, J. A., T. T. von Rosenvinge, and W. R. Webber, Acta Physica Hung., 29, Suppl. 1, 375, 1970.

85. Lingenfelter, R. E. and R. Ramaty, Proc. 12th Inter. Conf. Cosmic Rays, Hobart, Tasmania, 1, 377, 1971.

86. Linsley, J. and N. Herwitz, Rev. Sci. Instr.,26, 556, 1956.

87. Long, C.E., M. S. Thesis, Univ. of Minnesota, 1968.

88. Mathiesen, O., C. E. Long, P. S. Freier, and C. J. Waddington, Can. J. Phys., 46, S583, 1968.

89. Mewaldt, R. A., Ph.D. Thesis, Univ. of Wash.-St. Louis, 1971.

90. Mewaldt, R. A., J. I. Fernandez, M. H. Israel, J. Klarman, and W. R. Binns, Tech. Rpt., Washington Univ.-St. Louis, 1971.

91. Mewaldt, R. A., J. I. Fernandez, M. H. Israel, J. Klarmann, and W. R. Binns, Astrophys. & Space Sci., 22, 45, 1973.

92. Michaud, G. and W. A. Fowler, Astrophys. J., 173, 157, 1972.

93. Ormes, J. F., M. S. Thesis, Univ. of Minnesota, 1965.

94. Ormes, J. F., Ph.D. Thesis, Univ. of Minnesota, 1967.

95. Ormes, J. F., V. K. Balasubrahmanyan, F. B. McDonald, and R. D. Price, IEEE Trans. Nucl. Sci.,NS-15, 566, 1968.

96. Ormes, J. F., and V. K. Balasubrahmanyan, Acta Physica Hung.,29, Suppl. 1, 397, 1970a.

97. Ormes, J. F., V. K. Balasubrahmanyan, R. D. Price, M. J. Ryan, and R. F. Silverberg, IEEE Trans. Nucl. Sci.,NS-17, 3, 1970b.

98. Ormes, J. F., V. K. Balasubrahmanyan, T. Bowen, R. W. Huggett, T. A. Parnell, and K. Pinkau, NASA/GSFC Doc. X-661-71-1, 1971a.

99. Ormes, J. F., V. K. Balasubrahmanyan, R. D. Price, and M. J. Ryan, Bull. Am. Phys. Soc.,Series II, 18, 540, 1971b.

100. Ormes, J. F., V. K. Balasubrahmanyan, and M. J. Ryan, Proc. 12th Inter. Conf. Cosmic Rays,Hobart, Tasmania, 1, 178, 1971c.

101. Ormes, J. F., and V. K. Balasubrahmanyan, Nature, 241, 95, 1973.

102. Parker, E. N., Phys. Rev., 110, 1445, 1958.

103. Parker, E. N., Astrophys. J., 133, 1014, 1961.

104. Parker, E. N., Interplanetary Dynamical Processes, Interscience Publishers, New York, p.196-206, 1963.

105. Parker, E. N., Planet. Spa. Sci., 13, 9, 1965.

106. Parker, E. N., Planet. Spa. Sci., 14, 371, 1966.

107. Price, P. B., R. F. Fleischer, D. D. Peterson, C. O'Ceallaigh, D. O'Sullivan, and A. Thompson, Phys. Rev., 164, 1618, 1967.

108. Price, P. B., R. L. Fleischer, D. D. Peterson, C. O'Ceallaigh, D. O'Sullivan, and A. Thompson, Phys. Rev. Letters, 21, 630, 1968.

109. Price, P. B., D. D. Peterson, R. L. Fleischer, C. O'Ceallaigh, D. O'Sullivan, and A. Thompson, Acta Phys. Hung., 29, Suppl. 1, 417, 1970.

110. Quenby, J. J., Handbuch der Physik, 46/2, 310, 1967.

111. Ramaty, R. and R. E. Lingenfelter, Conf. Isotopic Composition of the Primary Cosmic Radiation, ed. P. M. Dauber, Danish Space Research Institute, p. 203, 1971.

112. Ramaty, R., V. K. Balasubrahmanyan, and J. F. Ormes, Science, 180, 731, 1973.

113. Reames, D. V., and C. E. Fichtel, Can. J. Phys., 46, S544, 1968.

114. Roelof, E. L., Ph.D. Thesis, Univ. of Calif.-Berkeley, 1966.

115. Rossi, B., High Energy Particles, Prentice-Hall, New York, 1952.

116. Rudstam, G., Z. Naturforschung, 21a, 1027, 1966.

117. Ryan, M. J., J. F. Ormes, and V. K. Balasubrahmanyan, Phys. Rev. Letters, 28, 985, 1972.

118. Rygg, T., Ph.D. Thesis, Univ. of Maryland, 1970.

119. Shapiro, M. M. and R. Silberberg, Acta Physica Hung., 29, Suppl. 1, 485, 1970a.

120. Shapiro, M. M., and R. Silberberg, Ann. Rev. Nucl. Sci., 20, 323, 1970b.

121. Shapiro, M. M., R. Silberberg, and C. H. Tsao, Acta Physica Hung., 29, Suppl. 1, 463, 1970a.

122. Shapiro, M. M., R. Silberberg, and C. H. Tsao, Acta Physica Hung., 29, Suppl. 1, 471, 1970b.

123. Shapiro, M. M., R. Silberberg and C. H. Tsao, Acta Physica Hung., 29, Suppl. 1, 479, 1970c.

124. Shapiro, M. M., R. Silberberg, and C. H. Tsao, Proc. 12th Inter. Conf. Cosmic Rays, Hobart, Tasmania, 1, 221, 1971.

125. Shapiro, M. M., R. Silberberg and C. H. Tsao, Proc. 13th Conf. Cosmic Rays, Denver, 1, 578, 1973.

126. Silberberg, R. and C. H. Tsao, Astrophys. J. Suppl.,25, 315, 1973.

127. Silverberg, R. F., J. F. Ormes, and V. K. Balasubrahmanyan, J. Geophys. Res., 78, 7165, 1973.

128. Smith, L. H., A. Buffington, G.F. Smoot, L. W. Alvarez, and M. A. Wahlig, Astrophys. J., 180, 987, 1973.

129. Symon, K. R., Ph.D. Thesis, Harvard Univ, 1948.

130. Truran, J. W. and W. D. Arnett, Astrophys. J., 160, 181, 1970.

131. Tsao, C. H., M. M. Shapiro, and R. Silberberg, Proc. 13th Inter. Conf. Cosmic Rays, Denver, 1, 107, 1973.

132. Urch, I. H. and L. J. Gleeson, Astrophys. & Space Sci., 17, 426, 1972.

133. von Rosenvinge, T. T., and W. R. Webber, Nucl. Instr. & Meth.,66, 1, 1968.

134. von Rosenvinge, T. T., Ph.D. Thesis, Univ. of Minnesota, 1969.

135. von Rosenvinge, T. T., W. R. Webber, and J. F. Ormes, Astrophys. & Space Sci.,3, 4, 1969a.

136. von Rosenvinge, T. T., W. R. Webber, and J. F. Ormes, Astrophys. & Space Sci.,3, 80, 1969b.

137. von Rosenvinge, T. T., W. R. Webber, and J. F. Ormes, Astrophys. & Space Sci.,5, 342, 1969c.

138. Waddington, C. J., Astrophys. and Spa. Sci.,5, 3, 1969.

139. Waddington, C. J., P. S. Freier, and C. E. Long, Acta Physica Hung., 29, Suppl. 1, 367, 1970.

140. Webber, W. R., Handbuch der Physik, 46/2, 181, 1967a.

141. Webber, W. R., Proc. 10th Int. Conf. Cosmic Rays, 1, 146, 1967b.

142. Webber, W. R., and J. F. Ormes, J. Geophys. Res.,72, 5957, 1967.

143. Webber, W. R., S. V. Damle, and J. C. Kish, Proc. 12th Inter. Conf. Cosmic Rays, Hobart, Tasmania, 1, 229, 1971.

144. Webber, W. R., Cosmic Ray Charge Measurements - A 1972 Summary, 1972.

145. Webber, W. R., S. V. Damle, and J. C. Kish, Astrophys. and Spa. Sci., 15, 245, 1972.

146. Webber, W. R., J. A. Lezniak, J. C. Kish, and S. V. Damle, Astrophys. & Spa. Sci. 12, 123, 1973a.

147. Webber, W. R., J. A. Lezniak, and J. C. Kish, Nucl. Instr. & Meth., 111, 301, 1973b.

148. Webber, W. R., J. A. Lezniak, J. C. Kish, and S. V. Damle, Nature, 241, 96, 1973c.

149. Whiteside, H., C. J. Crannell, H. Crannell, J. F. Ormes, M. J. Ryan, and W. V. Jones, Nucl. Instr. & Meth., 109, 375, 1973.